INFORMATION TO USERS

This manuscript has been reproduced from the microfilm master. UMI films the text directly from the original or copy submitted. Thus, some thesis and dissertation copies are in typewriter face, while others may be from any type of computer printer.

The quality of this reproduction is dependent upon the quality of the copy submitted. Broken or indistinct print, colored or poor quality illustrations and photographs, print bleedthrough, substandard margins, and improper alignment can adversely affect reproduction.

In the unlikely event that the author did not send UMI a complete manuscript and there are missing pages, these will be noted. Also, if unauthorized copyright material had to be removed, a note will indicate the deletion.

Oversize materials (e.g., maps, drawings, charts) are reproduced by sectioning the original, beginning at the upper left-hand corner and continuing from left to right in equal sections with small overlaps. Each original is also photographed in one exposure and is included in reduced form at the back of the book.

Photographs included in the original manuscript have been reproduced xerographically in this copy. Higher quality 6" x 9" black and white photographic prints are available for any photographs or illustrations appearing in this copy for an additional charge. Contact UMI directly to order.

UMI®

Bell & Howell Information and Learning
300 North Zeeb Road, Ann Arbor, MI 48106-1346 USA
800-521-0600

Université d'Ottawa • University of Ottawa

Process Model for 2D Braiding of Elliptical Cross-section Preforms

A thesis submitted to the
School of Graduate Studies in partial
fulfilment of the requirements for the degree
of Master of Applied Science

© By
Stephen A. Eustace

Department of Mechanical Engineering
University of Ottawa
Ottawa, Ontario, Canada

1998

ABSTRACT

One form of composite material consists of an amorphous matrix (generally a polymer) with a set of fibres contained in fibre bundles or strands, embedded within it. Often the strands are arranged in an interwoven fabric. Two-dimensional (2D) braiding provides one means of creating such a fabric.

The composite's properties depend very much on the configuration of the strands. This configuration depends on aspects of the braiding process, such as machine size and machine speeds. Thus there is a need to establish the relationships between the process parameters and the resulting configuration for braiding processes.

In this research effort, relationships of this type were developed for hollow tubular fabric "preforms" with an elliptical cross-section that varies in size along the product's length. These relationships take the form of both single line equations and algorithms with several inherent equations and decision steps. The algorithms give the property distributions over the preform surface. Relationships were developed for both steady state and transient processes.

The algorithms, which were run for various process and mandrel conditions, gave reasonable results. When run for circular cylindrical preforms, the results agreed with previously published work.

ACKNOWLEDGEMENTS

I would like to thank my supervisors, Dr. A.E. Fahim and Dr. M.B. Munro, for providing me with valuable guidance and assistance during the course of this research. I would also like to thank the Natural Sciences and Engineering Research Council for their scholarship in support of this work.

TABLE OF CONTENTS

LIST OF FIGURES

LIST OF TABLES

CHAPTER 1

INTRODUCTION AND LITERATURE REVIEW

1.1 Introduction

Composite materials can have light weight, high strength, high stiffness, and low production cost. As such, they are gaining widespread acceptance in the aerospace, sports equipment, and other industries. One form of composite material consists of an amorphous matrix (generally a polymer) with fibres imbedded within it. The fibres have a high strength and modulus of elasticity. The strength and stiffness of the fibres are combined with the flexibility of the polymer in the composite. The fibres are grouped together in strands within the polymer. Generally the strands are arranged in a pattern, often a pattern of interwoven strands, or "fabric". Two-dimensional (2D) braiding

provides one means of creating such a fabric.

Conventional 2D braiding results in a tubular fabric. Thus it is only used for creating shells or hollow items. However, a cylindrical tube is not the only shape which may be fabricated. A tube of fabric could be laid in a mould and injected with the polymer to create a more complex shape, such as a tennis racket frame. Alternatively, the braiding process itself can be controlled to create a tubular shell with a cross-section that varies along the shell's length.

Good mechanical properties in such materials are often required. These properties depend very much on the orientation, configuration, and density of the fibres. Since the ability to produce a specified strand configuration is desirable, the relationships between strand configuration and mechanical properties are sought. Also, relationships between aspects of the process (speeds, etc.) and the resulting configuration are sought. It is the purpose of this thesis to develop relationships of the latter type for some applications, specifically, hollow tubular products with an elliptical cross-section which varies in size along the products' length. This thesis will consider dry fibre products (ie. without a polymer matrix) called preforms. Matrix impregnation occurs after the production of the fibre preform.

This thesis presents formulae and methods for finding basic fabric configuration properties resulting from braiding onto certain shapes of mandrels under various process conditions (or parameters), such as machine size, machine speeds, etc. The configuration properties to be analysed in this thesis are the braid angle, the strand spacing and the cover factor. There are other parameters which can be used to describe a configuration of strands, such as 'fibre volume fraction'; however, the three above are commonly used. A brief description of the braiding process is given.

During braiding a mandrel is set up in a braiding machine as shown in Figures 1-1 and 2-2. After starting the process, the mandrel moves axially away from the circle of strand carriers. The carriers move about the circle, half of them in one direction and half in the other direction, passing each other on alternate sides. This creates a woven fabric on the mandrel. The fabric grows along the mandrel until the mandrel is covered.

As a carrier moves around the circle and as the mandrel moves forward, a strand is deposited in the shape of a helix. The angle of this helix is known as the 'braid angle'. It is measured with respect to the longitudinal direction of the mandrel. Because this angle partly describes the configuration of the finished fabric, it is referred to herein as a 'configuration property'. After braiding, the braid angle may be different at different locations along the mandrel. The braid angle at which the strand was laid down at

depends on how fast the mandrel was moving relative to the speed of the carriers at that time and other factors. In this thesis it is assumed, during the braiding process, that portions of the strand that have contacted the mandrel do not slide on the mandrel after placement.

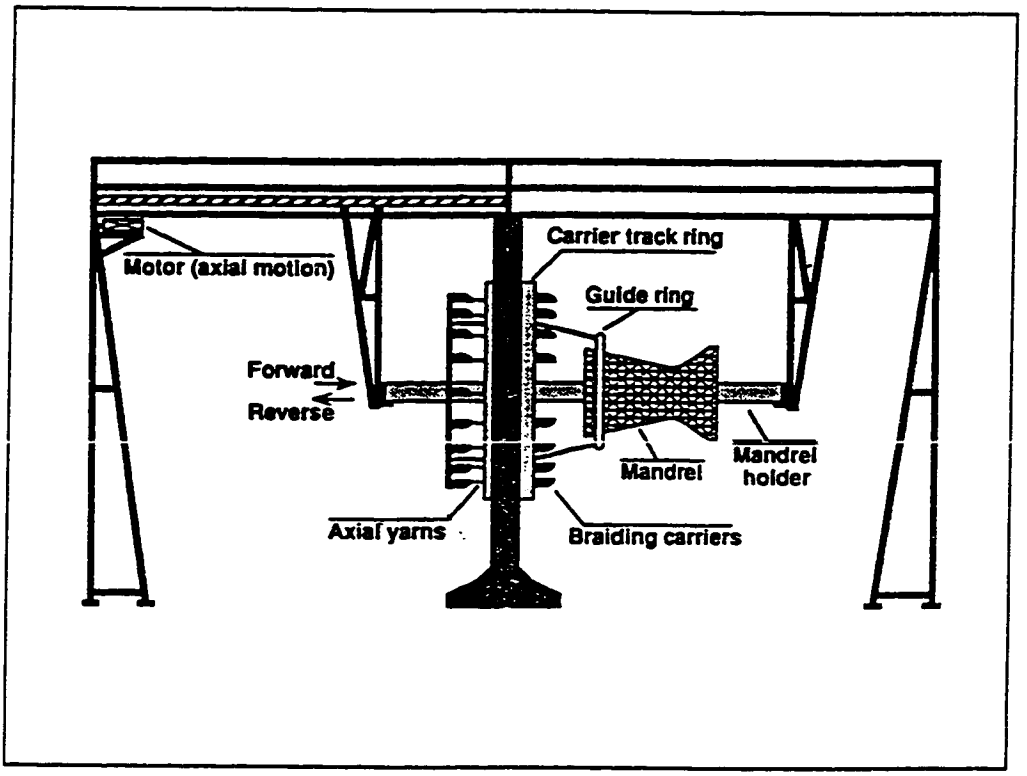

Figure 1-1 The Braiding Process. From Du, Popper, and Chou, [2].

Many strands are laid down on the surface of the mandrel. The circumferential distance between two adjacent strands on the surface laid down by carriers travelling in the same angular direction (ie. parallel strands) shall be referred to as the 'strand spacing'. This clearly is another configuration property.

The third configuration property studied herein is the cover factor. The cover factor for a region of a surface covered by a fabric is defined as the area covered by strands divided by the total area of the region. This property is further defined in Chapter 3, and is calculated using the braid angle and strand spacing.

1.2 Literature Review

Since braided composites are relatively new, very few papers have been published developing the relationships between the resulting configuration properties and the parameters (eg. carrier speed) of the braiding process. As stated, the fabric when impregnated with a polymer, forms a stress bearing shell of composite material. Much work has been done on determining the material properties of such materials based on the orientation (or configuration properties) of the strands of such fabrics. Some work has been done on using the relationships between process speeds and configuration properties to control the speeds automatically to get the desired properties.

Pastore and Ko [1] studied relationships between composite fabric material strength and configuration properties. They also developed the basic relationships between configuration properties and machine speeds for cylindrical mandrels, presuming steady state processes. These relationships were then used to develop a controlled braiding system to produce a desired profile of configuration properties along the length of the pre-form.

Du, Popper, and Chou [2] considered mandrels of circular section whose diameter varied along the length of the mandrel. They developed equations relating the positions and speeds of the mandrel, carriers, and strands, at any given time to the braid angle of the fabric formed at that time. These were used to create differential equations which describe the rate of growth of the fabric. They describe a technique to numerically integrate the latter equations and also use the former equations to calculate the set of braid angles along the length of the mandrel. This well constructed method thus gives the valuable relationships between the process parameters and the basic configuration properties. They also describe an "inverse" solution whereby the desired set of braid angles is given and the necessary set of speeds is found.

Michaeli and Rosenbaum [3] also developed a computer control system for a 2D braiding machine. The system was designed to produce a desired set of braid angles along the length of a mandrel. They also studied how far the desired path of the strand can be from a geodesic path before slipping occurs. Such deviation is possible (and usual) due to friction between the strands and the mandrel and each other, due to the inter-woven configuration. They showed that this allowable deviation for braiding can be 30% higher than for a comparable strand winding process.

Applications of braided tubular fabric are presented by J.B. Sainsbury-Carter [4]. He briefly discusses the merits of different types of fibre materials used. He also describes techniques for fabricating objects of various shapes from the fabric and resin, such as,

expandable foam cores, heated female moulds, and shrink tape. Included in the discussion are typical curing temperatures and pressures.

L.R. Sanders [5] adapted a commercial textile braider to use fibreglass, Kevlar, and graphite fibres. He developed a compatible resin system so that pre-impregnated strands could be braided. He performed a comprehensive study on the effect of temperature during the process on the strengths of these fibres. He also studied the effect of temperature on the strengths of the composite materials produced with these fibres.

McDonnell Douglas Astronautics Company [6] successfully adapted a braiding machine to produce a composite material missile launcher. They are also adapting the process for use on aircraft structural components by researching the properties of various braided composites. They studied methods of attaching other components onto the product during braiding and multi-layering for increasing the thickness, so that complex products could be produced. For the launcher they developed a multiple piece mandrel which defined a complex shape and held other product components. They added a control system to automatically control machine speeds in different areas so as to produce the braid angles which they determined were required. They developed equipment for automatic transportation, resin impregnation, curing, and removal of excess material.

Soebroto, Hager, Pastore, and Ko [7] created an integrated design system for braided tubular composites. They developed design curves relating braiding parameters to braid

geometry and experimentally verified them. A fabric geometry model was created for the modelling of the composite's strength properties.

1.3 Problem Definition

Du, Popper, and Chou [2] developed a model of the process of creating a preform with a circular cross-section that varies in size along its length, by the 2D braiding process. A model of the (2D) braiding of a preform with an elliptical cross-section that varies in size along its length has not been published. This thesis develops such a model. The model yields the distributions of configuration properties over the preform surface when braided using specified time profiles of the process parameters, for transient and steady states.

1.4 Thesis Outline

In Chapter 2 relationships are given between parameters of the process (for example, machine speeds, preform dimensions, and machine dimensions) and the strand configuration for the case of circular cylindrical preforms produced by a steady state process. Also Du, Popper, and Chou [2] developed a numerical process (in lieu of

analytical relations) for finding the configuration properties along the length of a preform of any revolute shape given the set of process parameters which may be time dependent. This process and the inherent equations are described in Chapter 2.

In Chapter 3 a formula is developed for the "cover factor" of a fabric. This is one of the quantities (or properties) commonly used in describing the strand configuration at a point in a fabric which shall be referred to herein as "configuration properties".

In Chapter 4 preforms with constant elliptical cross-section braided in a steady state process are considered. Certain assumptions are made. Formulae are developed giving the configuration properties around the preform's perimeter. An algorithm is developed which outputs the property distributions in a table.

In Chapter 5 preforms with elliptical cross-sections with section size varying along the length are considered for both transient and steady state processes. An algorithm is developed which traces the path on the preform surface on which each strand lies. Equations are also developed to get the configuration properties over the preform surface from this data. These equations are incorporated into the algorithm. The algorithm outputs a table of strand co-ordinate points and the properties at those points for the entire preform surface.

The algorithms were run for many process and mandrel conditions to examine their

accuracy. In Chapter 6 the results of these runs are discussed. The results of the algorithms are compared for the same set of process parameters. Assumptions made are discussed in light of the results.

Conclusions and recommendations for further study are presented in Chapter 7 .

CHAPTER 2

CONFIGURATION PROPERTIES FOR PREFORMS WITH CIRCULAR CROSS-SECTIONS

The purpose of this thesis is to study configuration properties resulting from 2D braiding onto mandrels with elliptical cross-sections, both constant and varying along the length of the mandrel. The configuration properties have been studied by others for braiding onto mandrels with circular cross-sections, both constant and varying along the length of the mandrel. That work is presented briefly in this chapter as the work of this thesis is based on it. Also, a circular section is one case of an elliptical section (where the major and minor axes are equal) thus the results of this thesis can be compared for this case. In addition, some errors were found in the existing papers and are corrected herein.

2.1 Properties for Preforms with Constant Circular Cross-section When Braided in Steady State

This section presents a study of the fabric configuration properties obtained when braiding in steady state to produce a preform with a constant circular cross-section.

The derivation by Pastore and Ko [1] of the resulting braid angle, θ, which is uniform over the surface, is repeated here. For the process running at steady state, during one revolution of the carriers a tow is laid down as shown in Figure 2-1. The figure shows that;

$$\theta = \tan^{-1} \frac{2 \pi r}{a} \qquad (1)$$

where; a = the longitudinal distance traveled by the contact point of the strand on the mandrel during one revolution

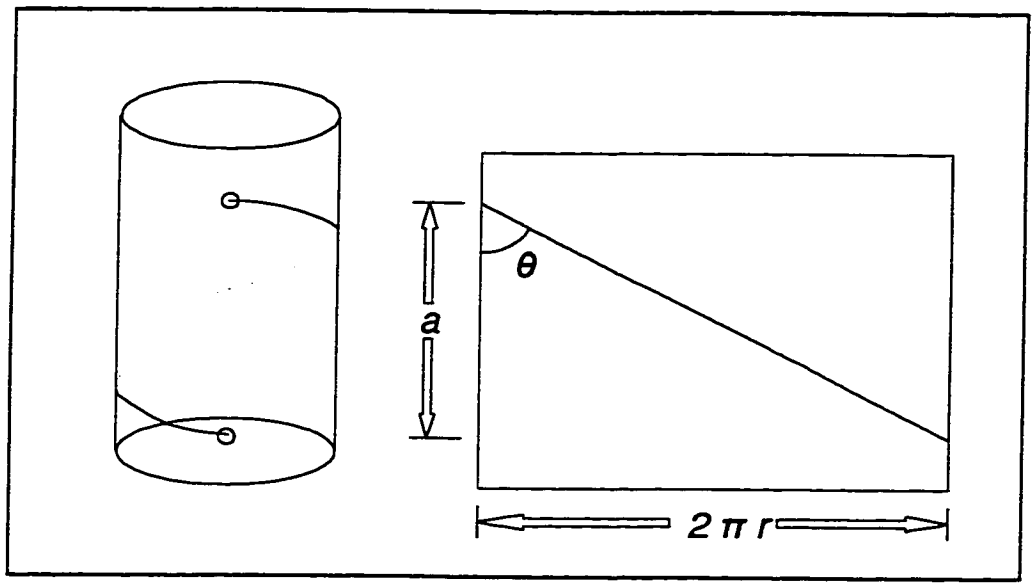

Figure 2-1 The Path of a Single Strand on a Mandrel with Constant Circular Cross-section when Braided in Steady State

Because the process is in steady state, a is equal to the distance that the mandrel travels during one revolution. Thus;

$$a = v_t \left[\frac{2\ \pi\ radians}{\omega_c}\right] \tag{2}$$

where; v_t = mandrel traverse velocity

ω_c = angular velocity of carriers

(radians/unit time)

Therefore;

$$\theta = \tan^{-1}\left(\frac{r\ \omega_c}{v_t}\right) \tag{3}$$

The strand spacing, S, is easily calculated. Because of circular symmetry, the distance between any two same direction strands in the braided fabric is the same all around the perimeter. Therefore;

$$S = \frac{(2\ \pi\ r)}{N_s} \tag{4}$$

where; r = radius of mandrel

N_s = number of same-direction tows

Pastore and Ko calculate the cover factor based on braid angle and strand spacing.

2.2 Properties For Preforms With Varying Circular Cross-section when Braided in a Steady or Transient State

This section's material is derived from Du, Popper and Chou [2] and is included because the work of Chapter 5 is based on it. Du et al. developed a method to find the configuration properties which result from braiding with machine speeds which are pre-specified functions of time (typically constant speeds).

Figures 1-1, 2-2 and 2-3 illustrate the braiding process at one instant in time. Figure 1-1 indicates a 'guide' ring or 'formation' ring. This is a ring which the strands pass through before contact with the mandrel. Its use is to assist in producing low braid angles if desired, and is optional.

2.2.1 Process Relationships

Variables are defined as shown in Figures 2-2 and 2-3.

Rg = radius of circle of carriers or formation ring (if present)

t = time since beginning of process

h = contact distance at time t

ho = initial h

z = location of ring of strand contact points ('Deposit plane' in the figures) with respect to starting end of mandrel, at time t

zo = initial z

Rm = radius of mandrel at contact ring

γ = slope angle of mandrel at contact ring

V_y = fibre volume fraction

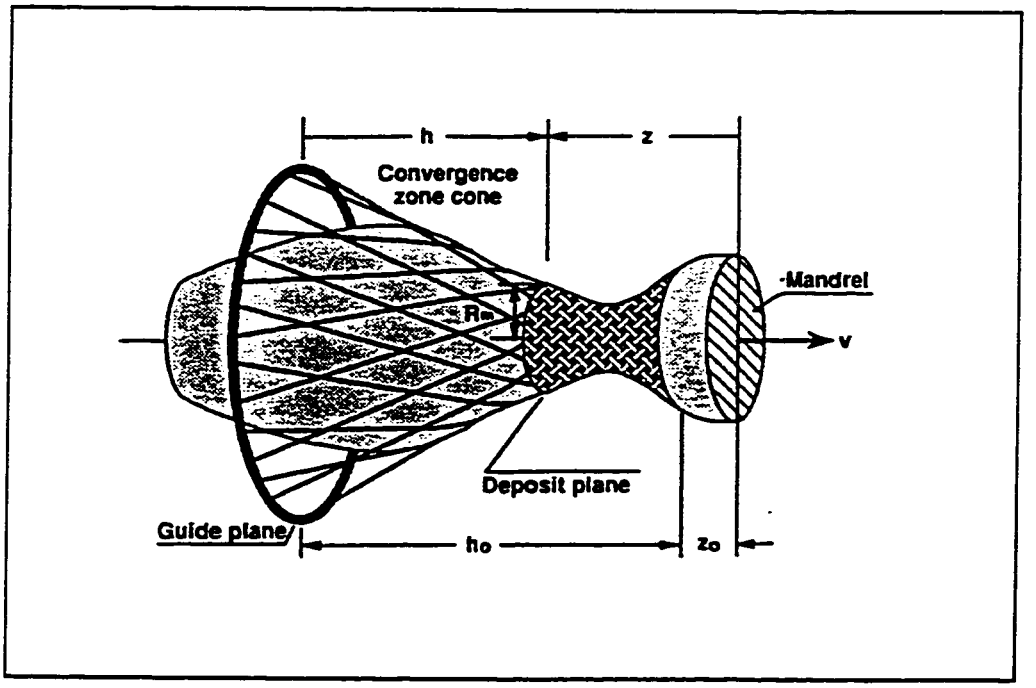

Figure 2-2 Deposition of Strands (Du, Popper, and Chou, [2]).

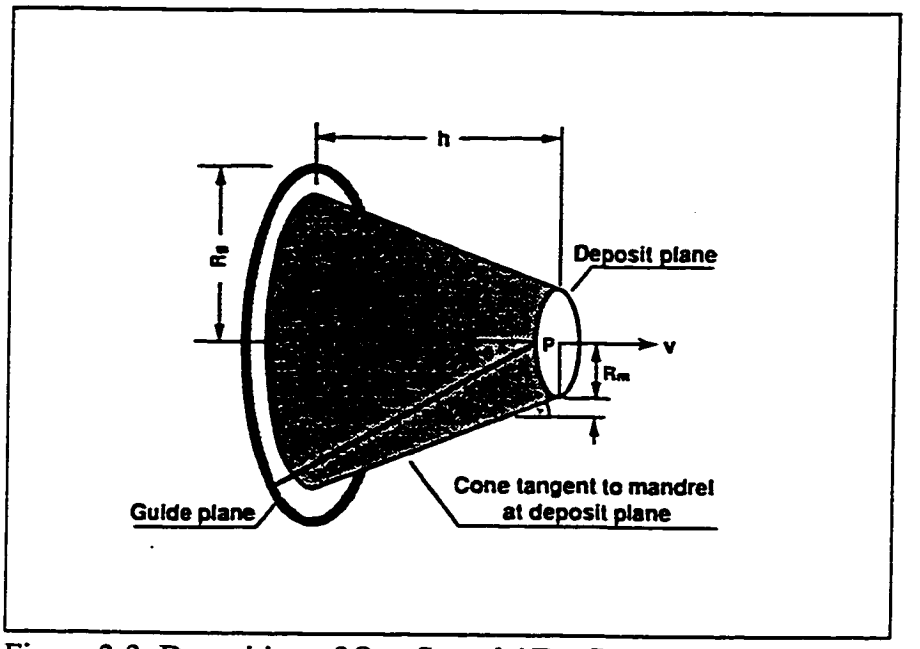

Figure 2-3 Deposition of One Strand (Du, Popper, and Chou, [2]).

The following equations are extracted from Du, Popper and Chou [2].

$$\theta = \tan^{-1}\left[\frac{Rg\cos\gamma}{h}\sqrt{1-\left(\frac{Rm + h\tan\gamma}{Rg}\right)^2}\right] \tag{6}$$

$$\theta = \tan^{-1}\left[Rm\cos\gamma\,\frac{\omega}{\frac{dz}{dt}}\right] \tag{5}$$

$$\frac{dh}{dt} + \frac{Rm\,\omega\,h}{Rg\sqrt{1-\left[\frac{Rm\,h\tan\gamma}{Rg}\right]^2}} = v_t \tag{7}$$

$$z = z_0 + \int_0^t [\, v_t - \frac{dh}{dt}] \, dt \tag{8}$$

$$V_y = \frac{w \sin\gamma}{2\, Rm \cos\theta \sin[\frac{\pi \sin\gamma}{N_s}]} \tag{9}$$

$$C = 1 - (1 - V_y)^2 \tag{10}$$

Equation 6 has been corrected from that in Du et al., i.e. "dz/dt" replaces "z". Noting that they define $\omega = d\beta / dt$, the change is evident from Figure 5 in Du et al. (see Figure 2-4 herein).

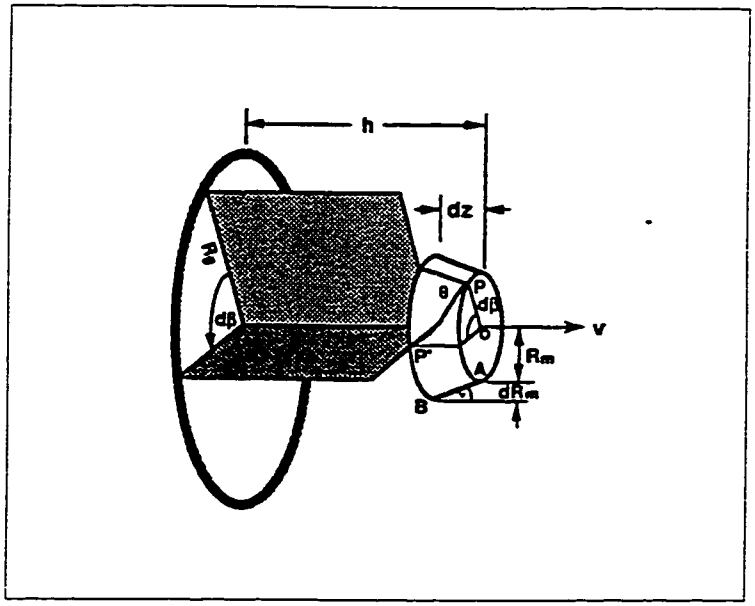

Figure 2-4 Yarn Deposit Within Time Increment dt, from Du, Popper, and Chou [2]

For a straight cylinder braided at constant speed Du et al. solved equation 7 analytically, and found h as a function of time. Though not presented in their paper, using this and equation 5, the braid angle could be found as a function of time. Using h(t), z as a function of time could also be obtained. Thus, if desired, the braid angle as a function of z, a configuration property profile, could be found.

For large values of time Du et al.'s equations reduced to equation 3 obtained in Section 2.1 for steady state braid angle.

2.2.2 Method For Finding Configuration Properties Over the Preform Surface

Finding the set of configuration properties which occurs for given machine speeds is known as the "forward" solution. The initial value of h is known; it is selected by the machine operator. It could be a precalculated value based on equation 5 to give a desired braid angle at the starting end of the mandrel. Du et al. state that to find the configuration property profile the initial values of the other variables are first calculated from the above equations. Then a small time interval, Δt, is considered. Δh is then found using equation 7. Thus h at the end of the interval is found as follows;

$$h = \text{previous } h + \Delta h$$

From equation 8;

$$z = \text{previous } z + v_t \, \Delta t - \Delta h$$

Since r and γ are functions of z, they can now be found. Considering the next Δt, equation 7 is used to find the next Δh. This process is continued until z reaches the end of the mandrel. This yields a set of h values which enables the calculation of the braid angle profile using equation 5.

Consider braiding onto a mandrel with a circular cross-section that is constant along the length at constant pre-selected machine component speeds. The strands are wrapped on as shown in Figure 2-2. Note that there is a longitudinal distance between the carrier circle (or formation ring, if present) and the ring of points at which the strands contact the mandrel. This shall be referred to as the contact distance, h. At the start of the braiding process the machine operator attaches the strands to the mandrel as shown in Figure 2-2. Thus the initial contact distance is selected as desired. After starting the process the contact distance then changes over a time period until it stabilizes at a greater or lesser value. This signifies that a steady state has been reached. The configuration properties also change during the transient period and stabilize when the steady state is reached.

2.2.3 Method For Finding Speed Profile Required For Desired Configuration Property Profile

Du et al. also developed a method to find the speed functions required to give a desired

configuration property distribution (for example, constant cover factor). Though outside of the immediate scope of this thesis, this is presented in brief because it may be used by others in the future to predict the required machine speeds for the production of elliptical sectioned preforms.

For some applications a machine is run in a fashion intended to give a specified configuration property profile, such as constant cover factor. Finding the machine speed profile required is known as the "inverse" solution. If the angular velocity of the carriers is set constant, the traverse velocity profile is required, or vice-versa. Knowing the initial braid angle, the initial value of h is found from equation 5. The machine is set to this position. A small segment of the mandrel is considered, Δz. For this segment the required Δt and v_t are found using equations 7 and 8. This process is repeated for the next segments giving the speed profile that is required to produce the desired configuration property profile.

CHAPTER 3

COVER FACTOR DERIVATION

As stated in the previous chapter, one configuration property considered in this thesis is the cover factor. The cover factor for a region of a surface covered by a fabric is defined as the area covered by strands divided by the total area of the region. Only one source was found which presents a formula for the cover factor, namely Pastore and Ko [1]. However, this formula is unclear, therefore a correct formula is developed herein. The cover factor of a fabric at any point depends on the spacing of the strands and the angle at which they lay, the braid angle.

3.1 Derivation Of Cover Factor Formula

A unit cell is an area of the fabric such that the entire fabric is made up of and only of "copies" of this area. Thus for a uniform fabric the cover factor everywhere is equal to the cover factor of a unit cell.

Figure 1 in Pastore and Ko [1] (see Figure 3-1) shows a region of fabric and a rectangle showing their selection of a unit cell. The unit cell selected for this analysis is shown in Figure 3-3.

There are many patterns of woven fabric. That shown in Figure 3-2 is referred to as a 1 to 1 fabric. That shown in Figure 3-1 is like a 1 to 1 fabric except that it has vertical strands also. However, Pastore and Ko's analysis is for a 1 to 1 fabric, like that of Figure 3-2.

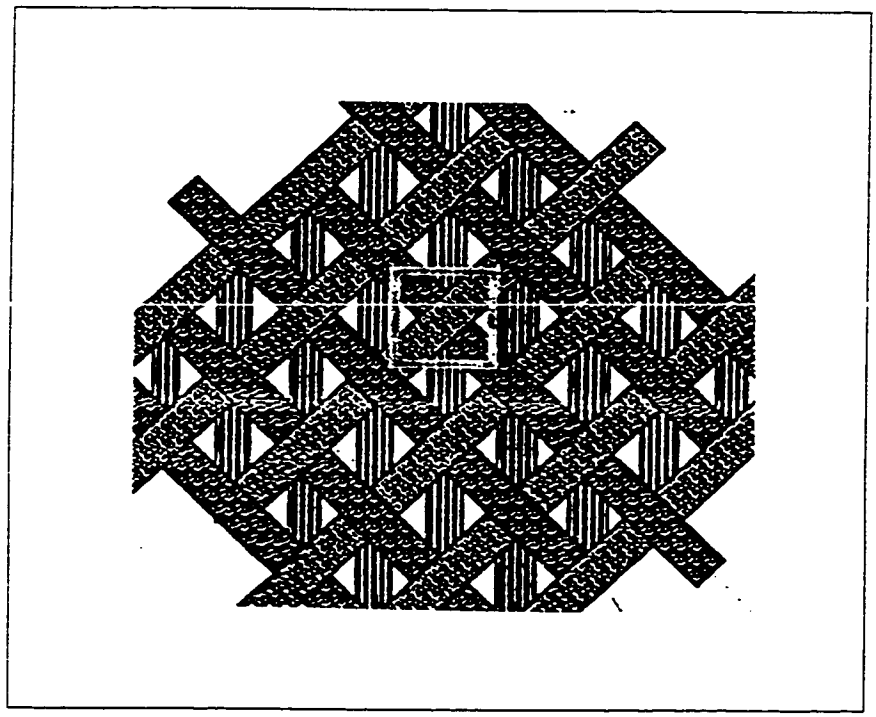

Figure 3-1 Unit Cell, from Pastore and Ko [1]

The cover factor shall be derived for a 1 to 1 fabric based on the given strand spacing, S, and the braid angle, θ. Figure 3-2 shows a 1 to 1 fabric with a braid angle of θ and a strand spacing of S. Figure 3-3 shows a unit cell. The cover factor is;

$$C=A_c/A_t \tag{11}$$

where; A_c = area covered by strands

A_t = total area of the unit cell

C = cover factor

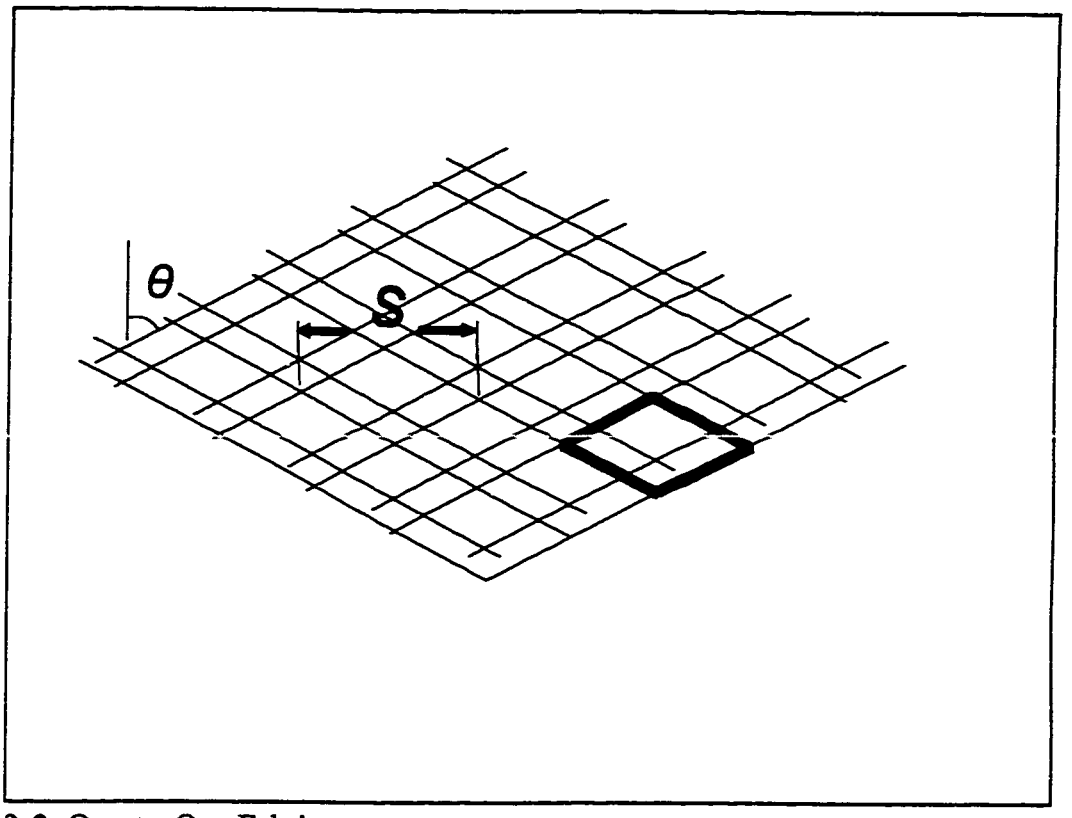

3-2 One-to-One Fabric

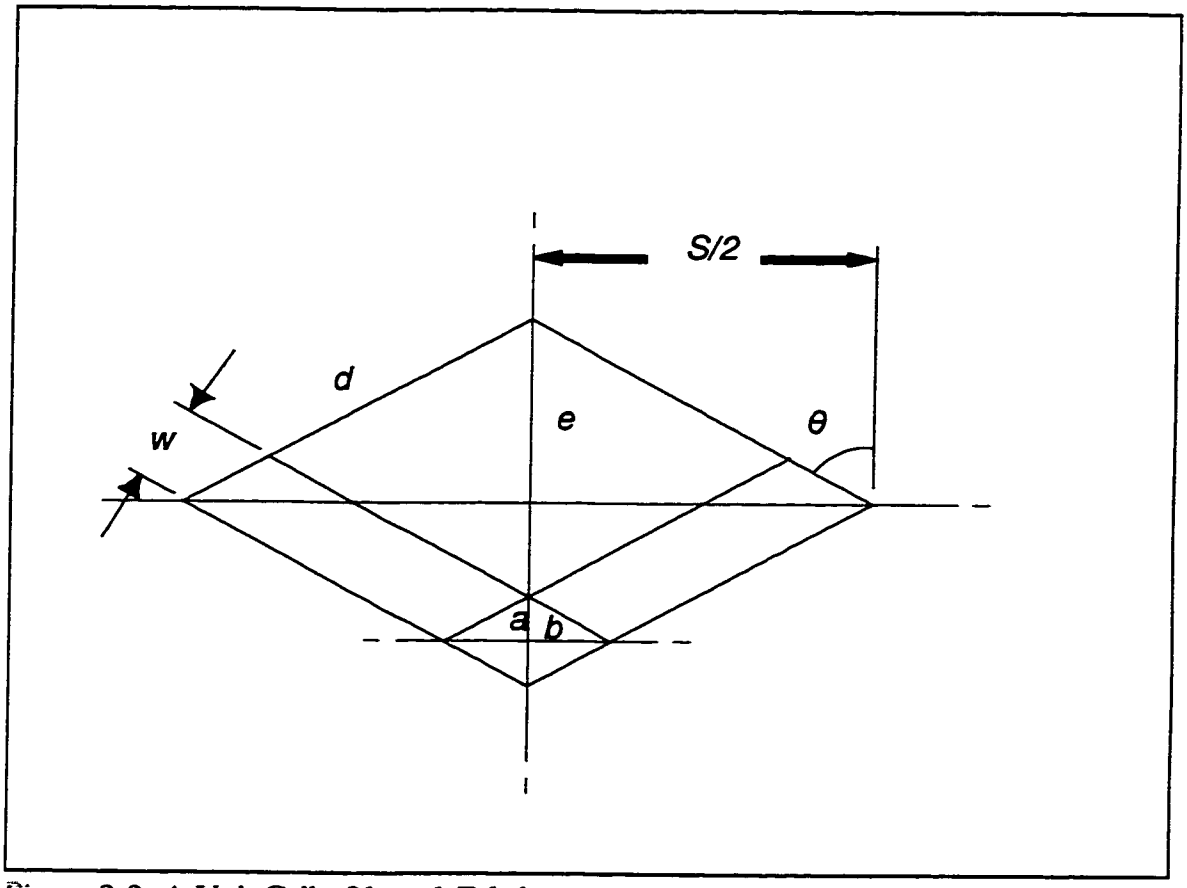

Figure 3-3 A Unit Cell of 1-to-1 Fabric

Note that the width of the unit cell shown in Figure 3-3 is equal to the strand spacing S.

With reference to the figure, A_t is given by;

$$A_t = 4.\frac{1}{2}.\frac{S}{2}.e \tag{12}$$

and;

$$e = \frac{S}{2\tan\theta} \tag{13}$$

Therefore;

$$A_t=\frac{S^2}{2\tan\theta} \tag{14}$$

The covered area, A_c, is the sum of the areas covered by the two strand lengths, 2 A_L, minus the diamond shaped area of overlap, A_D. Again from Figure 3-3 A_L is found to be;

$$A_L=w\ d \tag{15}$$

and;

$$d=\frac{S}{2\ \sin\theta} \tag{16}$$

where; w = width of a strand

Thus;

$$A_L=\frac{w\ S}{2\ \sin\theta} \tag{17}$$

From the figure, A_D is given by;

$$A_D=2\ a\ b \tag{18}$$

where;

$$a=\frac{w}{2\ \sin\theta} \tag{19}$$

and;

$$b=a\ \tan\theta \tag{20}$$

Combining equations 18 to 20 yields;

$$A_D = \frac{w^2}{2 \sin\theta\cos\theta} \tag{21}$$

Thus;

$$A_c = 2 A_L - A_D \tag{22}$$

or;

$$A_c = \frac{w}{\sin\theta} \left[S - \frac{w}{2 \cos\theta} \right] \tag{23}$$

Substituting into equation 11 yields;

$$C = \frac{2 S w \cos\theta - w^2}{S^2 \cos^2\theta} \tag{24}$$

This formula is used in this thesis whenever calculating the cover factor. Pastore and Ko's formula is given as follows;

$$C = \frac{2 x w \cos\theta - w^2}{x^2 \cos^2\theta} \tag{25}$$

where; x = 'unit cell width' = $2 \pi r / N$ (for circular cylindrical mandrel)

N = 'number of carriers on machine'

For a circular cylindrical mandrel, equation 4 for the distance S was developed herein. Inspection of equations 4, 24, and 25 shows that Pastore and Ko's formula for C is the same as that derived herein except that their 'N' should be specified to be the number of

'same-direction' carriers on the machine (not the total number of carriers on the machine).

For a fabric of 100 % coverage, Ko, Pastore, and Head [8] give θ to be;

$$\theta = \cos^{-1}\frac{N_T\, w}{4\,\pi\, r} \qquad \textbf{(26)}$$

For r = 2 cm, w = .2 cm, N_T =36, this yields; θ = 73.35 deg.

Substituting these four values into equation 24 yields C = 1 , as expected. Substituting the four values into equation 25 yields C = 1 if 'N' is taken as the number of 'same-direction' carriers. If 'N' is taken as the total number of carriers, equation 25 yields C = .0006 , which is incorrect. Thus 'N' should have been declared by Pastore and Ko to be the number of 'same-direction' carriers.

3.2 Jamming Test Formula

When the carrier velocities are increased with respect to the mandrel traverse velocities, higher braid angles result. This "rotates" the strands, hence reducing the gaps in-between them. If rotated sufficiently, the "edges" of the strands come into contact with each other thus producing a 100% cover factor. If rotated more, then the strands bunch up. This condition is known as "jamming". In this condition, equation 24 is no longer valid. Thus before calculating a cover factor, it is necessary to test to ensure that the strands are not jammed. For a given braid angle the strand spacing below which jamming occurs shall

be derived.

Figure 3-4 shows two strands just at the jammed state. From the figure, g is calculated to be;

$$g=\frac{w}{\cos\theta} \tag{27}$$

where g is defined in the figure

and w is strand width

Jamming occurs when the strand spacing, S, falls below g. Therefore, jamming occurs for;

$$S < \frac{w}{\cos\theta} \tag{28}$$

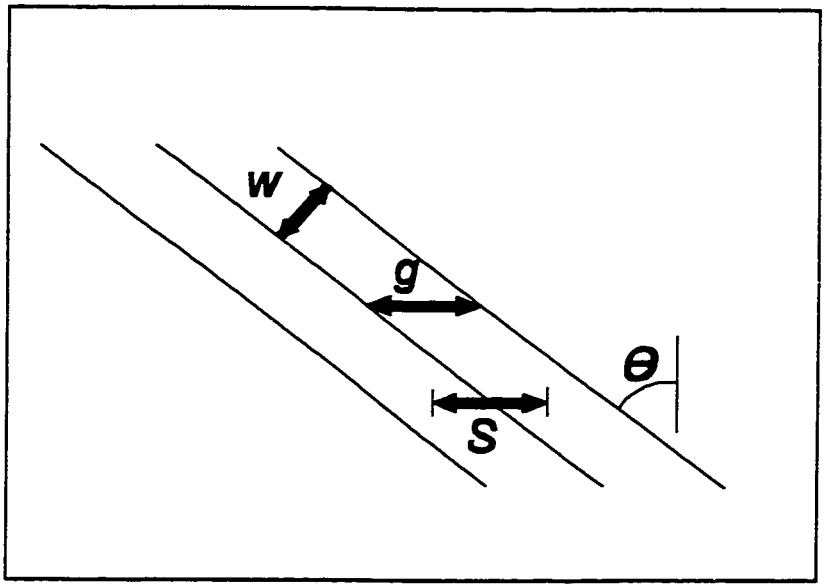

3-4 Strand Spacing When Jammed

CHAPTER 4

CONFIGURATION PROPERTIES FOR PREFORMS WITH CONSTANT ELLIPTICAL CROSS-SECTIONS

4.1 Introduction

In this chapter, formulae and an algorithm are developed for the configuration properties for fabrics formed by 2D braiding on a mandrel with a constant elliptical cross-section along the length of the mandrel under a steady state condition.

During braiding, each strand runs from a carrier to a "contact point" on the mandrel. The "curve" formed by this set of points is referred to herein as the contact ring.

The assumptions of this analysis are;

- the absence of a formation ring
- the strand stays on the mandrel where it is put, ie. it does not slide on the surface.
- the strands constrain each other to a planar contact ring.
- the strand is in a straight line between the carrier and the mandrel

How strands affect each other during braiding is currently unknown. The assumption that the strands are straight between the carrier and the mandrel may not be true. However this analysis still provides a first step in studying the process.

The "contact distance" is the longitudinal distance from the carriers to the contact ring. The planar contact ring assumption and the steady state consideration dictate that the contact distance is constant for this analysis.

The formulae for strand spacing and braid angle for this situation will now be derived for a given point on the mandrel surface. These configuration properties will vary from the top to the side of the mandrel; however, they remain constant longitudinally, as the process was presumed steady state. The formula for cover factor, equation 24, is based on braid

angle and strand spacing and was derived in Chapter 3.

4.2 Derivation of Strand Spacing

Figure 4-1a shows a strand being placed on a mandrel of constant cross section. Line 6-2 represents the strand. The configuration properties will now be derived for point 6, whose co-ordinates are known.

Figure 4-1b shows strand 6-2 and the adjacent strand at a general instant in time during the process. Points 2 and 3 represent carriers. The strand spacing is the distance between the contact points of two adjacent strands. The strand stays where it is placed; therefore, the spacing between the two contact points during the process is equal to the spacing between the two strands at that point in the finished fabric.

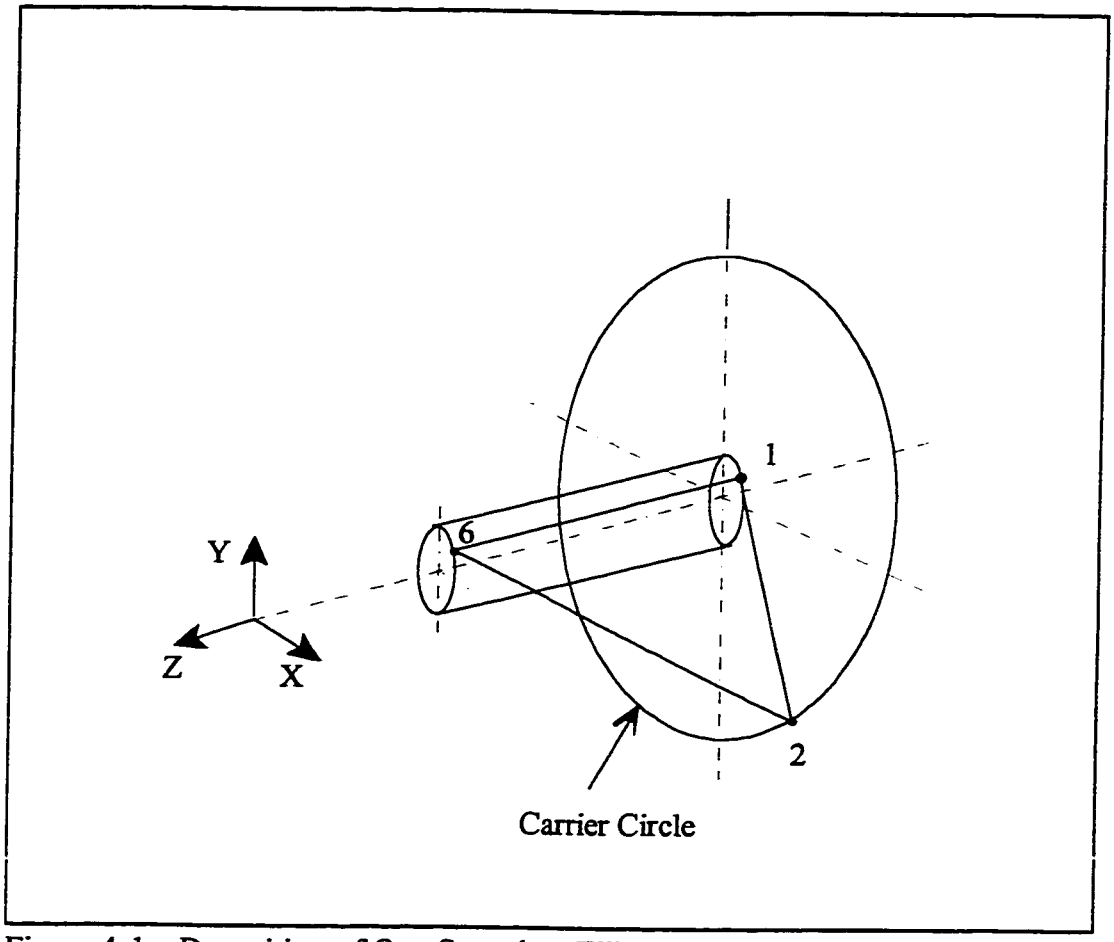

Figure 4-1a Deposition of One Strand on Elliptical Mandrel

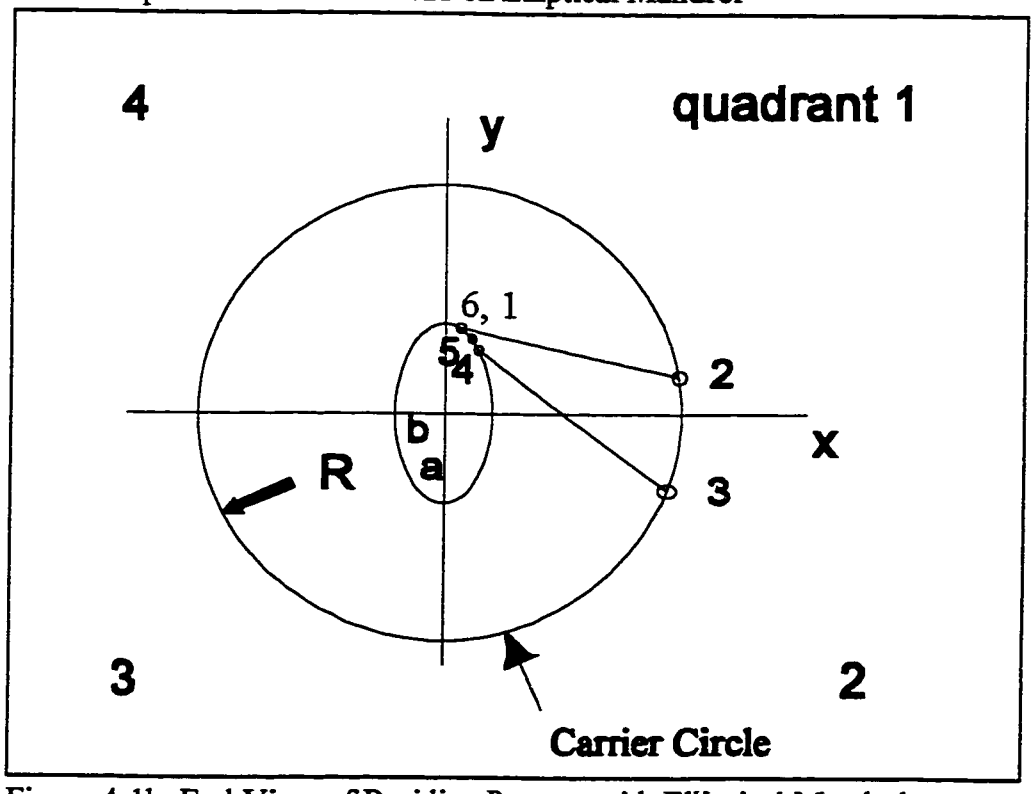

Figure 4-1b End View of Braiding Process with Elliptical Mandrel

The calculated strand spacing is for the mid-point, point 5, located between the contact points. Thus the mid-point must be found in order to have a point and a property at that point. An algorithm will be developed, which finds strand spacings at many points (ie. mid-points). Strand spacings at other points can then be found by interpolation from the results.

When a strand is wrapped around an object the portion of the strand between the carrier and the mandrel always remains tangent to the surface of the object at the point of contact. Therefore this portion of the strand is within a plane, 1-2-6, tangent to the mandrel at point 6. Line 6-1 is defined as the intersection of the tangent plane and the mandrel surface. Point 1 is where this line intersects the carrier circle plane.

The first step of the analysis is to find the carrier, point 2. This will be done by intersecting line 1-2 with the carrier circle. Before this, the equation of line 1-2 must be found. This equation is determined because x1 = x6 , y1 = y6 , and line 1-2 has the same slope as the ellipse at point 1. For an ellipse;

$$\frac{x^2}{b^2} + \frac{y^2}{a^2} = 1$$

Therefore;

$$y = \pm a\sqrt{1 - \frac{x^2}{b^2}}$$

And;

$$\frac{dy}{dx} = \pm \frac{ax}{b\sqrt{b^2 - x^2}}$$

Therefore, line 1-2 has the slope;

$$M = e_2 \frac{ax_1}{b\sqrt{b^2 - x_1^2}} \tag{4}$$

where $e_2 = \pm 1$

The value of e_2 depends on which quadrant point 1 is in. From the figure the following table is found;

quadrant	1	2	3	4
e_2	-1	1	1	-1

Also ;

$$y_1 = e_1 a \sqrt{1 - \frac{x_1^2}{b^2}} \tag{5}$$

And from the figure, for quadrants 1, 2, 3, and 4, e_1 is given respectively by 1, -1, -1, and 1.

Let line 1-2 be;

$$y = Mx + B \tag{6}$$

Point 1 is on the line. Substituting in x_1, y_1, and M, and noting that $e_2 = -e_1$, yields B;

$$B = \frac{e_1 ab}{\sqrt{b^2 - x_1^2}} \tag{7}$$

M is already known, thus line 1-2 is now determined. To find point 2, this line is intersected with the circle;

$$x^2 + y^2 = R^2 \tag{8}$$

where R = radius from centre-line to carriers

This yields;

$$x_2 = \frac{-MB + e_3\sqrt{R^2(1+M^2) - B^2}}{(1 + M^2)} \tag{9}$$

where $e_3 = \pm 1$

x_2 has two possible values because the line intersects the circle in two places. Given the quadrant of point 1, examining the figure shows whether the larger x_2 value is that desired

or the smaller value. Thus e_3 can be determined. Doing so yields, for quadrants 1, 2, 3, and 4, e_3 values of 1, -1, -1, and 1 respectively.

Substituting into equation 31 yields y_2;

$$y_2 = Mx_2 + B \tag{10}$$

Point 3 can now be found. All of the same-direction carriers always remain a certain angular distance apart from each other. This angle is called φ. The angle φ is given by;

$$\varphi = \frac{2\pi}{N_s} \tag{11}$$

where N_s is the number of same-direction carriers on the braiding machine.

Clearly the polar co-ordinates of point 2 are;

$$r_2 = R \tag{12}$$

and;

$$\gamma_2 = \tan_s^{-1} y_2/x_2 \tag{13}$$

where γ is defined counter-clockwise and $\tan_s^{-1}$ is the angle resulting from $\tan^{-1}$, with the sign corrected also (based on the signs of y and x).

Point 3 equals point 2 rotated about the origin by $-\varphi$, thus;

$$r_3 = R \tag{14}$$

and;

$$\gamma_3 = \gamma_2 - \varphi \tag{15}$$

Therefore;

$$x_3 = R \cos \left[\tan_s^{-1} \frac{y_2}{x_2} - \varphi \right] \tag{16}$$

and;

$$y_3 = R \sin \left[\tan_s^{-1} \frac{y_2}{x_2} - \varphi \right] \tag{17}$$

To find point 4 line 3-4 will be intersected with the ellipse. Line 3-4 will be found next;

$$y = M^1 x + B^1 \tag{18}$$

The slope, M^1, is the slope of the ellipse at point 4, therefore;

$$M^1 = e_6 \frac{a x_4}{b \sqrt{b^2 - x_4^2}} \tag{19}$$

where $e_6 = \pm 1$

The sign of the slope depends on which quadrant point 4 is in. From the figure, for quadrants 1, 2, 3, and 4, e_6 is given respectively by -1, 1, 1, -1.

Also, point 3 is on line 3-4, thus the line's equation is;

$$y = M^1(x - x_3) + y_3 \tag{20}$$

The equation of the ellipse portion to be intersected is;

$$y = e_5 \frac{a}{b} \sqrt{b^2 - x^2} \tag{21}$$

where $e_5 = \pm 1$

The value of e_5 depends on which quadrant point 4 is in. From the figure, for quadrants 1, 2, 3, and 4, e_5 is given respectively by -1, 1, 1, -1.

Note however that as x_4 is unknown, e_5 and e_6 are still unknowns. Point 4 is the intersection of these two equations. Therefore, combining these equations, yields;

$$e_5 \frac{a}{b} \sqrt{b^2 - x_4^2} = e_6 \frac{a\, x_4}{b\sqrt{b^2 - x_4^2}} (x_4 - x_3) + y_3 \tag{22}$$

Solving for x_4 and reducing yields;

$$e_5 a\ (b^2 - x_4^2) - e_6\ a\ x_4\ (x_4 - x_3) = y_3 b \sqrt{b^2 - x_4^2} \tag{23}$$

It is seen from the tables for e_5 and e_6, that e_6 always equals $-e_5$. This yields;

$$e_5(\ a(b^2 - x_4^2) + a x_4 (x_4 - x_3)) = y_3 b \sqrt{b^2 - x_4^2} \tag{24}$$

Rearranging equation 49 gives;

$$\frac{e_5 a (b^2 - x_4 x_3)}{y_3 b} = \sqrt{b^2 - x_4^2} \tag{25}$$

Noting that $e_5 = \pm 1$, and squaring, yields;

$$\frac{a^2}{y_3^2 b^2}(b^4 - 2b^2 x_4 x_3 + x_4^2 x_3^2) = b^2 - x_4^2 \tag{26}$$

Solving this equation yields;

$$x_4 = \frac{b^2\ (a^2 x_3 + e_7 y_3 \sqrt{b^2 y_3^2 + a^2 x_3^2 - a^2 b^2}\ )}{b^2 y_3^2 + a^2 x_3^2} \tag{27}$$

where $e_7 = \pm 1$

Since equation 50 was squared to give equation 51, equation 51 has two solutions.

However, only one is the correct solution for equation 50. It is therefore necessary to determine which solution (ie. which e_7) is correct. Note that which solution is correct depends on the value of e_5. When e_5 is +1 equation 50 has one solution and when e_5 is -1 it has a different solution. Clearly both solutions will solve equation 51. Thus these two solutions correspond to the two solutions of equation 51.

From equation 46 it is seen that an e_5 of +1 means that the ellipse curve to be intersected with is the upper half of the ellipse and that an e_5 of -1 means that the ellipse curve to be used is the lower half of the ellipse. From Figure 4-1 it is therefore seen that the two solutions of equation 51, ie. of a line through point 3 and tangent to the ellipse, correspond to one line which is tangent to the ellipse, in the upper half, and a second line which is tangent to the ellipse in the lower half. Point 3 is known. Which half of the ellipse is involved (and hence which value of e_5) depends on the location of point 3.

Inspection of the figure reveals that when point 3 is in the upper two quadrants the tangent point wanted is that with the lesser value of x. Thus the correct x_4 value is the lesser of the two possibilities. Thus e_7 is -1. When point 3 is in the lower two quadrants the greater x_4 value is correct. Because y_3 is negative here, this means that e_7 is again -1 (see equation 52). Thus for both cases e_7 is -1. This yields;

$$x_4 = \frac{b^2(a^2x_3 - y_3\sqrt{b^2y_3^2 + a^2x_3^2 - a^2b^2})}{b^2y_3^2 + a^2x_3^2} \qquad \textbf{(28)}$$

Next, for y_4 , as stated;

$$y_4 = e_5 \frac{a}{b} \sqrt{b^2 - x_4^2} \tag{29}$$

Thus e_5 must be determined. As stated previously e_5 is positive if the strand contacts the upper half of the ellipse, and negative if the strand contacts the lower half of the ellipse. On which half the strand contacts the ellipse can be determined from the location of point 3. If point 3 is in quadrant 1 then the upper half is contacted. Rotating point 3 clockwise, entering quadrant 2, the half contacted remains the upper. However, when x_3 decreases below b the half contacted becomes the lower half. For quadrant 3 it remains the lower half. In quadrant 4, when x_3 increases above -b, the half contacted becomes the upper half and remains so until point 3 is back in quadrant 1.

As point 3 is known, e_5 can now be considered a known quantity. After finding point 3 a person could determine e_5 from the figure, as stated above, or a program could do a test on x_3 and y_3 to determine e_5. The test is expressed as follows;

if (x_3<-b or (x_3<b and y_3<o)) then e_5 = -1, (otherwise e_5 = 1).

Thus y_4 is determined by;

$$y_4 = e_5 \frac{a}{b} \sqrt{b^2 - x_4^2} \tag{30}$$

Point 4 is now determined. The strand spacing will be found next. This is the distance along the perimeter arc between points 1 and 4 (see Figure 4-1). For a change in x, dx, there is a corresponding travel along the arc of ds. The change in y is dy which is given by;

$$dy = \frac{dy}{dx} dx \tag{31}$$

ds is equal to;

$$ds = \sqrt{(dx)^2 + (dy)^2} \tag{32}$$

Thus;

$$ds = dx \sqrt{1 + (\frac{dy}{dx})^2} \tag{33}$$

The length of the arc will be the sum of the ds's along the arc, which is;

$$S = \sum \sqrt{1 + (\frac{dy}{dx})^2 \, dx} \tag{34}$$

$$S = \int_{x1}^{x4} \sqrt{1 + [\frac{dy}{dx}]^2} \, dx \tag{35}$$

Substituting in dy/dx for an ellipse (equation 32) yields;

$$S = \int_{x1}^{x4} \sqrt{1 + \frac{a^2x^2}{b^2(b^2-x^2)}}\, dx \tag{36}$$

This is the strand spacing. The analytical equation for this integral could not be found in Spiegel [9], Abramowitz and Stegun [10], nor CRC Handbook of Chemistry and Physics [11]. Thus a geometrical approximation is used. The arc is approximated with a straight line.

Therefore, the strand spacing, S, is;

$$S = \sqrt{(y_4-y_1)^2 + (x_4-x_1)^2} \tag{37}$$

The braid angle is also required for this region. As stated previously, the strand spacing applies to the mid-point of the arc. Thus the braid angle is required at this point also. Thus it is necessary to find this point. The point is located on the arc, displaced by one half of the strand spacing (clockwise) from point 1. Thus, again, equation 61 could be used where S is known in this case or a geometrical approximation can be used, as is done herein.

Figure 4-2 shows a straight line from point 1 to point 4. A second line perpendicularly bisecting this line will intersect the ellipse arc at a point very close to its mid-point. This will be taken as the mid-point.

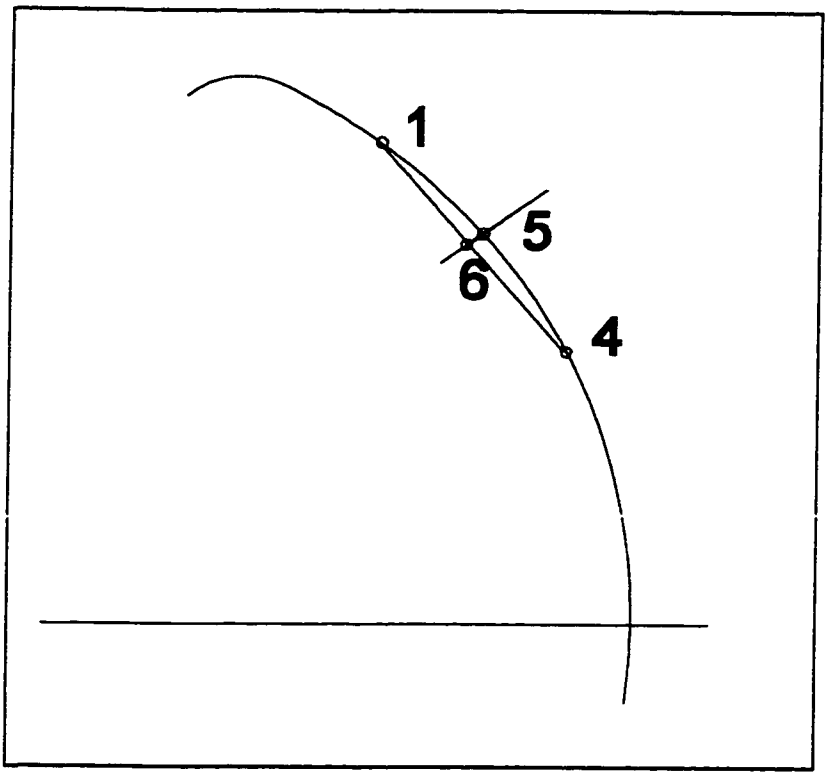

Figure 4-2 Approximation of Mid-point Between Strands

The slope of line 1-4 is;

$$M_{14} = \frac{y_4 - y_1}{x_4 - x_1} \tag{38}$$

From basic geometry the slope of line 6-5 is then;

$$M_{65} = -\frac{1}{M_{14}} \tag{39}$$

$$M_{65} = \frac{x_1 - x_4}{y_4 - y_1} \tag{40}$$

The centre of line 1-4 is;

$$x_6 = \frac{x_4 + x_1}{2} \tag{41}$$

$$y_6 = \frac{y_4 + y_1}{2} \tag{42}$$

Therefore the equation of line 6-5 is;

$$y = M_{65}\,(x - x_6) + y_6 \tag{43}$$

For point 5, this is intersected with the ellipse arc;

$$y = e_8 \frac{a}{b} \sqrt{b^2 - x^2} \tag{44}$$

where $e_8 = \pm 1$

Combining and solving yields;

$$x_5 = \frac{M_{65}^2 x_6 - M_{65} y_6 + e_9 \frac{a}{b} \sqrt{a^2 - M_{65}^2 x_6^2 + 2M_{65} y_6 x_6 - y_6^2 + l}}{\frac{a^2}{b^2} + M_{65}^2} \tag{45}$$

where $e_9 = \pm 1$

The two solutions correspond to the two intersections with the ellipse. It can be seen from the figure that when x_6 (equation 66) is positive, the greater solution for x_5 is the appropriate one, thus for this case $e_9 = +1$. When x_6 is negative, the lesser solution is correct, thus for that case $e_9 = -1$.

The y co-ordinate is;

$$y_5 = M_{65} (x_5 - x_6) + y_6 \tag{46}$$

This gives the "mid-point" to which the properties found apply.

4.3 Derivation of Braid Angle

The braid angle at the mid-point is desired. Figure 4-3 shows the strand laid down in the small region around point 5. By definition;

$$\theta = \tan^{-1} \frac{e}{d} \tag{47}$$

where e and d are as shown in the figure

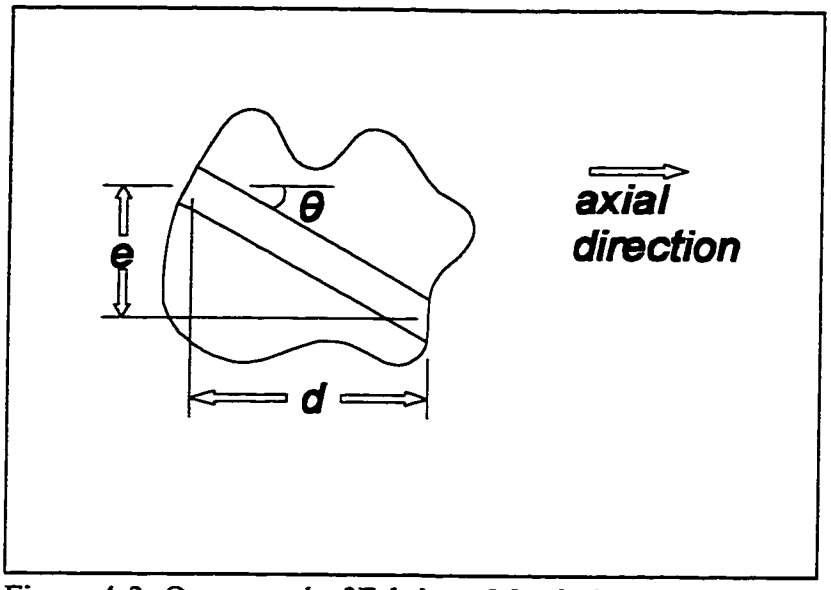

Figure 4-3 One strand of Fabric on Mandrel

As previously assumed, the strand remains on the path that the contact point took across the surface. Therefore e is the distance travelled by the contact point in the circumferential direction around the mandrel surface in a certain small time and d is the distance travelled in the axial direction in the same time. Therefore;

$$\theta = \tan^{-1} \frac{v_c}{v_a} \tag{48}$$

where; v_c = speed of contact point in circumferential direction

v_a = speed of contact point in axial direction

Because the constraint assumed in this Chapter is a planar contact ring (hence a constant contact distance), the axial velocity of the contact point relative to the mandrel surface is equal to the traverse velocity of the mandrel.

$$v_a = v_t \tag{49}$$

where; v_t = traverse velocity of mandrel

Thus it is necessary to find v_c. Figure 4-4 shows the end view of the braiding process, showing a strand passing by point 5. From the figure it can be seen that;

$$v_c = \sqrt{v_x^2 + v_y^2} \tag{50}$$

where; v_x = x component of v_c

v_y = y component of v_c

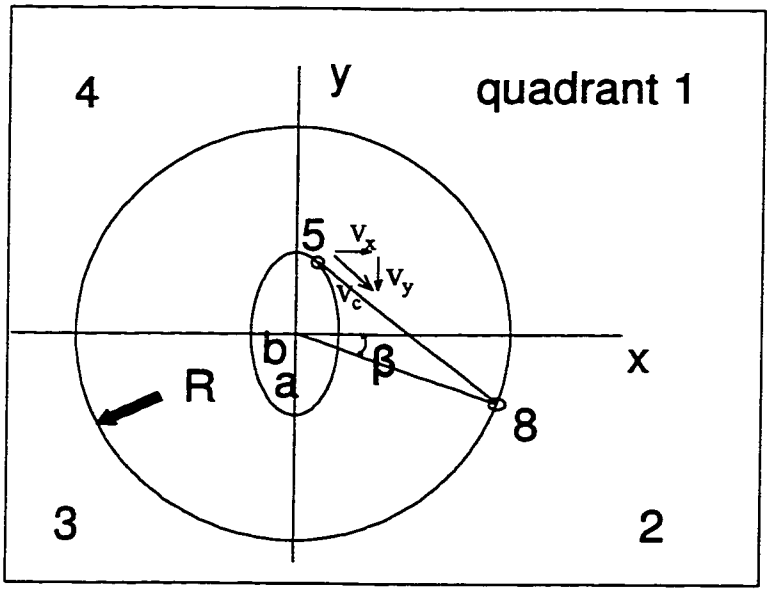

Figure 4-4 Braiding Process, Elliptical Mandrel, End View

v_y is found in terms of v_x;

$$v_y = \frac{dy}{dt} = \frac{dy}{dx}\frac{dx}{dt} = \frac{dy}{dx} v_x \tag{51}$$

Using the previously shown equation for dy/dx yields;

$$v_y = \pm \frac{a\, x_5}{b\sqrt{b^2 - x_5^2}} v_x \tag{52}$$

Thus, from equation 75;

$$v_c = |v_x| \sqrt{1 + \frac{a^2 x_5^2}{b^2(b^2 - x_5^2)}} \tag{53}$$

Thus, to find the braid angle, $|v_x|$ must be found. v_x can be related to ω_c as follows;

$$v_x = \frac{dx_5}{dt} = \frac{dx_5}{d\beta}\frac{d\beta}{dt} = \frac{dx_5}{d\beta}\omega_c = \frac{1}{\frac{d\beta}{dx_5}}\omega_c \tag{54}$$

Therefore;

$$| v_x | = \frac{1}{| \frac{d\beta}{dx_5} |} \omega_c \tag{55}$$

Note that $dx_5/d\beta$ is not used because this a function of β, and β is an unknown. $d\beta/dx_5$ is a function of x_5, a known value, and so it is used instead.

$|d\beta/dx_5|$ is found as follows;

$$\frac{d\beta}{dx_5} = \frac{d\beta}{dx_8}\frac{dx_8}{dx_5} \tag{56}$$

And hence;

$$|\frac{d\beta}{dx_5}| = |\frac{d\beta}{dx_8}| \, |\frac{dx_8}{dx_5}| \tag{57}$$

From Figure 4-4 it is seen that;

$$\beta = e_4 \cos^{-1}\frac{x_8}{R} + f \tag{58}$$

where $e_4 = \pm 1$

and e_4 and f are constants which depend on which quadrant point 8 is in.

Differentiating equation 83 gives;

$$\frac{d\beta}{dx_8} = e_4 \frac{-1}{\sqrt{R^2 - x_8^2}} \tag{59}$$

Therefore;

$$\left|\frac{d\beta}{dx_8}\right| = \frac{1}{\sqrt{R^2 - x_8^2}} \tag{60}$$

dx_8/dx_5 will be found next. Using point 5 and equation 34 yields;

$$x_8 = -MB + e_{12} \frac{\sqrt{R^2(1+M^2) - B^2}}{1 + M^2} \tag{61}$$

where;

$$M = e_{11} \frac{ax_5}{b\sqrt{b^2 - x_5^2}} \tag{62}$$

$$B = \frac{e_{10}ab}{\sqrt{b^2 - x_5^2}} \tag{63}$$

and e_{10}, e_{11}, and e_{12} are taken from the tables for e_1, e_2, and e_3, respectively, based on the location of point 5. Point 8 is the same function of point 5, as point 2 is of point 1.

It can be seen from their tables that $e_2 = -e_1$, and $e_3 = e_1$. Thus $e_{11} = -e_{10}$, and $e_{12} = e_{10}$. Substituting in M and B, and differentiating, yields;

$$\frac{dx_8}{dx_5} = -e_{10}^2 a^2 D - 2e_{10}^2 a^2 x_5^2 D^2 + \frac{e_{10}(R^2(x_5 + x_5^3 D)/b^2 - b^2 xD)}{C(1/(e_{10}^2 a^2 D) + x^2/b^2)} - \frac{2e_{10}^3 a^2 (x_5 + x_5^3 D)C}{(b/B + e_{10}^2 a^2 x_5^2/b)^2} \tag{89}$$

where;

$$D = \frac{1}{b^2 - x_5^2} \tag{90}$$

$$C = \sqrt{R^2 \left(1 + \frac{e_{10}^2 a^2 x_5^2 D}{b^2} \right) - e_{10}^2 a^2 b^2 D} \qquad (91)$$

Taking the absolute value of this, $| dx_8 / dx_5 |$ and $| d\beta / dx_8 |$ are determined, and hence $| d\beta/dx_5 |$ is determined.

In summary, the braid angle at point 5 is;

$$\theta = \tan^{-1} \frac{v_c}{v_a}$$

where v_c and v_a are determined using equations 74 to 91.

4.4 Algorithm

This section presents an algorithm which constructs a table containing a set of points on the mandrel surface (ie. around the ellipse) and gives the fabric properties at each point. The table only contains points on the right half of the ellipse (see Figure 4-1) as symmetry then determines the other half. Also, due to symmetry, only the strands of clockwise direction are considered.

The cover factor is determined by the braid angle and strand spacing of two opposing sets of strands. The algorithm calculates it based on only one set and assumes that the other set has the same braid angle and strand spacing.

Figure 4-5 presents the algorithm. In the flow chart, "calculate" means calculate using the equations developed in this chapter.

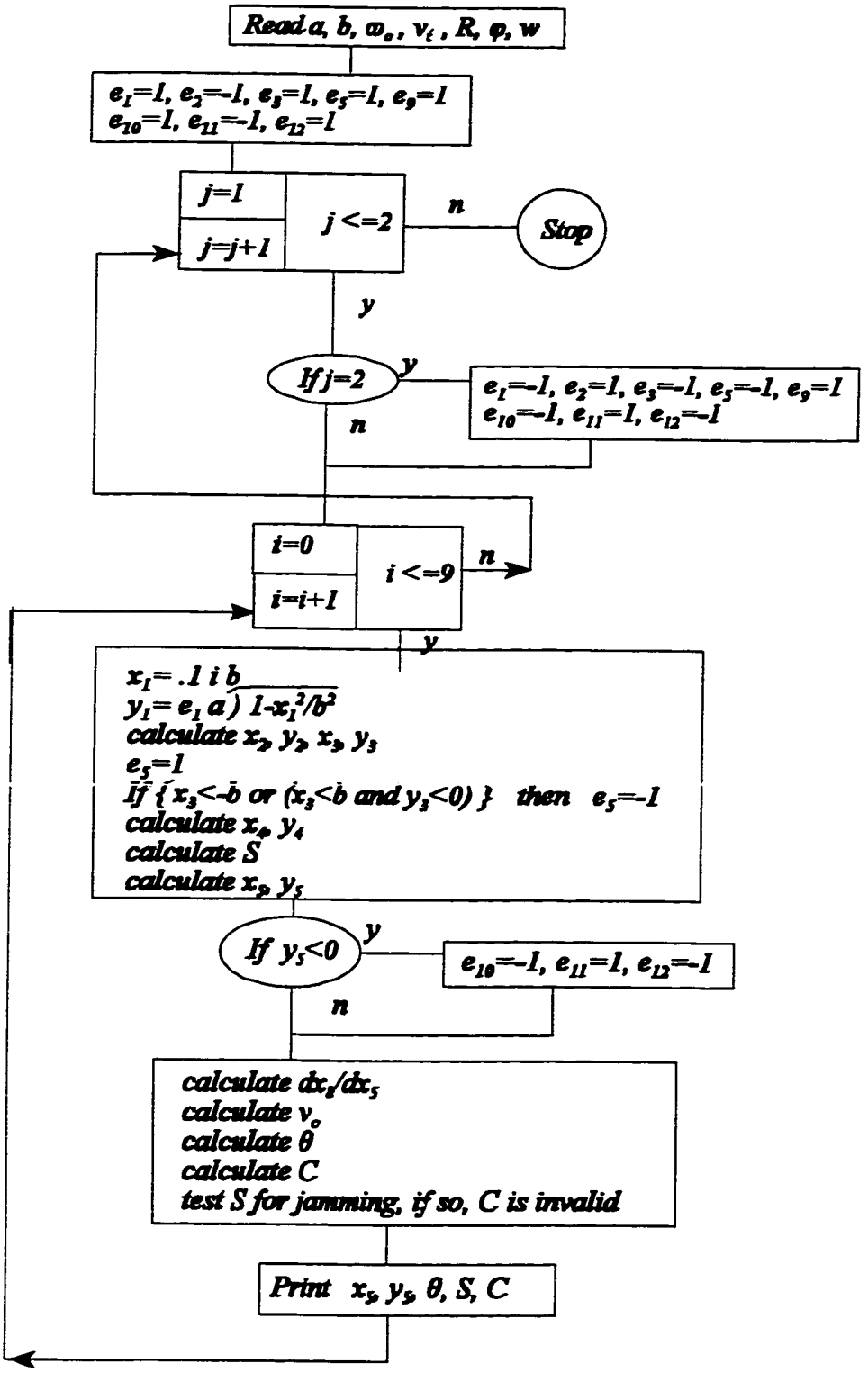

Figure 4-5 Algorithm 1

CHAPTER 5

CONFIGURATION PROPERTIES FOR ELLIPTICAL CROSS-SECTION PREFORMS WITH CROSS-SECTION SIZE VARYING ALONG LENGTH

5.1 Algorithm 2 Analysis

This chapter presents a model of braiding onto an elliptical section mandrel with cross-section size varying along the mandrel under transient or steady state conditions. An algorithm, Algorithm 2, is developed which generates a table of representative points over the surface of the mandrel and the configuration properties at those points.

In this case a planar contact ring and a constant contact distance will not be assumed. It will be assumed that a strand is laid down without any influence or interference by other strands. This different assumption is made in order to permit the analysis of mandrels with a section size that varies along its length and also both transient and steady states.

The other assumptions of this analysis are as before, namely, the absence of a forming ring and that the strand does not slide on the surface of the mandrel.

The algorithm will find the path on which each strand lies, on the mandrel surface. Clearly an algorithm is first needed which will find the path that one strand lies on. As stated before, the final path is equal to the path on the surface over which the strand contact point travels. Thus this "contact" path will be determined.

The algorithm will be given the initial x, y, z co-ordinates of the contact point at the starting end of the mandrel using a co-ordinate system on the mandrel surface. It then

uses a time step, dt, in finding the new location to where the contact point has moved, ie. the next contact point. It will then consider the next time step, dt, and find the next contact point. It will continue until the end of the mandrel is reached.

Clearly the formulae to obtain the next contact point when given a current contact point and a time step are needed.

5.1.1 Point-To-Point Analysis

Figures 5-1 and 5-2 show the process at a general instant in time. The mandrel is shown in Figure 5-1. Point 1 is an arbitrary point on the mandrel, the current contact point. The elliptical cone shape shown in Figure 5-2 is defined to be the cone which is tangent to the mandrel surface at z_1. Line 1-3 represents the strand, which is tangent to the mandrel surface at point 1. Figure 5-3 shows the portion of mandrel traversed over by the contact point during the time dt. Again, point 1 is the "current" contact point, the same as point 1 in Figure 5-2. Point 5 is the point that the contact point travels to, ie. the "next" contact point. Thus it is desired to find point 5.

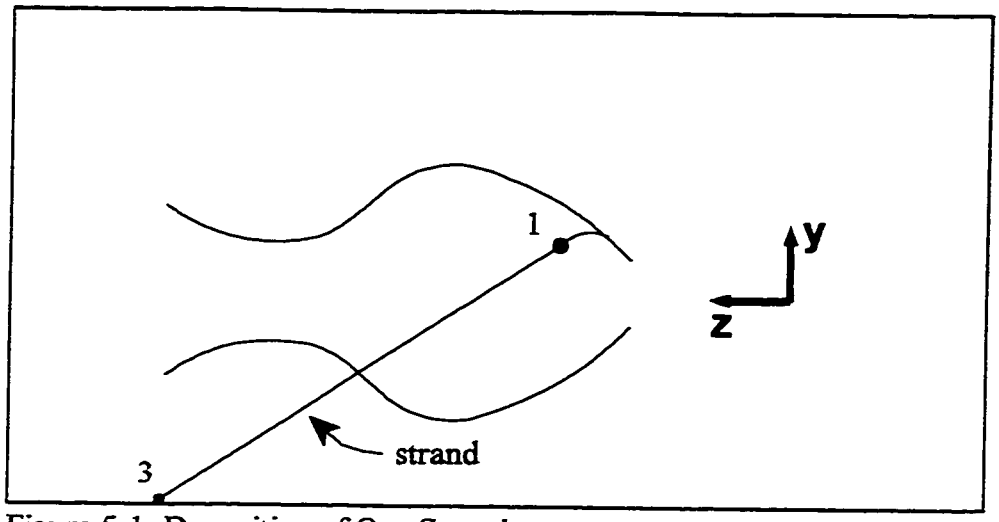

Figure 5-1 Deposition of One Strand

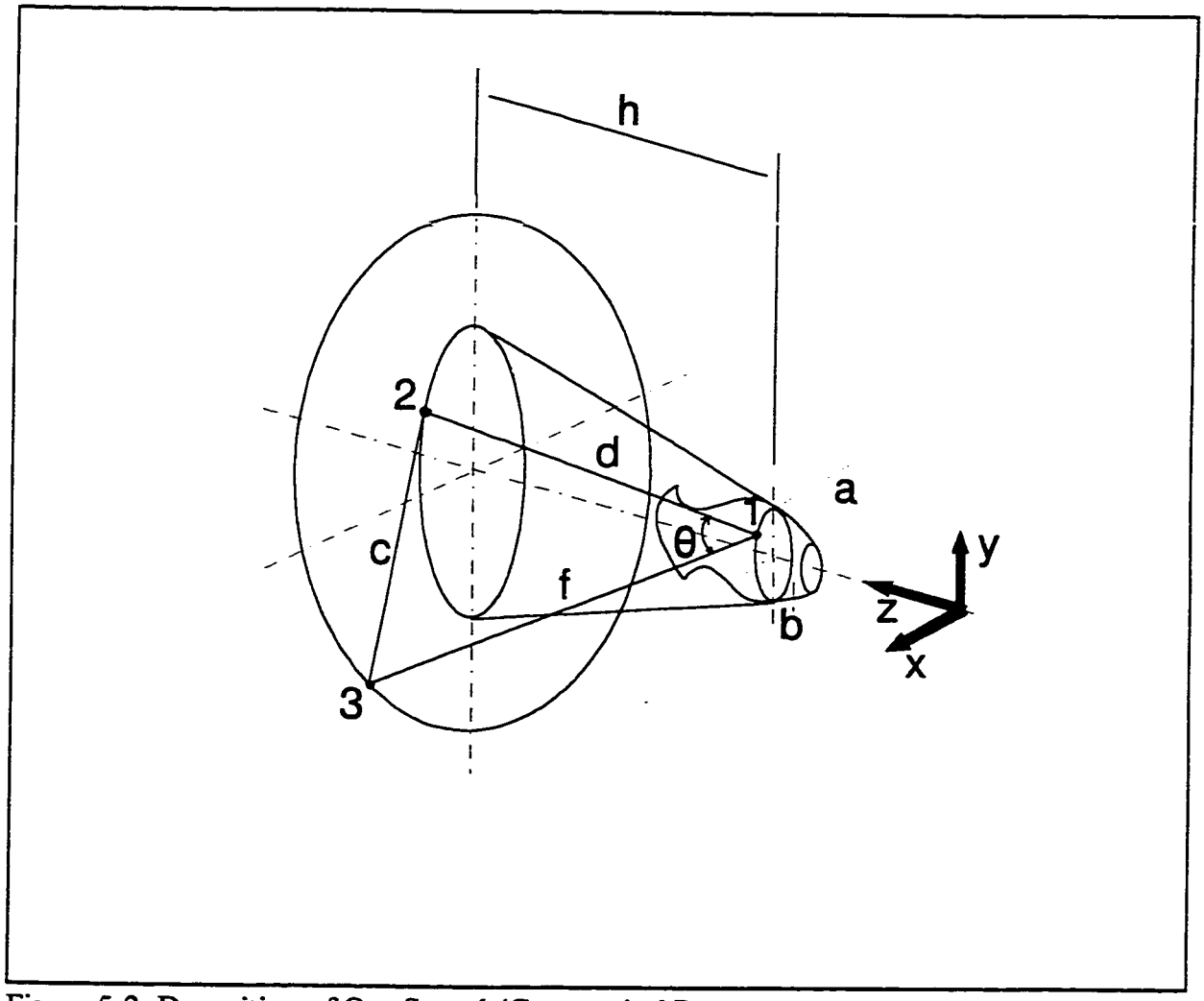

Figure 5-2 Deposition of One Strand (Geometrical Parameters)

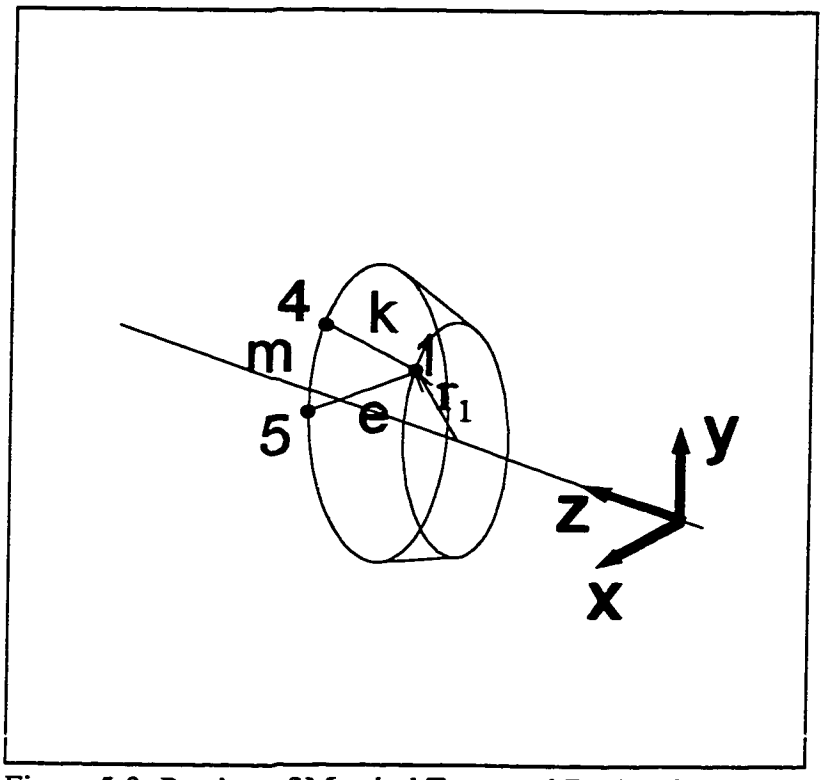

Figure 5-3 Portion of Mandrel Traversed During dt

The method of finding point 5 presented herein involves first finding dz and then using it to calculate point 5.

Thus dz will be found (the z-direction travel of the contact point over the time period dt). Line f (Figure 5-2) represents the strand. It is, due to the process, tangent to the tangent cone. There is a plane containing line f, and tangent to the tangent cone. The intersection of this plane and the tangent cone will be called line d. It is seen that the triangle 1-2-3 is tangent to the tangent cone. As the strand portion just laid down is in the same direction as

the taut strand, the braid angle is given by the angle 2-1-3.

In Figure 5-3, line k is the line where a plane tangent to the tangent cone and containing point 1, touches the tangent cone. In other words, line k is a small part of line d. Line e is where the strand lies; therefore, by definition, angle 4-1-5 is the braid angle.

Thus line k is collinear with line d, and line e is collinear with line f. Lines d and f intersect a plane perpendicular to z to give points 2 and 3, and lines k and e intersect a perpendicular plane to give points 4 and 5. Therefore, triangle 1-4-5 is similar to triangle 1-2-3. Hence ;

$$\frac{d}{c} = \frac{k}{m} \tag{92}$$

It will be seen that all of these lengths can be found in terms of dz. Solving the equation will then yield dz. Thus these quantities will be found in terms of dz.

Before d can be calculated, it is necessary to define a term "G". G will be the growth rate of the mandrel section size at the location on the mandrel, z.

That is, G is a function of z, defined as follows;

$$G = \frac{\frac{dr}{dz}}{r} \tag{93}$$

where r is any dimension of the mandrel section, such as the major axis of the ellipse, or the distance from the centre to the point at 45° on the ellipse.

For a given dimension then, G is the change in that dimension for a change in z, as a fraction of the original dimension. Thus for the case of this analysis, at any distance z, G is the same for any defined dimension (eg. major axis) of the section.

Because the ellipse major-axis is a known function of z (the mandrel shape is given), G will hereafter be considered a known value.

If r increases linearly with z, then;

$$G = \frac{r_2 - r_1}{(z_2 - z_1)\, r_1} \tag{94}$$

Rearranging;

$$r_2 - r_1 = G(z_2 - z_1)\, r_1 \tag{95}$$

And;

$$r_2 = (G(z_2 - z_1) + 1)\, r_1 \tag{96}$$

Now d will be determined. r_1 will be defined as the distance from the z-axis to point 1, and r_2 as the distance from the z-axis to point 2. From equation 95 ;

$$(r_2 - r_1) = G(z_2 - z_1)\, r_1 \tag{97}$$

Thus;

$$(r_2 - r_1) = G\, h\, r_1 \tag{98}$$

From Figure 5-2 and Pythagoras's Theorem, it is seen that;

$$d = \sqrt{h^2 + (r_2 - r_1)^2} \tag{99}$$

Thus;

$$d = \sqrt{h^2 + G^2 h^2 r_1^2} \tag{100}$$

$$d = h\sqrt{1 + G^2 r_1^2} \tag{101}$$

To proceed with equation 92, it is necessary to find c. From Figure 5-2, it is seen that;

$$c = \sqrt{(x_3 - x_2)^2 + (y_3 - y_2)^2} \tag{102}$$

Thus x_2, y_2, x_3, and y_3 are needed. From equation 96 and Figure 5-2, it is found;

$$x_2 = (Gh + 1)\, x_1 \tag{103}$$

$$y_2 = (Gh + 1)\, y_1 \tag{104}$$

Point 3 is the intersection of the line tangent to the ellipse at point 2, and the carrier circle. Thus point 3 is derived from point 2, in the same way that point 2 of Chapter 4 is derived from point 1, in Chapter 4. From equation 34, thus;

$$x_3 = \frac{-MB + e_3 \sqrt{R^2(1+M^2) - B^2}}{(1 + M^2)} \tag{105}$$

where;

$$M = e_2 \frac{a\, x_2}{b\sqrt{b^2 - x_2^2}} \tag{106}$$

and;

$$B = \frac{e_1 ab}{\sqrt{b^2 - x_2^2}} \tag{107}$$

and e_1, e_2 and e_3 are from their tables in Chapter 4, based on the quadrant of point 2.

And from equation 31;

$$y_3 = Mx_3 + B \tag{108}$$

Thus c is now 'known'.

k will be determined next. From Figure 5-3, and Pythagorus's Theorem;

$$k = \sqrt{(dz)^2 + (r_4 - r_1)^2} \tag{109}$$

Also;

$$r_4 - r_1 = G\ dz\ r_1 \tag{110}$$

Thus;

$$k = dz\sqrt{1 + G^2 r_1^2} \tag{111}$$

It is next necessary to find m. From Figure 5-3, it is seen;

$$m = \sqrt{(x_5 - x_4)^2 + (y_5 - y_4)^2} \tag{112}$$

From equation 96 and Figure 5-3;

$$x_4 = (G\ dz + 1)x_1 \tag{113}$$

$$y_4 = (G\ dz + 1)y_1 \tag{114}$$

Values of x_5 and y_5 are needed next. During dt the strand carrier moves about on the carrier circle by an amount dß. Also, $d\beta = \omega_c\, dt$, thus dß is a known value. Thus before the time step, a strand runs from a carrier to a point tangent to the mandrel ellipse. Then, after the time step, the strand runs from a point shifted by dß on the carrier ring to a new point tangent to the mandrel ellipse. The displacement which occurs for such a tangent point, corresponding to an angular displacement of a carrier point has already been developed in Chapter 4. There it is the strand spacing for carriers spaced apart by φ. These equations will be used to determine x_5 and y_5.

Equations 29 to 55 determine point 4 (of Chapter 4). Using the ellipse at z_1, and substituting in point 1 of this chapter results in an x_4 and y_4 (of Chapter 4) given by equations 53 and 55.

This point is exactly where point 5 would be if the ellipse size was not changing. If the ellipse is growing then x_5 and y_5 will be very slightly larger than these values, due to the ellipse's expansion. However, as smaller dz's are chosen this error drops to zero, thus giving excellent approximations of x_5 and y_5. Thus these values will be used for x_5 and y_5 in solving equation 92 for dz.

Equations 53 and 55 are based on variables x_3 and y_3, etc. which are developed in Chapter 4. Therefore the final result is not given in the form of one equation, but in the form of many. Thus all of these equations are not repeated here, because the only change to them

is that x_4, y_4 should be replaced with x_5, y_5.

Thus x_5, y_5, and m are now known values. It is now possible to substitute in all the variables of equation 92 and solve it for dz. Inspection reveals, however, that this is a very high order equation, hence yielding many solutions for dz. A method of selecting the proper dz value has not been revealed. Therefore a very slight approximation will be made. x_4 and y_4 are given from before by;

$$x_4 = (G\ dz + 1)\ x_1 \tag{115}$$

$$y_4 = (G\ dz + 1)\ y_1 \tag{116}$$

Because dz is infinitesimally small, G dz + 1 is approximately 1. Thus in solving for dz, it will be presumed;

$$x_4 = x_1 \tag{117}$$

$$y_4 = y_1 \tag{118}$$

Now substituting variables into equation 92 yields an equation where dz occurs only once. Substitution yields;

$$\frac{h\sqrt{1 + G^2 r_1^2}}{\sqrt{(x_3-x_2)^2+(y_3-y_2)^2}} = \frac{dz\sqrt{1 + G^2 r_1^2}}{\sqrt{(x_5-x_4)^2+(y_5-y_4)^2}} \quad \textbf{(119)}$$

where x_2, y_2, x_3, y_3, x_4, y_4, x_5, y_5 are as derived above.

Reduction and re-arrangement gives;

$$dz = \frac{h\sqrt{(x_5-x_4)^2+(y_5-y_4)^2}}{\sqrt{(x_3-x_2)^2+(y_3-y_2)^2}} \quad \textbf{(120)}$$

Thus dz is now a known value. This value will now be used to find point 5, the next contact point. Clearly;

$$z_5 = z_1 + dz \quad \textbf{(121)}$$

x_5 and y_5 were determined approximately, but the slight increase in ellipse size was not accounted for. The found x_5, y_5 is a point on an ellipse of the size of the ellipse at z_1. Point 5 should be on an ellipse at $z = z_1 + dz$. Therefore the approximation will be improved by increasing the co-ordinates by the percentage increase of the ellipse. This yields;

$$x_5 = (G\ dz + 1)\ x_5(\textit{found previously}) \quad \textbf{(122)}$$

$$y_5 = (G\ dz + 1)\ y_5\ (\textit{found previously}) \quad \textbf{(123)}$$

Thus the next contact point has been determined.

This point can now be used to find the next contact point after it. In an algorithm, x_1, y_1, z_1 are next assigned these values and then the same set of equations is used again for the next iteration. Note also, however, that during the time dt, h has changed. Therefore, h must be updated before doing the next analysis. Because the strand has moved up the mandrel by dz, h has decreased by dz. However, also, because the mandrel has moved away by v_t dt, h has increased by this amount. With "n" for new and and "o" for old, this yields;

$$h_n = h_o - dz + v_t\, dt \tag{124}$$

5.1.2 Calculation Of Braid Angle

After repeating the process several times, a set of points is obtained representing the path on which the strand lies, on the mandrel surface. During the calculations at each point, the braid angle can be found.

The braid angle at point 1 will be derived (see Figure 5-3). As stated, angle 4-1-5 equals the braid angle. The angle is given by the formula for an angle in a triangle, which is;

$$\theta = \cos^{-1} \frac{k^2+e^2-m^2}{2\,k\,e} \tag{125}$$

Lengths k and m are given in the previous section, and e is clearly;

$$e = \sqrt{(x_5-x_1)^2+(y_5-y_1)^2 + dz^2} \tag{126}$$

where the parameters are given in the previous section.

5.1.3 Calculation Of Strand Spacing

As stated, the algorithm will calculate a set of path points for several strands. The strand spacing will be found at each path point. To calculate a strand spacing, a strand's path points and the path points of the adjacent strand must be used. Figure 5-4 shows three such points.

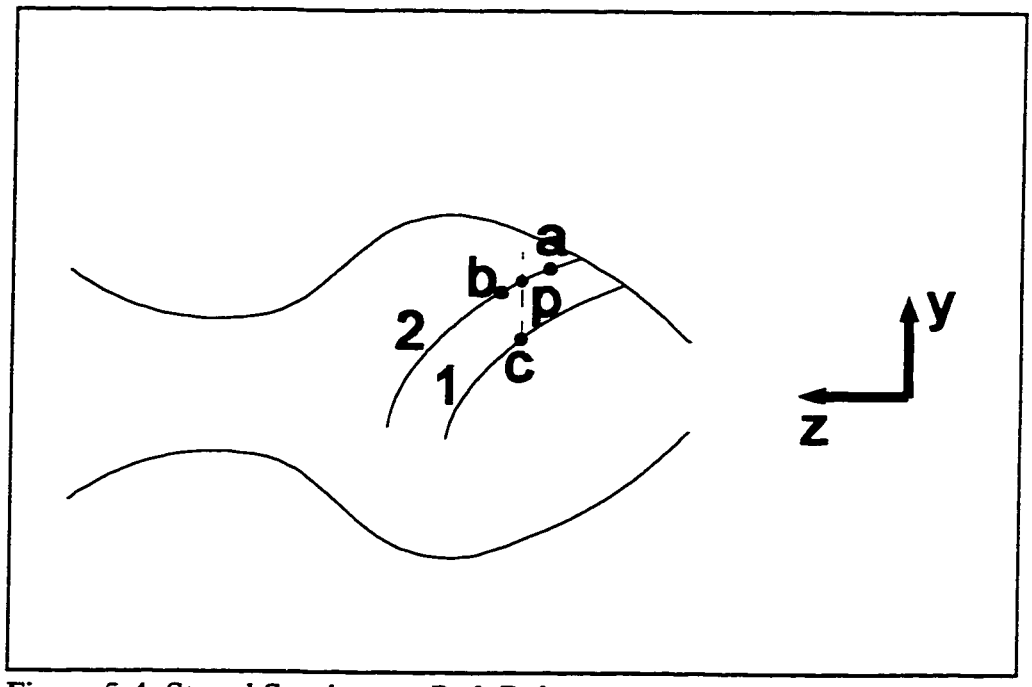

Figure 5-4 Strand Spacing at a Path Point

The strand spacing at path point c, between the two strands, will be found. Points a, b, and c are path points. Point p is defined as the point on strand 2 with the same z value as point c. Thus the strand spacing is the distance between points c and p. Point p will be found by interpolating between points a and b. This yields;

$$x_p = x_a + \frac{z_c - z_a}{z_b - z_a}(x_b - x_a) \tag{127}$$

and;

$$y_p = y_a + \frac{z_c - z_a}{z_b - z_a}(y_b - y_a) \tag{128}$$

Thus the strand spacing is;

$$S = \sqrt{(x_p - x_c)^2 + (y_p - y_c)^2} \quad (129)$$

5.2 Algorithm 2 Flow Chart

As stated, the algorithm finds the path that each strand lies on, on the mandrel surface. One feature of the algorithm is that it locates the initial contact point of all of the strands. In configuring the initial set up of the strands, they are presumed to all be attached to the very end of the mandrel. The only attachment information required by the algorithm is the longitudinal distance of the mandrel end from the carrier ring. Thus each strand's initial contact distance, h, is the same (this distance). The first strand is initially presumed to be attached at the very top of the mandrel, ie. $x = 0$, $y = a$. The location of the next strand is calculated by the algorithm.

As stated, during braiding all strands are always tangent to the mandrel where they contact the mandrel. Therefore the algorithm presumes that the first strand is attached tangent to the mandrel and that it runs to a carrier, and that the strand from the next carrier is also attached at a tangent point. This, therefore, locates the contact point of the next strand. Where such an adjacent contact point is, is given in Chapter 4. Therein it is called point 4 and is given by equations 29 to 55. Thus the algorithm uses these equations to find the adjacent strand contact point. It then uses this point and the equations to find the next strand's contact point, and so on.

The algorithm is presented in a flow chart. Therein, the word 'calculate' means calculate using the equations derived herein. x(i), y(i), z(i) are the co-ordinates of a path point for strand i. They are re-assigned (and printed out) as the program progresses, rather than storing all of the path points in an array of a size initially unknown.

The shape of the mandrel is input via a subroutine. As stated, the section size varies with z. However, the section shape, or a-to-b ratio (see Figure 5-2), remains constant. The ratio, b/a, is input as a constant. Therefore, now the function of 'a versus z' completely defines the mandrel shape. This function is present in the algorithm as a subroutine (see "afunc(z)"). Thus this subroutine must be edited in order to input the mandrel shape information.

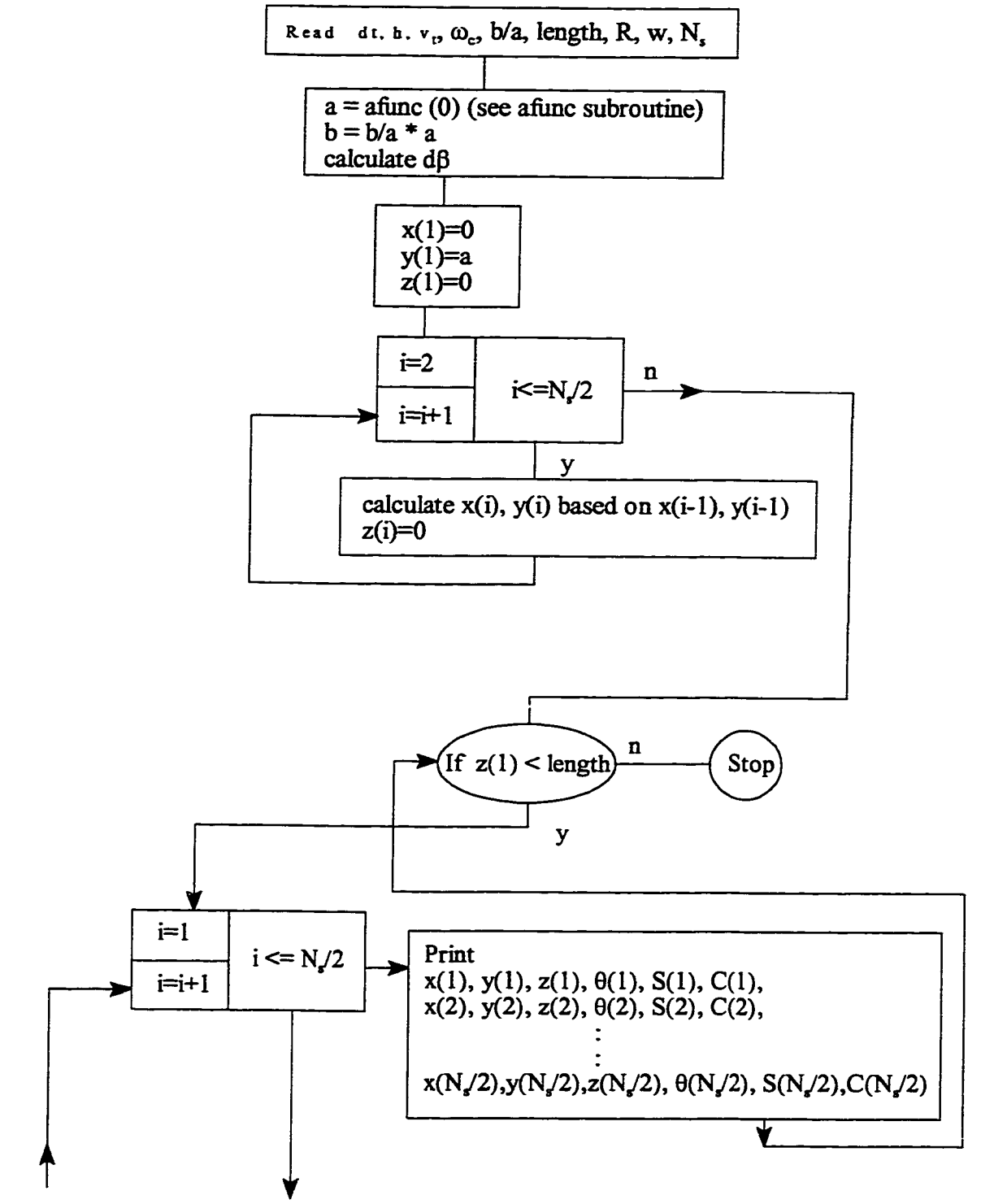

(continued on next page)

Figure 5-5 Algorithm 2

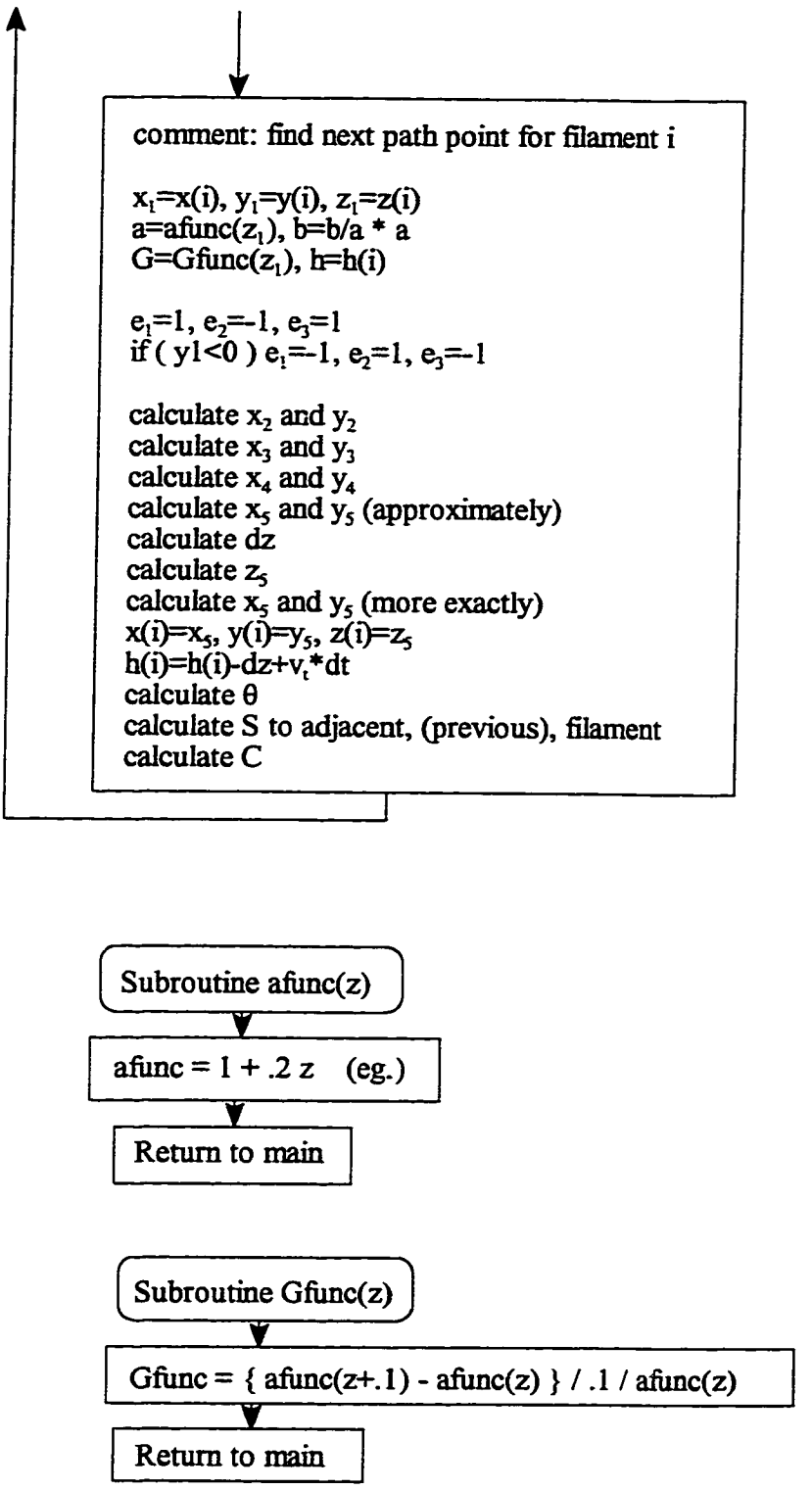

Figure 5-5 Algorithm 2 (cont'd)

5.3 Algorithm 3

The assumption made for Algorithm 2 was that the strand is not interfered with while being laid down on the mandrel by anything other than the carrier and the mandrel. The assumption of Algorithm 1 is that the strand is interfered with by other strands. The assumption is that the other strands push the contact point of the strand axially along the mandrel, confining it within a planar contact ring.

Thus the assumption of Algorithm 2 truly applies to free winding rather than braiding, however Algorithm 1 only models the steady state. Thus Algorithm 3 will be created which uses the principles of Algorithm 2 but which incorporates the assumption of Algorithm 1.

For Algorithm 3, again all of the same direction strands have their surface path determined. For each strand, the next path point (based on the previous one) is calculated in exactly the same way as for Algorithm 2. However, having done this, the average 'z' value (axial distance along the mandrel) of the contact points is taken. This value is then assigned to each of the contact points, to replace the calculated value. This effectively moves the contact point up or down axially along the mandrel, so as to keep it in a planar contact ring, thus establishing the assumption of Algorithm 1. Otherwise, the algorithm is identical to Algorithm 2.

The braid angles, strand spacings, and cover factors are then calculated as before.

CHAPTER 6

RESULTS AND DISCUSSION

6.1 Algorithm 1

A computer code was written for the algorithm which determines the configuration properties of fabric preforms formed by 2D braiding in steady state on a mandrel with constant elliptical cross-section (see Chapter 4, Algorithm 1). The results of several program runs are discussed in this section.

Each run of the program considers one set of process and mandrel conditions. This corresponds to one set of input variables or 'process parameters'. A sample output is included in Appendix A. The input conditions, hereafter referred to as Case 1, are:

$a = 2$ cm, $b = 1$ cm, $\omega_c = 0.116$ rad/sec, $v_t = 0.15$ cm/sec,

$N_s = 18$, $w_t = 0.125$ cm, $R = 16$ cm .

The results of four runs are plotted in Figures 6-1 a, b, and c. For each run the process parameters are the same as those of Case 1 except that the length of the semi-major axis, 'a', is varied, which creates four different aspect ratios. The values of 'a' are given in the figure. The three configuration properties (braid angle, strand spacing, and cover factor) are presented versus α, which is defined in Figure 6-2.

In order to facilitate reading the graphs, the angle α is defined clockwise from the y-axis so that an increasing α (which corresponds to a motion to the right on the graphs of Figure 6-1) also corresponds to a movement to the right on the perimeter in Figure 6-2.

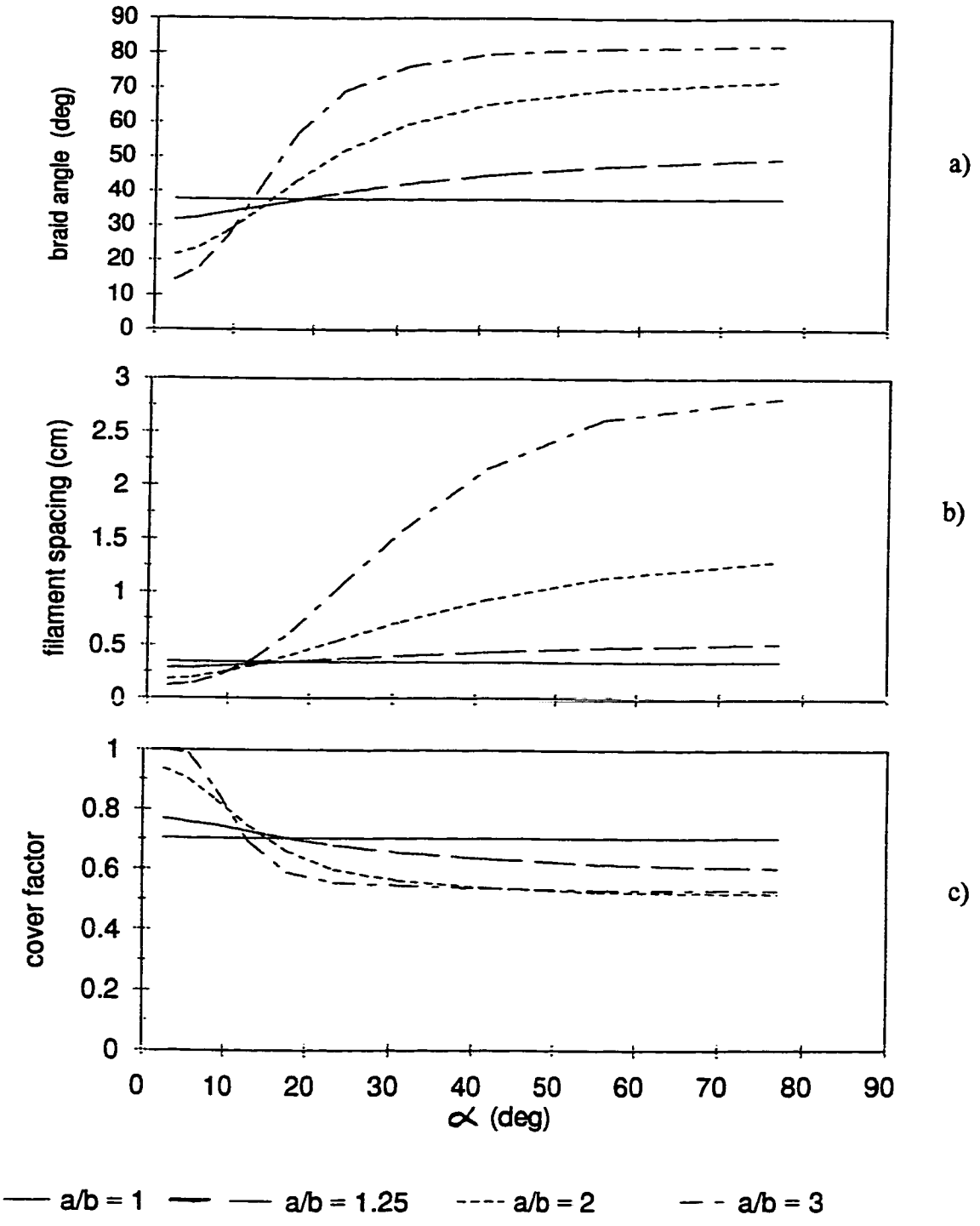

Figure 6-1 Configuration Properties For Four Cases, Algorithm 1, (Conditions per Case 1 except for 'a', as shown), a) braid angle, b) strand spacing, c) cover factor

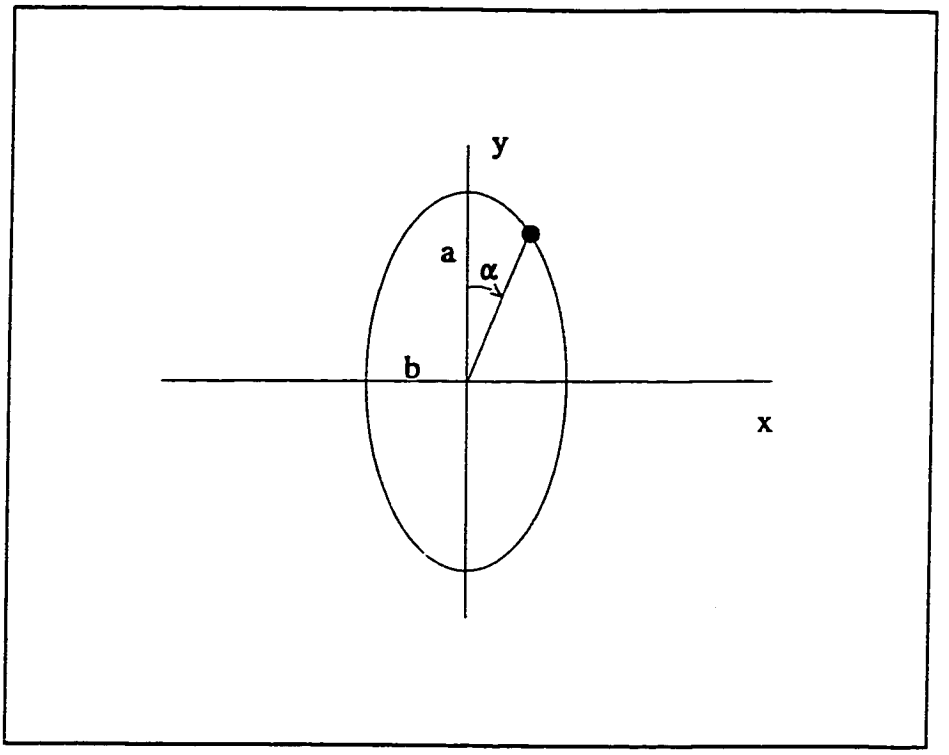

Figure 6-2 Location of Point on Perimeter

6.1.1 Braid Angle Distribution Around Perimeter

Each curve in Figure 6-1 a shows the calculated braid angle distribution around the first quadrant of an elliptical mandrel for a different value of 'a' and an otherwise common set of process parameters. It should be noted that the curves do not extend up to 90 degrees. This is simply because the next data point calculated is beyond 90 degrees (eg. 95 degrees) and so it is not on the graph.

The curves for aspect ratios greater than one show that the braid angle is higher at points near the minor axis of the elliptical mandrel than at points near the major axis. The region of the elliptical mandrel near the minor axis shall hereafter be referred to as the 'minor-axis

region', and the region of the elliptical mandrel near the major axis shall be referred to as the 'major-axis region'.

For an aspect ratio of 1 the calculated braid angle distribution is flat, ie. the braid angle is constant around the perimeter. The braid angle around the perimeter of a circular mandrel is expected to be constant due to symmetry as can be seen in published results, such as Pastore and Ko [1]. The braid angle calculated for this case (37.7 degrees) agrees with that predicted by the equations of Pastore and Ko, given in Chapter 2.

The braid angle variation can be explained by reviewing the process. As explained in the derivation of equation 73 (Section 4.3) the braid angle clearly depends on the longitudinal and circumferential speeds of the strand-mandrel contact point as the strand is laid on. It can be seen from the equation that for a constant longitudinal speed, v_t, a higher circumferential speed, v_c, will cause a higher braid angle.

For Algorithm 1, it is presumed that the longitudinal speed is constant, thus the circumferential speed shall be examined. Figure 6-3 shows a strand with its contact point in the 'major-axis region'. Recall that the strand remains tangent to the mandrel at all times. A small motion of the carrier, as shown, causes a small motion of the contact point. The figure also shows a strand with its contact point in the 'minor-axis region'. Clearly, the same motion of the carrier causes a much larger motion of the contact point. It is evident also, that this effect is more pronounced for mandrels of higher aspect ratio, (a/b).

Thus because the carrier speed is constant the circumferential speed, v_c, is higher in the minor-axis region than in the major-axis region. Therefore, the braid angle will be higher in the minor-axis region than in the major-axis region , and this braid angle difference is greater for mandrels of higher aspect ratio.

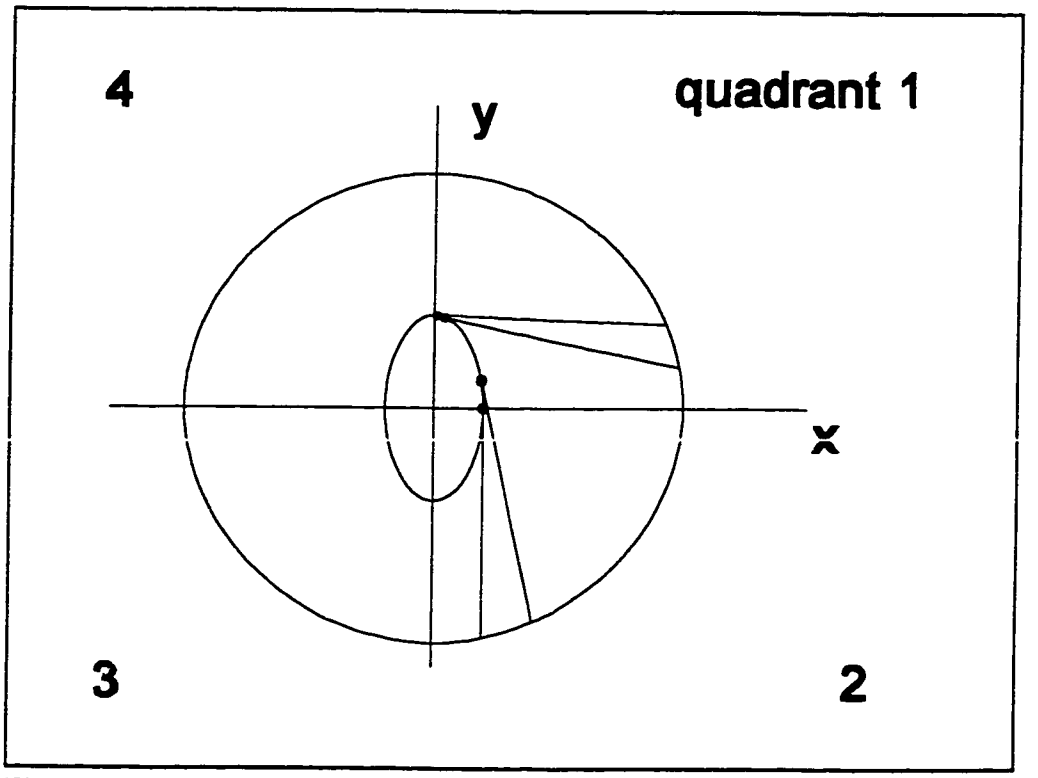

Figure 6-3 Strand Motions

Results for four mandrel shapes are shown. For each mandrel the minor-axis is the same, however the major-axis is different (see Figure 6-2). This shows the effect of increasing the aspect ratio, (a/b), on the distribution of braid angles. The curves show that as the aspect ratio is increased, the braid angle in the major-axis region decreases, while the braid

angle in the minor-axis region increases. The explanation for this was given in the previous paragraph.

6.1.2 Symmetry of Properties

Observation of any of the results (for example, Case 1 of Appendix A) shows that the braid angles in the second quadrant (Figure 6-3) of the elliptical mandrel decrease from the minor-axis region to the major-axis region. This is expected due to the symmetry of the mandrel. However the results are not exactly symmetric. This is displayed in Figures 6-4 a, b, c. The figure shows the braid angle, strand spacing, and cover factor for two quadrants super-imposed on the same axes for comparison of the symmetry. The input parameters and the output are those of Case 1 in Appendix A and are repeated on the figure.

The slight non-symmetry can be explained by considering Figure 6-5. A strand is shown in the figure running from the first quadrant of the ellipse to a carrier on the carrier circle. A strand running from the point on the ellipse mirrored in the x-axis to the carrier circle is also shown. Because the strand must be tangent to the ellipse this results in a strand running to the carrier circle which is much shorter than the first strand. This fact is discussed simply to show that the process of laying on the strand is clearly somewhat different at the second point than at the first. Thus it should be expected that the properties in the second quadrant do not mirror those in the first, ie. that the results are

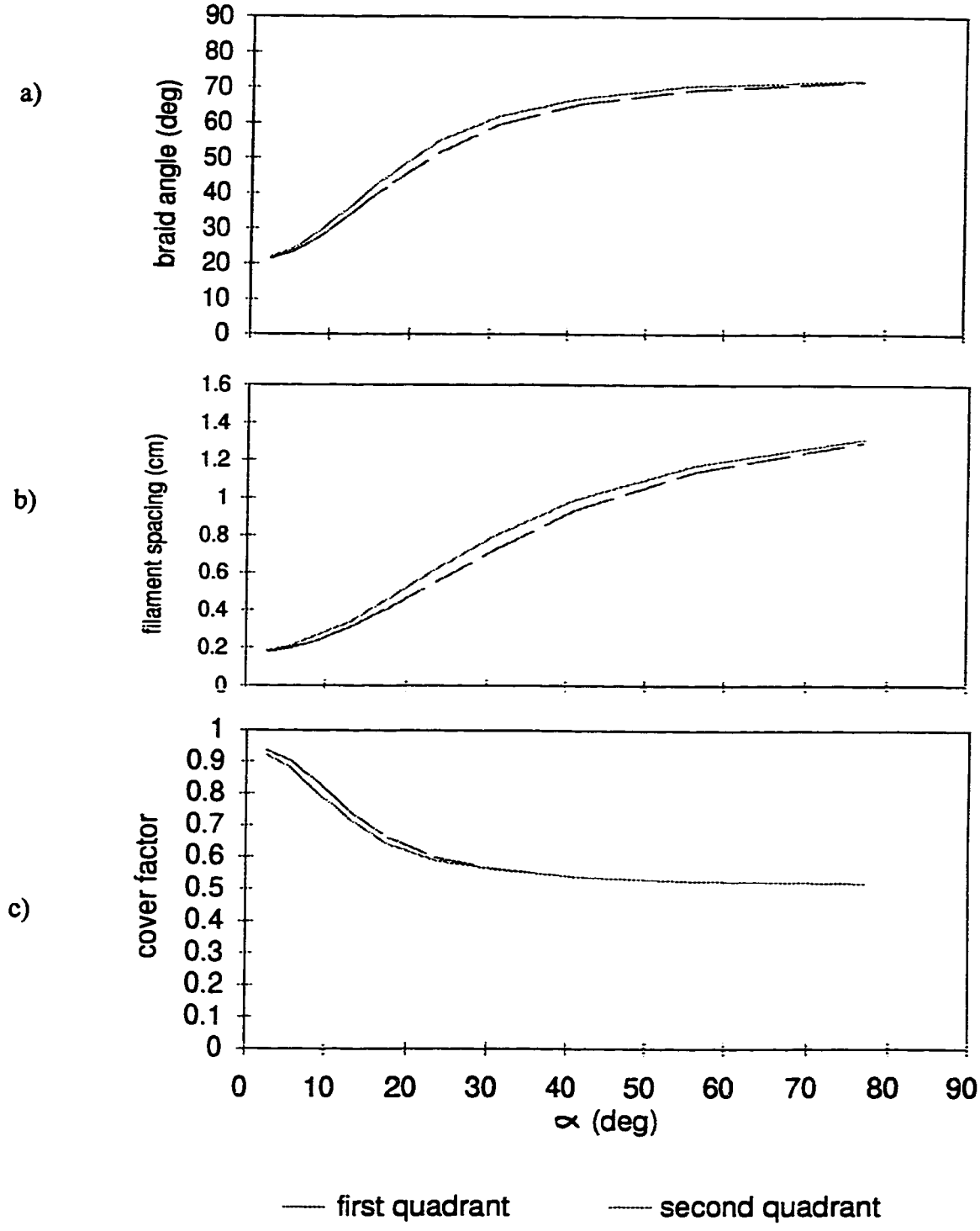

Figure 6-4 Configuration Properties as Functions of α , For Symmetry Comparison (Conditions per Case 1), a) braid angle, b) strand spacing, c) cover factor

not perfectly symmetric. However, because the properties are very close, configuration properties from only the first quadrant will be plotted.

The explanation given herein of the variation of braid angle around the perimeter indicates that it has its minimum and maximum at the major and minor axes of the ellipse. This can be seen to be the case in Figure 6-4.

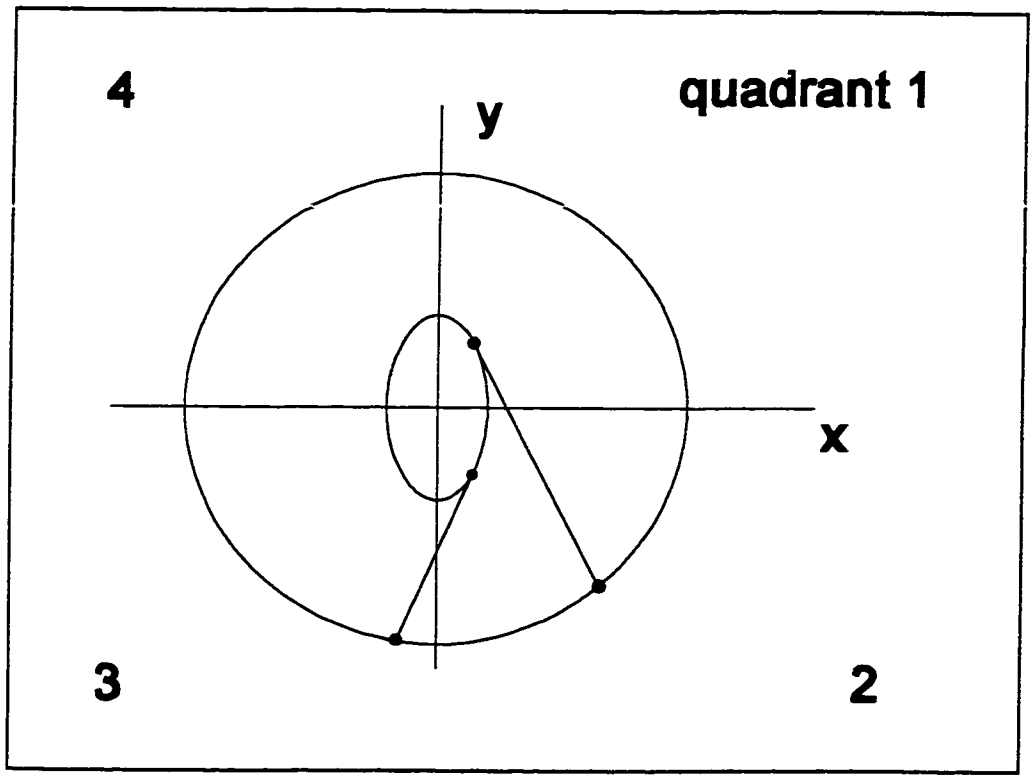

Figure 6-5 Non-symmetry of Process

6.1.3 Strand Spacing Distribution Around Perimeter

Each curve in Figure 6-1 b shows the calculated strand spacing distribution around the first quadrant of a mandrel ellipse for a different value of 'a' and an otherwise common set of process parameters. The curves for aspect ratios greater than one show that the strand spacing is higher in the minor-axis region than in the major-axis region.

For an aspect ratio of 1 the strand spacing distribution is flat, ie. the strand spacing is constant around the perimeter. The strand spacing around the perimeter of a circular mandrel is expected to be constant due to symmetry, as can be seen in published results, such as Pastore and Ko [1]. The strand spacing calculated for this case (0.349 cm) agrees with that predicted by the equations of Pastore and Ko, given in Chapter 2.

As explained in Section 6.1.1, for a given carrier displacement the corresponding displacement of the ellipse contact point will be smaller when in the major-axis region than when in the minor-axis region of the mandrel. Thus for two carriers spaced a given distance apart the distance between the corresponding two ellipse contact points will be smaller in the major-axis region than in the minor-axis region. Since the carriers always remain equidistant, the contact point spacing, and hence strand spacing, is therefore smaller in the major-axis region than in the minor-axis region.

The results plotted are from the same program sample runs as the data of Figure 6-1 a, ie.

the process conditions and mandrel shapes are the same. Again the presentation of four curves is intended to show the effect of an increasing aspect ratio on the strand spacing distribution. It can be seen that for a higher aspect ratio the range of strand spacing (along the quadrant perimeter) is greater. It was stated in Section 6.1.1 that equal carrier displacements correspond to larger contact point displacements in the minor-axis region than in the major axis region and that this effect is more pronounced for mandrels of higher aspect ratio. Therefore, for mandrels of higher aspect ratio, the range of strand spacing is greater.

6.1.4 Cover Factor Distribution Around Perimeter

Each curve of Figure 6-1 c shows the cover factor distribution around the first quadrant of the ellipse for a different aspect ratio. One observation is that (for aspect ratios not equal to 1) the cover factor decreases from the major-axis region to the minor-axis region.

As the aspect ratio approaches 1, the cover factor distribution becomes flat, ie. it is constant around the perimeter. Cover factors around the perimeter of any circular mandrel are, by symmetry, constant. The cover factor calculated for this case is not compared to that predicted by the equation of Pastore and Ko [1] because that equation is believed to be incorrect (see Chapter 3).

The presentation of four curves shows the effect of an increasing aspect ratio on the cover factor distribution. It is seen that for a higher aspect ratio the range of the cover factor is greater.

The algorithm generates the braid angle and strand spacing at a point and then calculates the cover factor with a simple formula based on these two variables, derived in Chapter 3 (equation 24). As can be seen therein, the derivation is very short and is based on simple geometry. Thus the cover factor's behavior can only be explained by the behavior of the braid angle and the strand spacing.

It is clear from Figure 3-2 that cover factor increases with braid angle. It is also clear from Figure 3-2 that cover factor decreases with increasing strand spacing. The derived formula for cover factor (equation 24) exhibits these relationships.

6.1.5 Other Effects

As previously stated, the purpose of this thesis is to develop mathematical relationships between the process parameters and the configuration properties, for the reasons given in Chapter 1. The relationships have been presented thus far as equations and algorithms. For the design of 2D braiding processes however, it is useful to see these relationships in a visual form. Therefore the results are plotted as functions of the process parameters.

Each of the process parameters was varied over a wide range while keeping the others the same. The results were plotted in an abbreviated fashion in order to present an overall picture of results for various mandrel shapes and sizes and machine speeds. The causes of the trends seen are also discussed.

Computer runs were made for many shapes and sizes of mandrels and machine speeds (process parameters) to provide the results shown in Figures 6-6, 6-7, and 6-8.

In Figure 6-6 a six curves are shown which correspond to three aspect ratios. For each aspect ratio computer runs were made for increasing mandrel sizes, from 6% of the carrier circle radius to 95% of the carrier circle radius. The resulting braid angle at the point on the ellipse at the intersection of the major-axis, 'major-axis braid angle', is plotted versus mandrel size. The braid angle at the minor-axis is also plotted, as a function of size, on the same graph.

The strand spacings and cover factors were plotted in the same way, in Figures 6-6 b, and c. The runs were made for one carrier to mandrel speed ratio to get the data of Figure 6-6. For Figure 6-7 runs were made for a higher speed ratio. For Figure 6-8 the speed ratio was yet higher. The aspect ratios and speed ratios are given in the figure captions.

The three aspect ratios chosen provide a wide range of mandrel cross-section shape, from almost circular to a very elongated ellipse. The 36 carrier braiding machine in the

Composite Materials Laboratory was observed while producing a fabric on a mandrel. A reasonable cover factor was obtained for the speed ratio used. This speed ratio condition was used for the results of Figure 6-7. For Figure 6-6 a 60% lower ratio was used, and for Figure 6-8 a 60% higher ratio was used, thus providing a wide range of speed ratios.

Also, the results have been non-dimensionalized to present general data. Appropriate variables were divided by the carrier circle radius, R, in order to non-dimensionalize them. Thus users of various sizes of machine could use this data if desired. The mandrel size is defined by a/R, the ellipse half-major axis divided by the carrier circle radius. The strand spacing is presented as S/R, the strand spacing divided by R. The cover factor is unmodified as it is already non-dimensional. The braid angle is left in degrees as there is no benefit in non-dimensionalizing it.

There are two speeds involved in the process, the mandrel speed, v_t, and the carriers' angular velocity, ω_c, which translates into a carrier speed of $\omega_c R$. However there is only one degree of freedom, which is the ratio of the two speeds, $\omega_c R/v_t$.

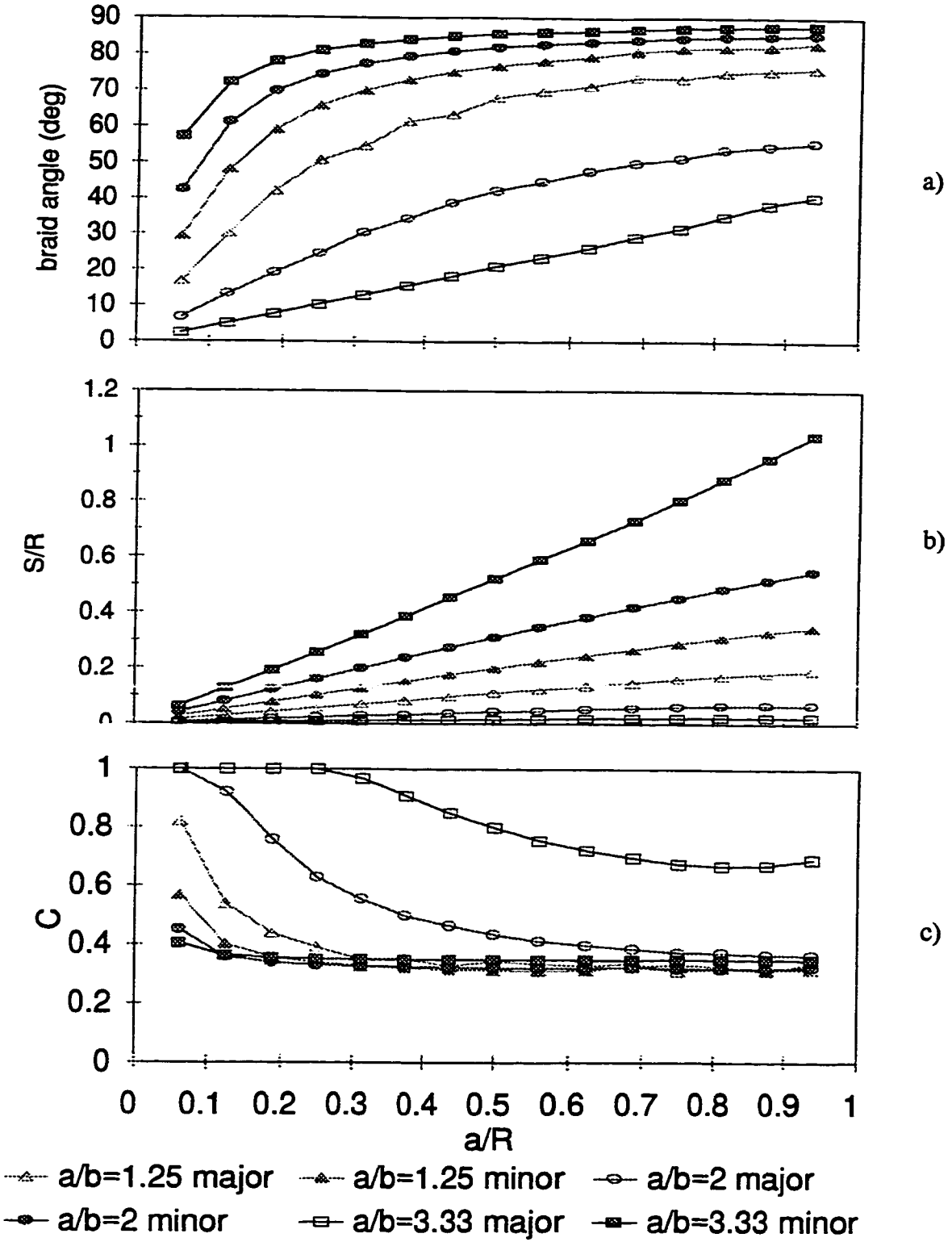

Figure 6-6 Configuration Properties at Major and Minor Axes versus Mandrel Size, Algorithm 1, (ω_c R / v_t = 7.42), a) braid angle, b) strand spacing, c) cover factor

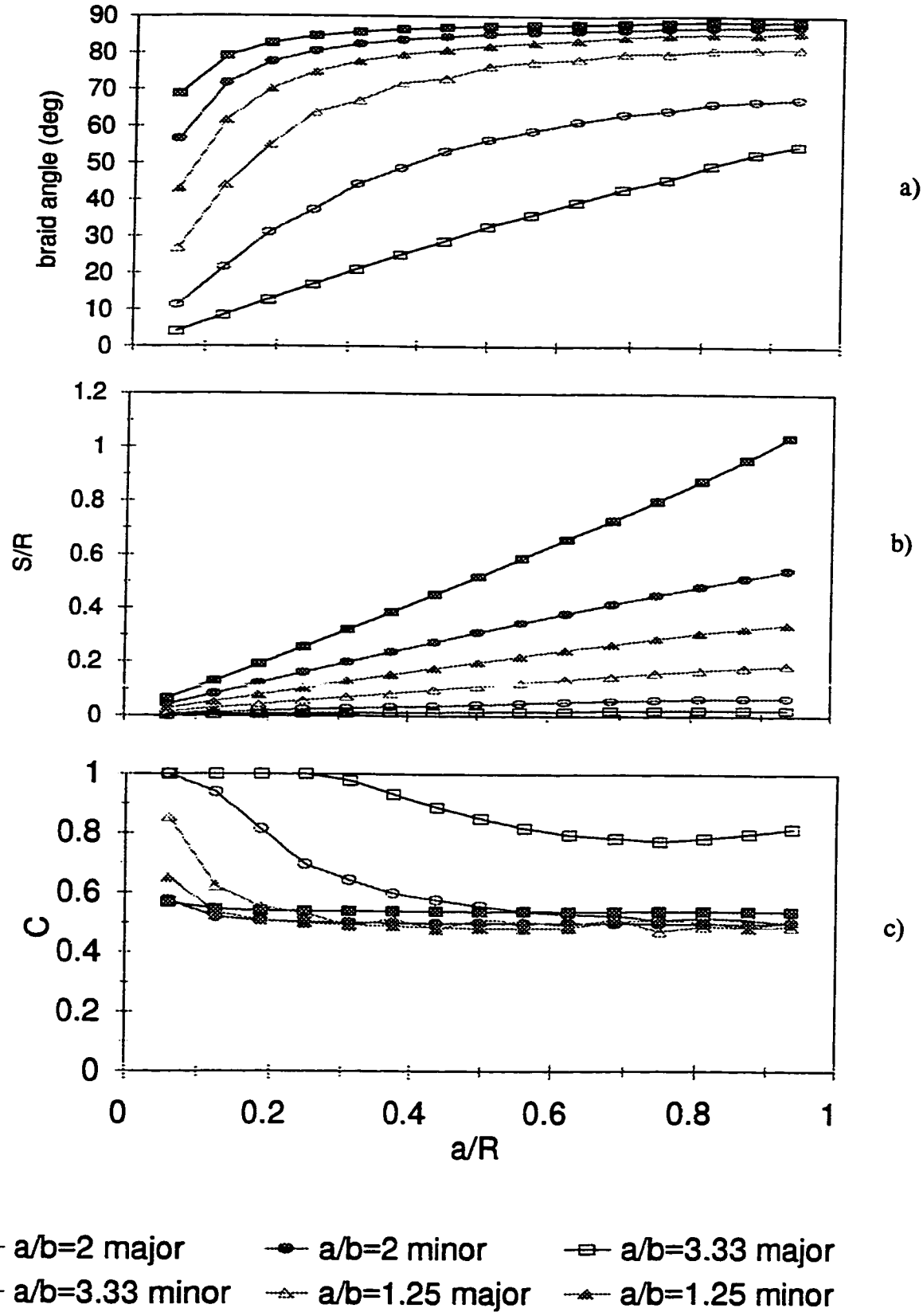

Figure 6-7 Configuration Properties at Major and Minor Axes versus Mandrel Size, Algorithm 1 ($\omega_c R / v_t = 12.37$) a) braid angle, b) strand spacing, c) cover factor

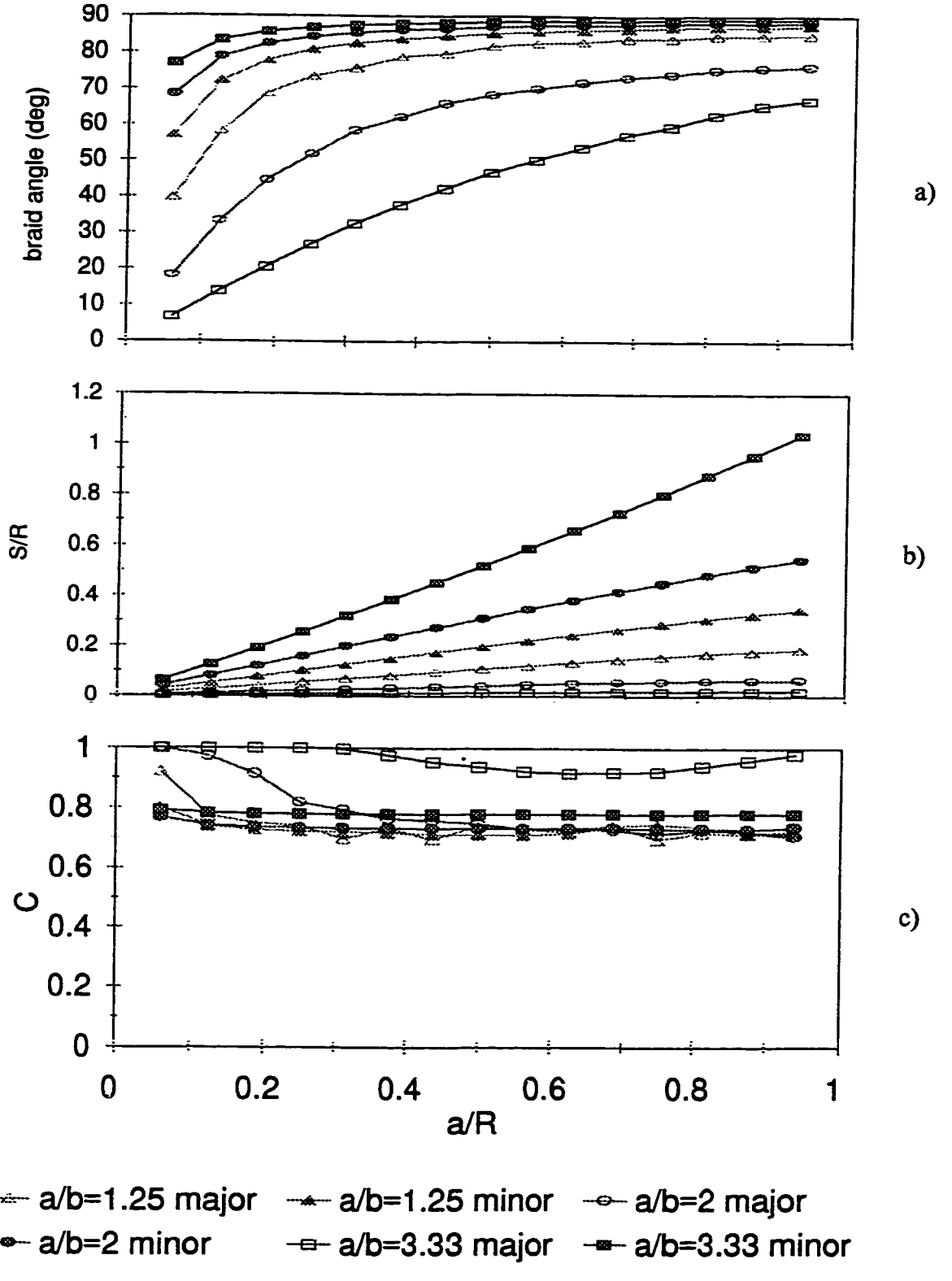

Figure 6-8 Configuration Properties at Major and Minor Axes versus Mandrel Size, Algorithm 1, (ω_c R / v_t = 20.62), a) braid angle, b) strand spacing, c) cover factor

6.1.6 Effect of Location on Perimeter

The braid angle results (Figures 6-6 to 6-8 a) show that for any aspect ratio, the curve of 'major-axis' braid angle is lower than the curve of 'minor-axis' braid angle. Thus at any mandrel size, the braid angle is lower in the major-axis region than in the minor-axis region. The reason for this was discussed in Section 6.1.1.

For any aspect ratio the curve of 'major-axis' strand spacings is lower than the curve of 'minor-axis' strand spacings. Thus at any mandrel size the strand spacing is lower at the major-axis than at the minor-axis. The reason for this was also discussed in Section 6.1.3.

The curves for 'major-axis' cover factor are higher than those for 'minor-axis' cover factor. Thus at any mandrel size the cover factor is higher at the major-axis than at the minor-axis. The reason for this was discussed in Section 6.1.4.

6.1.7 Effect of Mandrel Size

The resulting properties are greatly affected by the size of the mandrel. It can be seen from any of the braid angle figures that, for any aspect ratio, the braid angle versus mandrel size curve is an increasing curve, for both 'major-axis' and 'minor-axis' braid angles. Thus, for larger mandrels, the braid angle at any same point on the perimeter is

higher.

This is explained as follows. In Chapter 2, for circular-sectioned cylindrical mandrels equation 3 was developed;

$$\theta = \tan^{-1}[\frac{\omega_c \, r}{v_t}]$$

where θ is the braid angle, ω_c is the carrier velocity, v_t is the mandrel velocity, and r is the radius of the mandrel. This equation was developed by considering the segment of mandrel and the strand path laid down during one traverse around the mandrel. "Uncurling" this cylindrical segment reveals a right-angled triangle (Figure 2-1). It is seen that the braid angle is determined by the ratio of the lengths of the horizontal and vertical sides. The length of the vertical side is $2\pi v_t / \omega_c$, as explained in Chapter 2. This shows how the machine speeds affect the braid angle. A lower ratio of mandrel speed to carrier speed (or a higher ratio of carrier speed to mandrel speed) clearly creates a higher braid angle. The length of the horizontal side is simply the circumference, $2\pi r$. This shows how the mandrel radius affects the braid angle. For a larger mandrel radius processed at the same speeds, the braid angle is greater. The larger mandrel draws off much more strand during the same time period.

Consider an elliptical mandrel. When a "one traverse" segment is "uncurled", the right angled triangle is replaced by a slightly different shape, as shown in Figure 6-9. The

hypotenuse is replaced by an undulating curve, because the braid angles are lower at the major-axes than at the minor-axes. However the length of the vertical side is still $2\pi v_t/\omega_c$. which shows how machine speeds affect the braid angles. Again a lower ratio of mandrel speed to carrier speed clearly creates a set of higher braid angles. The length of the horizontal side is still simply the perimeter of the mandrel. Clearly a larger mandrel perimeter and hence a longer length, processed at the same speeds, creates a set of higher braid angles (see Figure 2-1 for definition of braid angle).

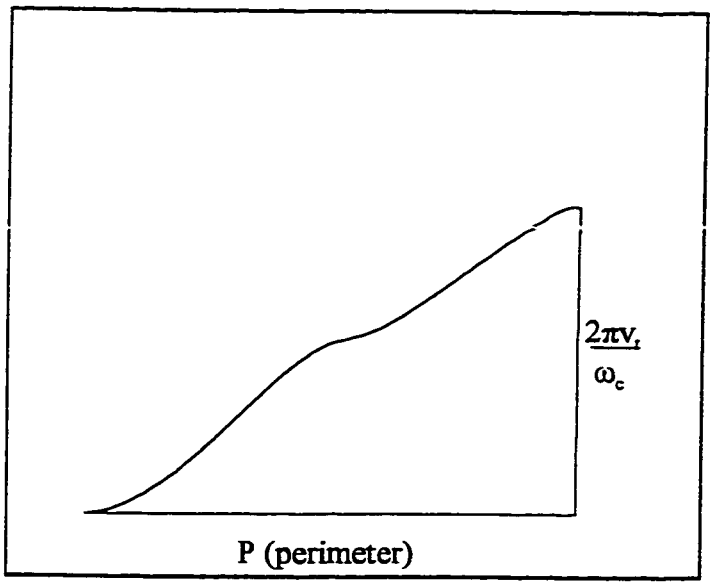

Figure 6-9 One Strand on Mandrel Surface 'Uncurled'

It can be seen that if a curve approaches 90 degrees, it becomes asymptotic to the 90 degree horizontal line. This is to be expected, as the braid angle cannot go beyond 90 degrees without the mandrel reversing direction.

The strand spacing versus mandrel size curves are all increasing curves. Thus for larger mandrels the strand spacings (at similar points on the perimeter) are higher. The reason for this is simple. When a mandrel size is increased, for example doubled, then because the number of same direction carriers and strands attached to it remains the same, one might expect each of the spacings between the strands, from small spacings near the major-axis to larger spacings near the minor-axis, to be doubled due to the geometric similarity of the two mandrels. However, the size of the larger mandrel is closer to the carrier circle radius and therefore the situation is not perfectly geometrically similar and so its distribution of the strand spacings is slightly different. Thus the strand spacing curves are not exactly linear.

The cover factor versus mandrel size curves are all decreasing curves. Thus, for larger mandrels, the cover factors are lower. The cover factor is calculated based on only strand width (a constant in our examples) and the two fabric properties previously calculated, namely, strand spacing and braid angle. Therefore the behavior of the cover factor could only be explained by examining the behavior of those two properties. As explained in this section, the cover factor decreases with the strand spacing and increases with the braid angle. From the figures, it can be seen that the braid angle increases slowly while the strand spacing increases more quickly, thus the net effect is that the cover factor decreases.

In general, the cover factor curves level off as the mandrel size approaches the carrier

circle radius. This can be explained by consideration of Figure 2-1. For a cylindrical mandrel, as the mandrel size is increased (and no other process parameters are changed) the 'triangle' shown changes in shape to one like Shape A (Figure 6-10) ie. a longer, narrower shape. If the perimeter of the mandrel of Figure 2-1 is doubled then the length of strand of one revolution is clearly not doubled. However if the perimeter of the mandrel of Shape A is doubled, then the length of strand is approximately doubled, as shown in Figure 6-10. Therefore, the amount of strand laid on is approximately doubled. Therefore, because the surface area and amount of strand laid on are both doubled, the cover factor remains approximately the same. Therefore, for large mandrels, like that of Shape A, an increase of size changes the cover factor only slightly, and so the cover factor is relatively constant as a function of size.

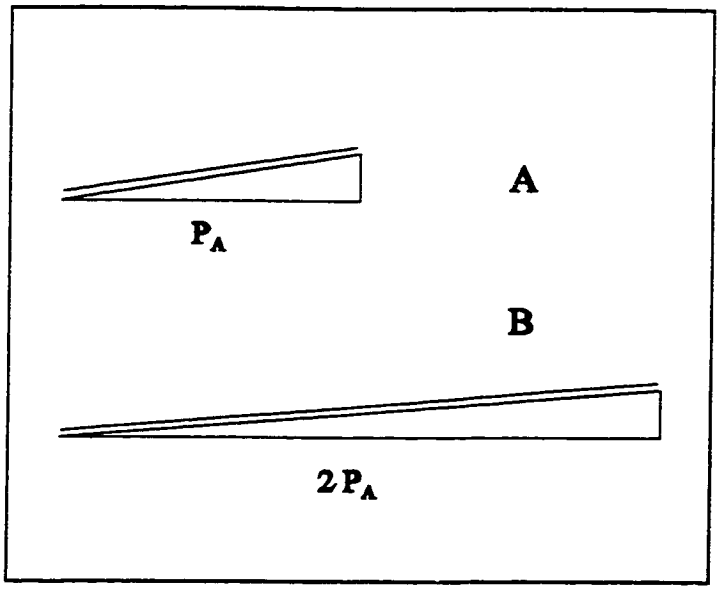

Figure 6-10 Doubling of Large Mandrel's Perimeter

6.1.8 Effect of Aspect Ratio

It can be seen from the braid angle figures that using a higher aspect ratio mandrel (higher a/b) lowers the 'major-axis' braid angle curve and raises the 'minor-axis' braid angle curve. Thus if other factors are kept the same, a higher aspect ratio causes a lower 'major-axis' braid angle and a higher 'minor-axis' braid angle. The reason for this was given in Section 6.1.1.

From the strand spacing figures, it can be seen that using a higher aspect ratio mandrel lowers the 'major-axis' strand spacing curve and raises the 'minor-axis' strand spacing curve. Thus other factors being the same, a higher aspect ratio produces a lower 'major-axis' strand spacing and a higher 'minor-axis' strand spacing. The reason for this was given in Section 6.1.3.

It can be seen from the cover factor figures that using a higher aspect ratio mandrel raises the 'major-axis' cover factor curve and lowers the 'minor-axis' cover factor curve. Thus other factors being the same, a higher aspect ratio causes a higher 'major-axis' cover factor and a lower 'minor-axis' cover factor. The reason for this was given in Section 6.1.4.

6.1.9 Effect of Speed Ratio

By comparing the three braid angle figures, it is seen that increasing the carrier speed to mandrel speed ratio shifts all of the curves upwards. Thus other factors being kept the same, a higher carrier to mandrel speed ratio causes a higher braid angle, at any point on the mandrel perimeter. The reason for this was given in Section 6.1.1.

Comparison of the three strand spacing figures shows that increasing the carrier to mandrel speed ratio does not affect the curves. Thus a higher speed ratio does not affect the strand spacing at any point on the mandrel perimeter. For a machine with 'n' carriers, there are 'n' strands (and 'n' strand spacings) located around the perimeter at any cross-section. Increasing the speed ratio does not increase the number of strands around the perimeter, thus the strand spacings are not changed.

Comparison of the three cover factor figures shows that increasing the carrier to mandrel speed ratio shifts all of the curves upwards. Thus other factors being the same, a higher carrier to mandrel speed ratio causes a higher cover factor at any point on the mandrel perimeter. Again, the cover factor varies increasingly with the braid angle and inversely with the strand spacing. As previously stated, increasing the speed ratio increases the braid angle and does not affect the strand spacing; therefore, it increases the cover factor.

6.2 Algorithms 2 And 3

6.2.1 Algorithm 2

A computer code was written for the algorithm of Section 5.1, Algorithm 2. A sample output is included in Appendix B. The input parameters (referred to as Case 2) are:

dt = .25 seconds (time-step)
h = 6.0 cm (initial, all)
υ_t = .15 cm/sec
ω_c = .116 rad/sec
b/a = .5
length = 30 cm
R = 16 cm
w_t = .125 cm
N_s = 18
a = 2.0 cm

These process parameters are the same as those of Case 1, except that dt and h are not necessary nor included for Case 1, as Algorithm 1 evaluates steady state only. The output data shows a set of points for each strand, which represent its path on the mandrel surface. Three sections of the data are shown; they correspond to the front, middle, and end of the mandrel. It can be seen that each strand wraps around the mandrel in a helix, as shown in Figure 6-11. Each strand's braid angle starts at approximately 70 degrees and stabilizes at approximately 50 degrees. The initial spacings of the strands range from 0.18 to 1.3 cm;

however, they stabilize at different values. Thus there is a transient period and a steady state period.

6.2.1.1 Optimum Time Step

An analysis was done to determine an optimum time step for process parameters and mandrel dimensions like those of Case 2. Algorithm 2 was run several times, using diminishing sizes of time step. For each run a 100 second interval of braiding onto a constant-section sized mandrel was simulated. The surface co-ordinates of the final path point of Strand 1 (Figure 6-11), one of the 18 strands around the mandrel (see Section 5.2, 'Algorithm 2'), are examined for convergence. The z co-ordinate of this point is plotted in Figure 6-12 as a function of the time step size.

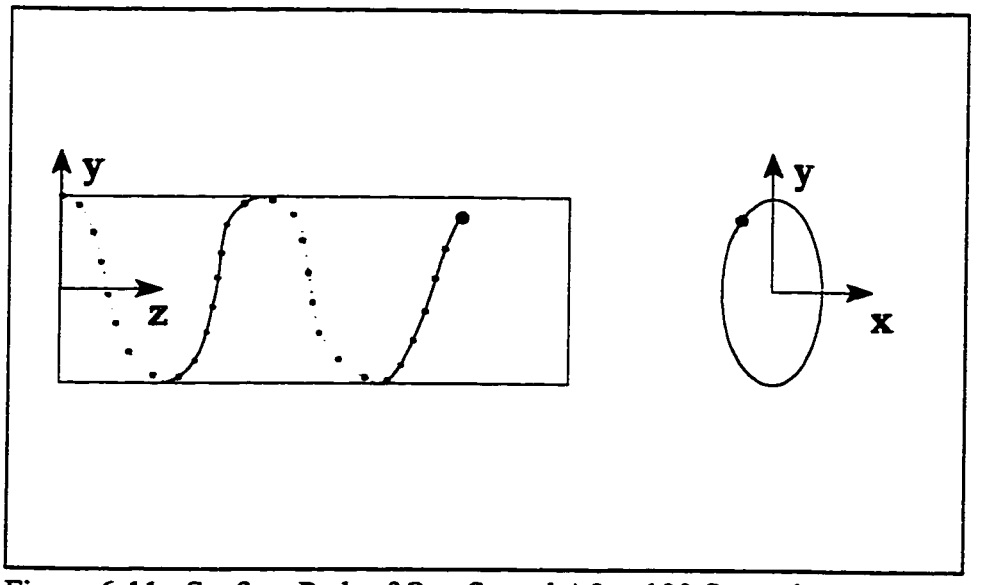

Figure 6-11 Surface Path of One Strand After 100 Seconds

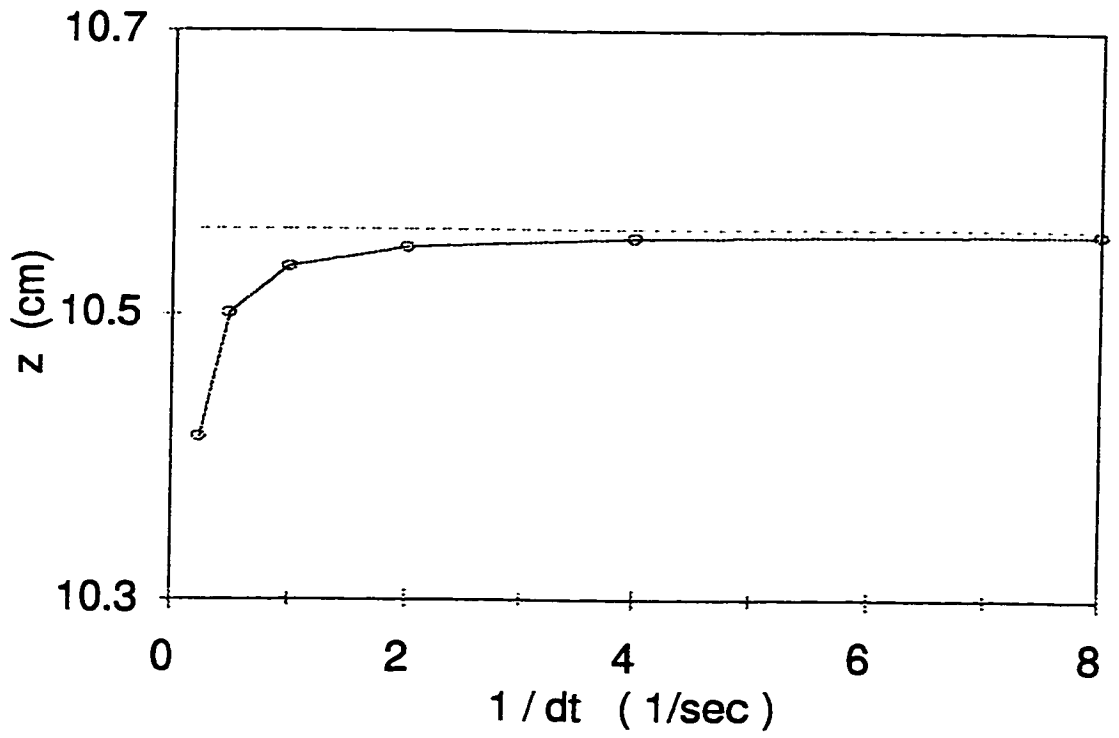

Figure 6-12 z Co-ordinate of Strand 1 Path Point After 100 Seconds. Mandrel Dimensions and Process Parameters per Case 2.

At a time step of 1 second the z value is converged to within 0.3 % of the asymptotic value. At a time step of 0.25 seconds, the z value is converged to within 0.05 % of the asymptotic value. The other co-ordinates of the path point, x and y, converge more quickly, at greater time steps. The final path points of the other strands converge in the same fashion. Thus a time step of 0.25 seconds is suitable for such process conditions. For process parameters or mandrel dimensions greatly different from those of Case 2 a similar time step analysis is recommended to determine an optimum time step.

6.2.1.2 Property Distributions Around Perimeter

Resulting steady state properties are shown in Figure 6-13 for two mandrel aspect ratios. The figure shows that the braid angles are relatively constant around the mandrel perimeter. This is different from the results of Algorithm 1, where they increase from major-axis to minor-axis. This is due to the different assumption or 'boundary conditions' of Algorithm 2. Recall that Algorithm 2 assumes that the strands do not interfere ('free winding') while Algorithm 1 assumes that they interfere so as to produce a flat contact ring. The strand spacing and cover factor results are different also.

The contact ring predicted by Algorithm 2 proves to be non-planar. It can be seen from the results, such as Case 2 in Appendix B, that the ring has higher z values in the second and fourth quadrants of the x-y plane and lower values in the first and third quadrants. Thus the contact ring is non-planar, as illustrated in Figure 6-14.

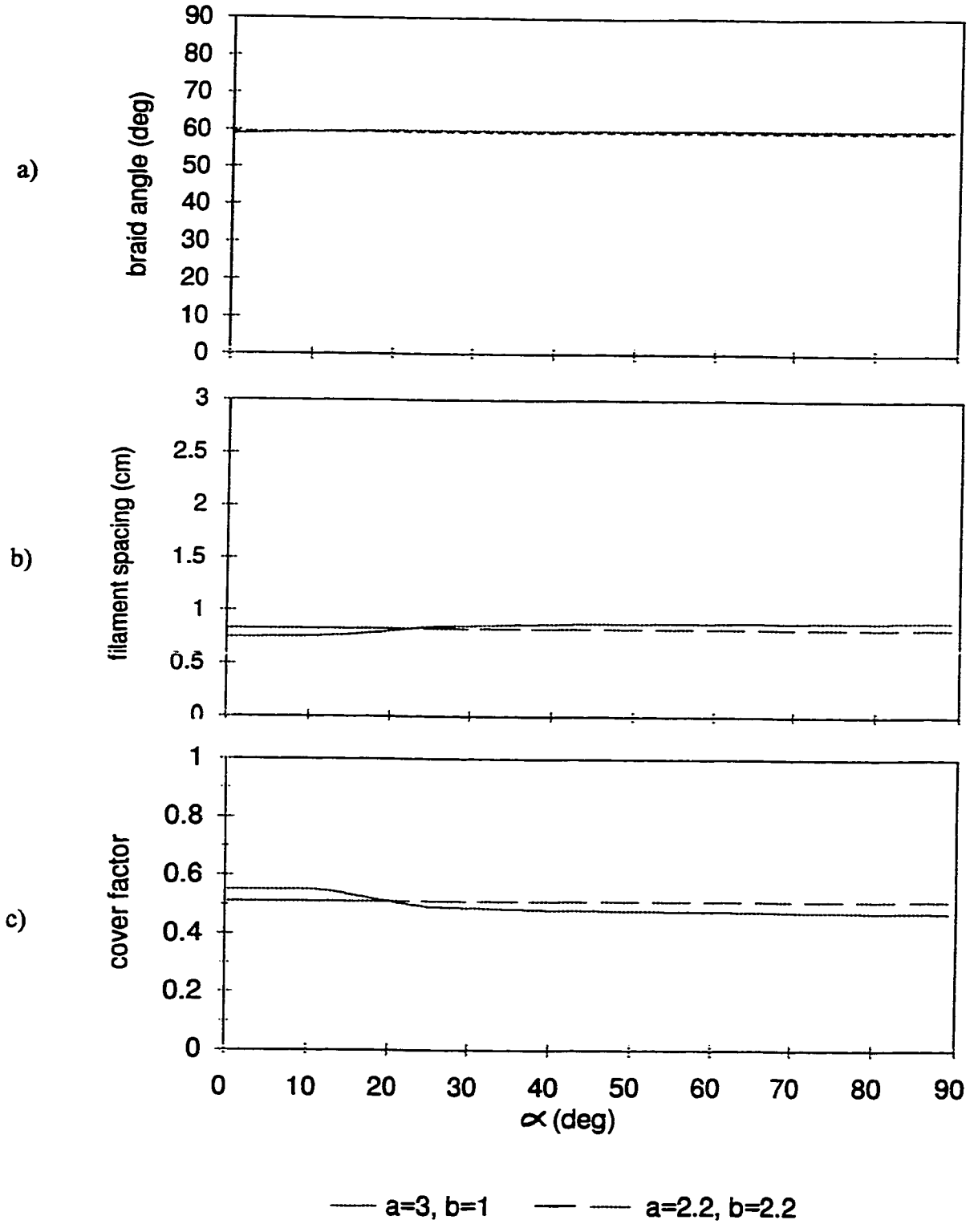

Figure 6-13 Property Distributions Around Perimeter, From Algorithm 2. (Conditions per Case 2, except a and b), a) braid angle, b) strand spacing, c) cover factor

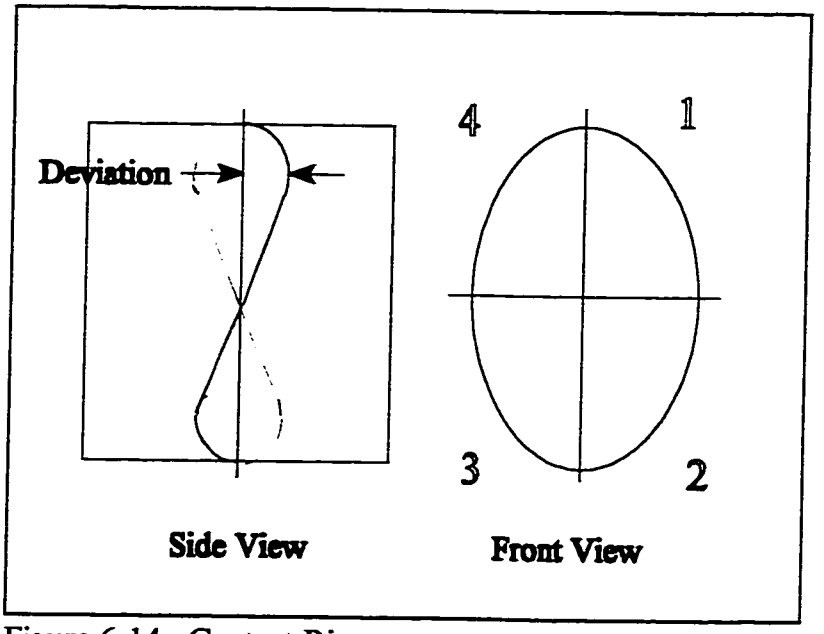

Figure 6-14 Contact Ring

The 'deviation' of the contact ring from planar is shown in Figure 6-14. The amount of this deviation depends on the process parameters. The deviation is plotted in Figure 6-15 as a function of aspect ratio for a few mandrel sizes. The figure shows that the deviation is slightly larger for larger mandrels. Also, the deviation increases with aspect ratio, with zero deviation for a circular mandrel.

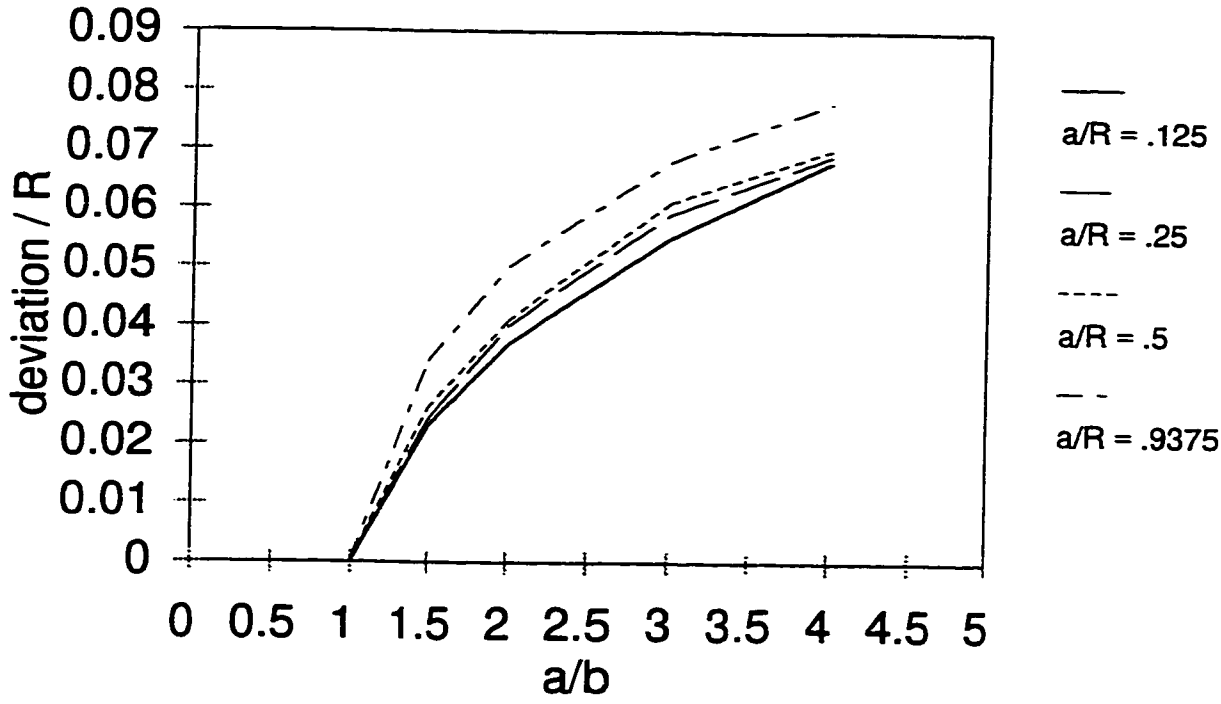

Figure 6-15 Deviation of Contact Ring versus Aspect Ratio
(v_t = .15 cm/sec, ω_c = .116 rad/sec, R = 16 cm).

This leads to the question of which assumption is more accurate. Consider the strands being wound in the opposite direction. Clearly they result in a ring of the opposite shape. However, during braiding there is only one contact ring. Thus the strands must affect each other in such a way that only one ring is created. They will force each other to create a roughly planar ring. Thus the assumption of Algorithm 2, that there is no interference of strands during the process, ie. that a strand is wound on to the mandrel freely, is shown not to be the case for braiding. Thus Algorithm 2 does not give results for the actual 2D braiding process.

6.2.1.3 Other Effects, Introduction

Computer runs were made for many shapes and sizes of mandrels to get the data shown in the graphs of Figure 6-16. Algorithm 2 outputs properties along the mandrel surface over a 'transient' portion and then the steady state portion. Algorithm 1 only analyzes and gives data for the steady state portion, which was presented in Figures 6-6 to 6-8. Thus, for comparison, steady state data of Algorithm 2 is presented in Figure 6-16. All runs were made using one pair of machine speeds to get the data of Figure 6-16. Runs were also made for other pairs of speeds; however, the effect of the speed ratio on the curves was simply the same as it had been for the curves of Algorithm 1. This is discussed further in this section.

The curves of Figure 6-16 correspond to three mandrel aspect ratios. For each aspect ratio computer runs were made for increasing mandrel sizes, from relatively small almost up to the carrier circle size. The resulting steady state configuration properties vary around the perimeter of the mandrel, as has been shown. For each mandrel size, the properties at the major-axis and minor-axis are plotted, as was done for Algorithm 1. The aspect ratios and machine speed ratio are as described in the figure.

The results have been non-dimensionalized as was done for algorithm 1. The mandrel size is defined by a/R, the ellipse half-major axis over the carrier circle radius. The strand spacing is presented as FS/R, the strand spacing over R.

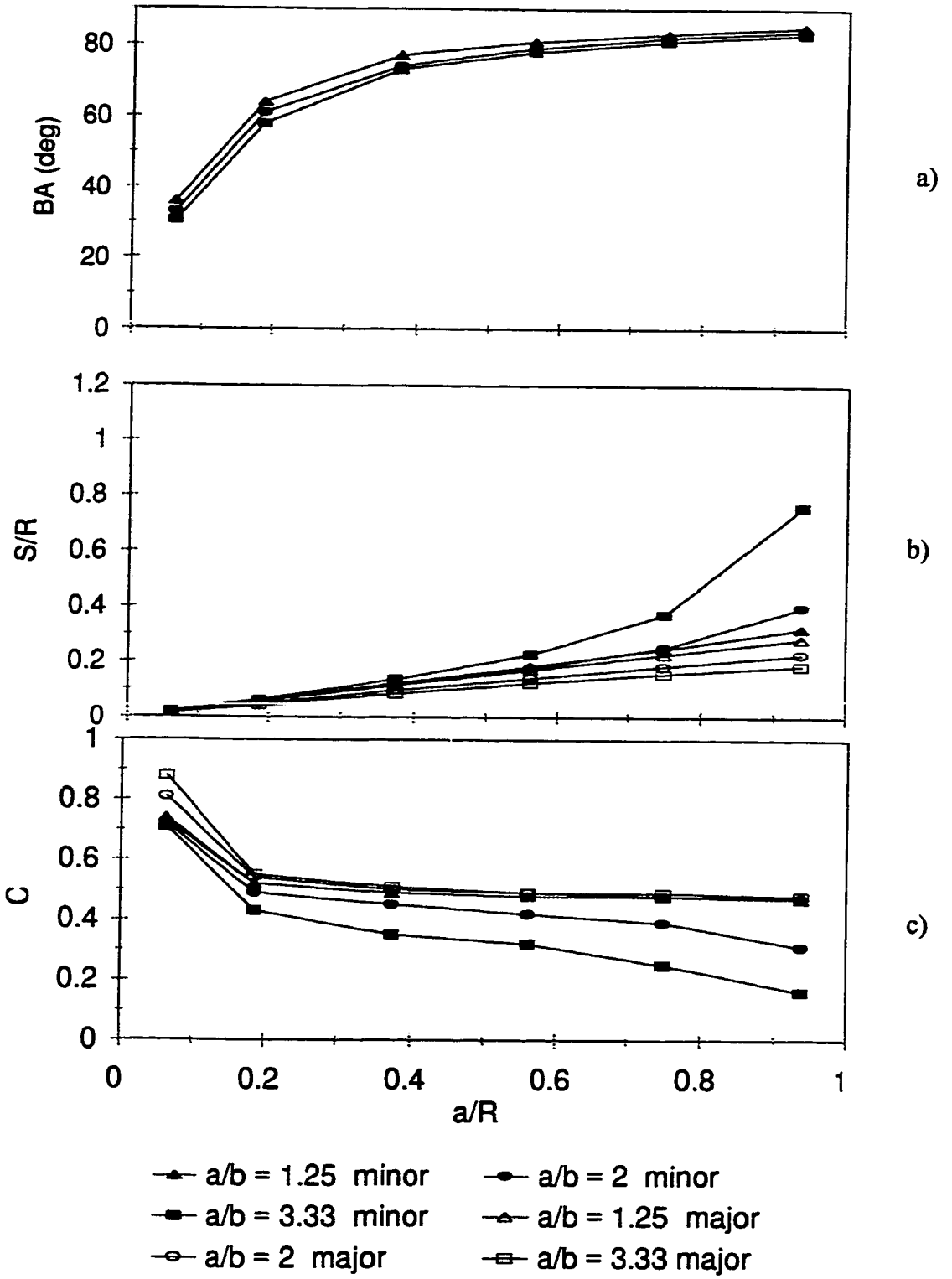

Figure 6-16 Configuration Properties at Major and Minor Axes versus Mandrel Size, Algorithm 2, (ω_c R / v_t = 12.37), a) braid angle, b) strand spacing, c) cover factor

6.2.1.4 Effect of Mandrel Size

For each aspect ratio the braid angle is approximately the same at the major and minor-axis and so the two curves are co-incident, thus only one curve appears. For any aspect ratio, the braid angle versus mandrel size curve is an increasing curve for both 'major-axis' and 'minor-axis'. Thus for larger mandrels, the braid angle, at any same point on the perimeter, is higher. The reason for this was given in Section 6.1.

The strand spacing versus mandrel size curves are all increasing curves. Thus for larger mandrels, the strand spacings, at similar points on the perimeter, are higher. The reason for this was given in Section 6.1. The strand spacings are different than those given by Algorithm 1 due to the different assumptions of Algorithm 2, as discussed in Section 6.2.1.2.

6.2.1.5 Effect of Aspect Ratio

It can be seen from the braid angle figure, that using a higher aspect ratio mandrel (higher a/b) does not lower the 'major-axis' braid angle curve and raise the 'minor-axis' braid angle curve, as was the case for Algorithm 1. Thus a higher aspect ratio does not cause a lower 'major-axis' braid angle and a higher 'minor-axis' braid angle. The braid angle

remains relatively constant around the perimeter.

From the strand spacing figure, it can be seen that using a higher aspect ratio mandrel lowers the 'major-axis' strand spacing curve and raises the 'minor-axis' strand spacing curve. Thus, other factors being the same, a higher aspect ratio produces a lower 'major-axis' strand spacing and a higher 'minor-axis' strand spacing, as was the case for Algorithm 1.

6.2.1.6 Effect of Speed Ratio

As stated previously, Algorithm 2 results showed that increasing the carrier speed to mandrel speed ratio simply shifts the braid angle curves upwards, as it did for Algorithm 1. Thus, other factors being kept the same, a higher carrier to mandrel speed ratio causes a higher braid angle, at any point on the mandrel perimeter. The reason for this is as was given in Section 6.1.

The results also showed that increasing the carrier to mandrel speed ratio does not affect the strand spacing curves. Thus a higher speed ratio does not affect the strand spacing, at any point on the mandrel perimeter. The reason for this was given in Section 6.1.

6.2.2 Algorithm 3

Recall that for Algorithm 3, the strands are constrained to a flat contact ring. Thus for a mandrel of constant cross-section, the resulting properties, once a steady state has been reached, should be the same as those of Algorithm 1 for the same process conditions. For comparison, the results for the conditions of Case 1, from Algorithms 1 and 3, are plotted in Figure 6-17. It is seen that the results are the same. Note that the plotted points for Algorithm 3 were interpolated from an output data table.

To establish that the results are the same over wide ranges of conditions, results were found for the various conditions of Figures 6-6 to 6-8. These are plotted in Figures 6-18 to 6-20, along with the original results from Algorithm 1, for comparison. It is seen that the results are the same. Note that the plotted points, for both algorithms, were interpolated from output data tables.

The results of Algorithm 1 were discussed in Section 6.1. As the results of Algorithm 3 are the same, this discussion of Section 6.1 applies here also.

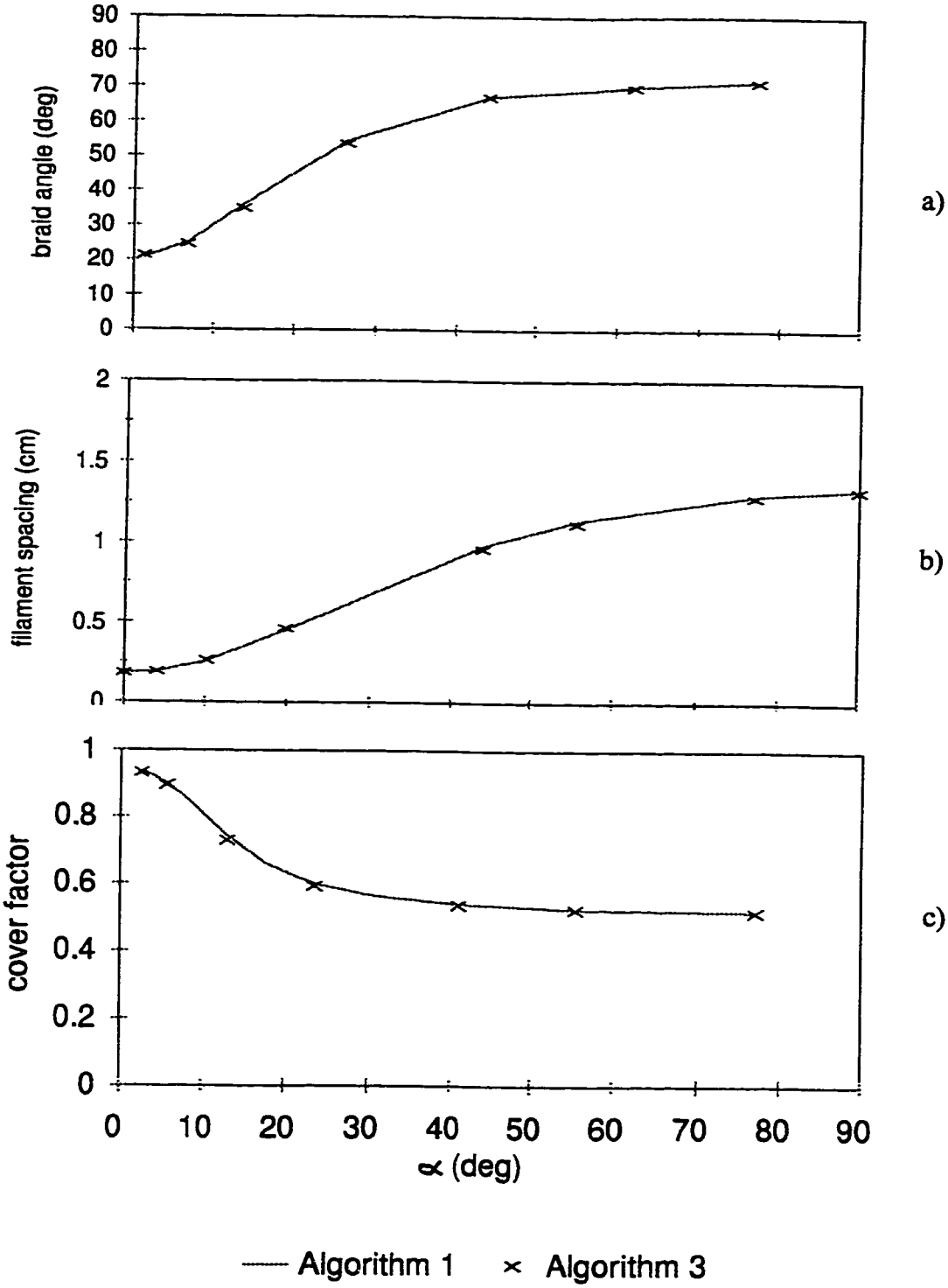

Figure 6-17 Comparison of Property Distributions Around Perimeter, (Conditions per Case 1), a) braid angle, b) strand spacing, c) cover factor

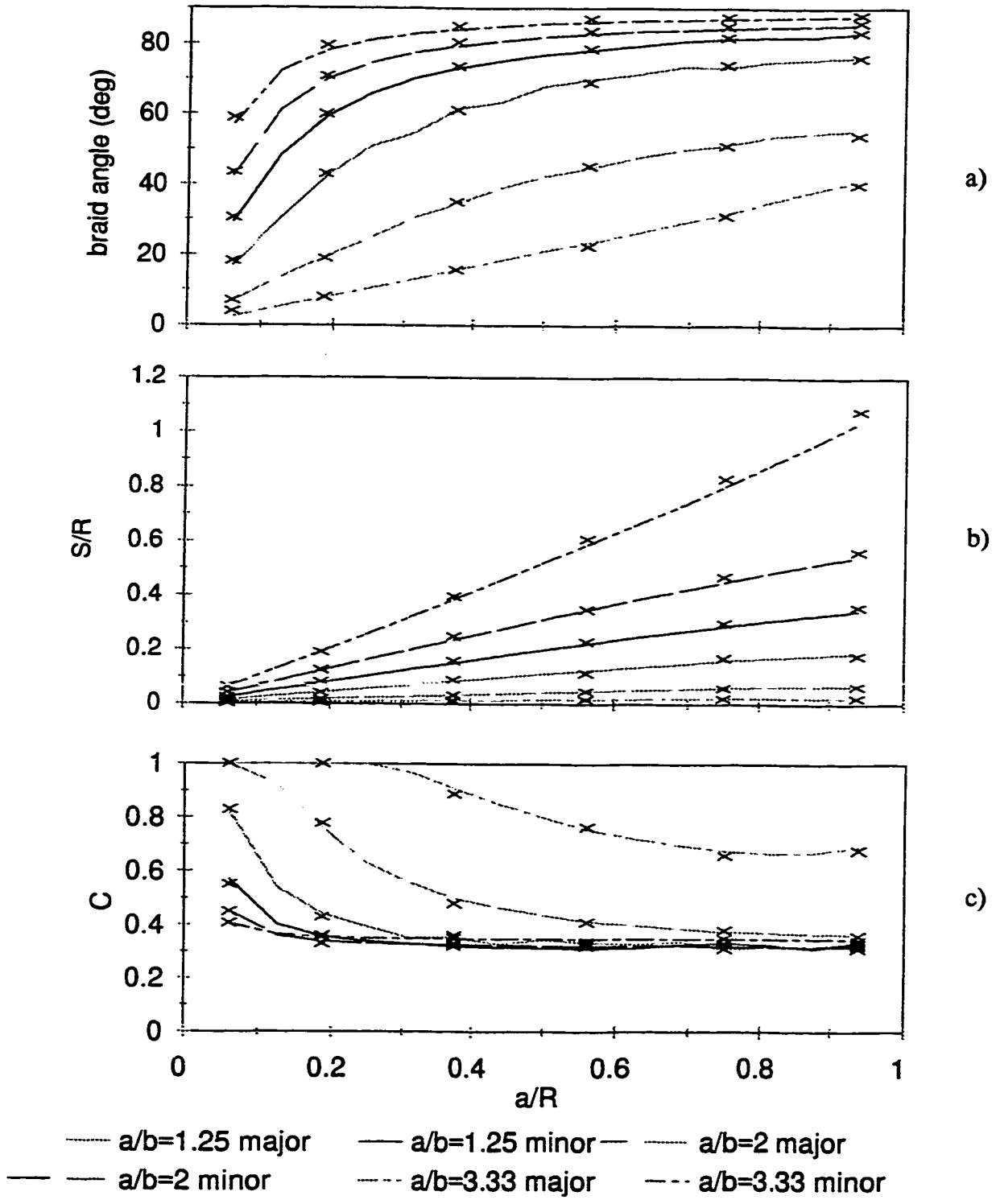

Figure 6-18 Configuration Properties at Major and Minor Axes versus Mandrel Size, Comparison of Algorithm 1, (curves), and Algorithm 3, (x's), ($\omega_c R / v_t = 7.42$), a) braid angle, b) strand spacing, c) cover factor

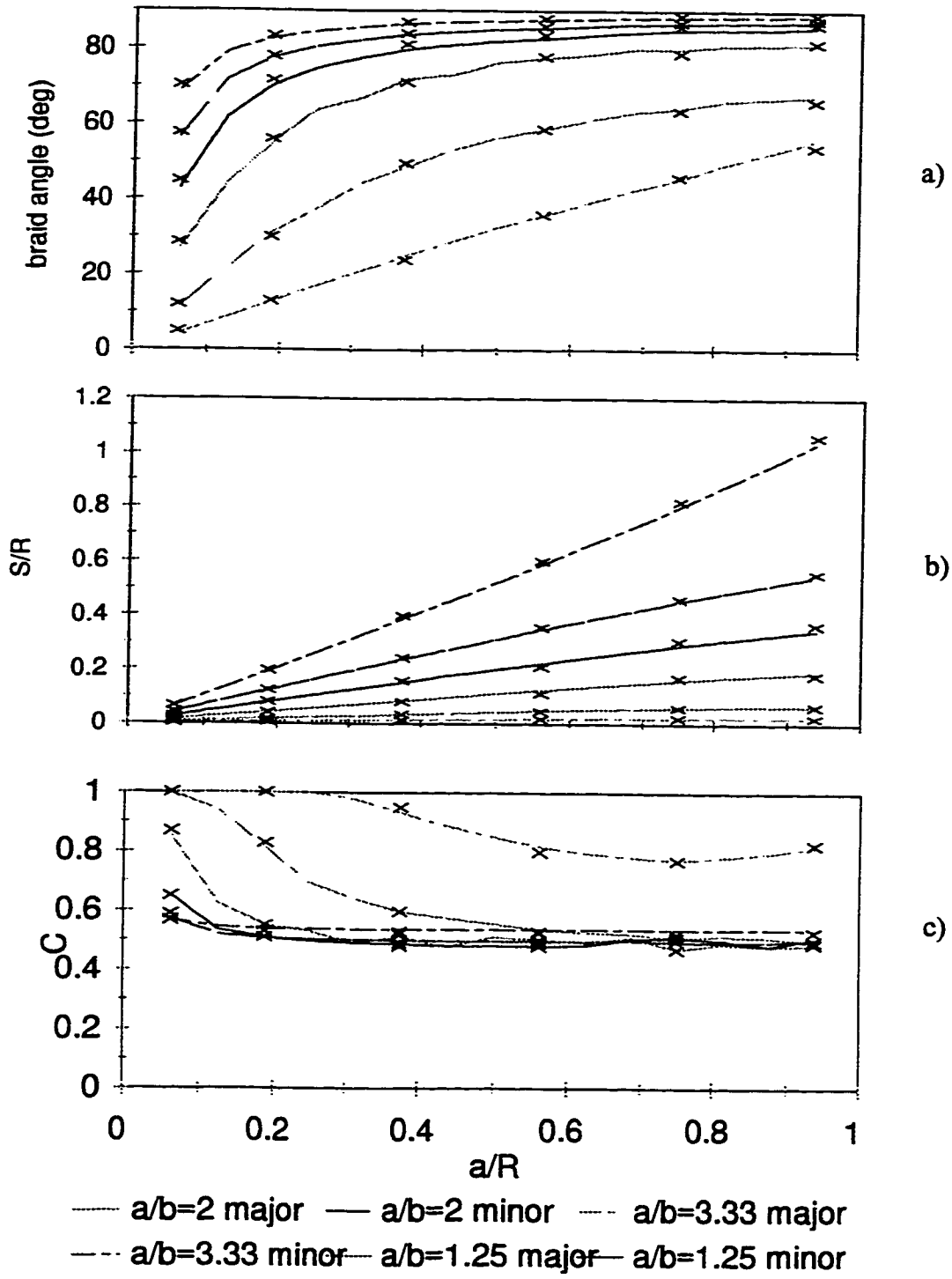

Figure 6-19 Configuration Properties at Major and Minor Axes versus Mandrel Size, Comparison of Algorithm 1, (curves), and Algorithm 3, (x's), (ω_c R / v_t = 12.37), a) braid angle, b) strand spacing, c) cover factor

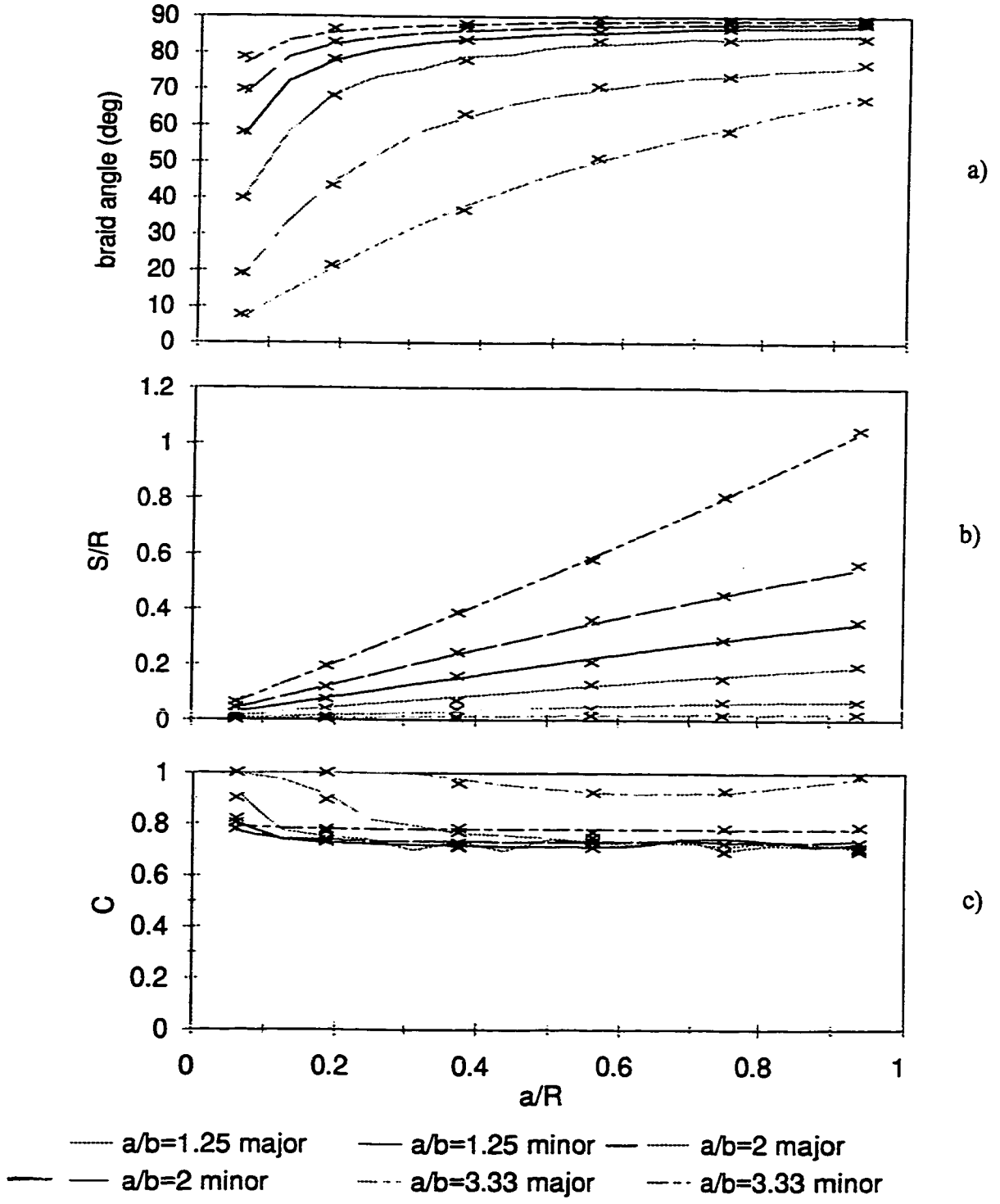

Figure 6-20 Configuration Properties at Major and Minor Axes versus Mandrel Size, Comparison of Algorithm 1, (curves), and Algorithm 3, (x's), (ω_c R / v_t = 20.62), a) braid angle, b) strand spacing, c) cover factor

CHAPTER 7

CONCLUSIONS AND RECOMMENDATIONS

7.1 Conclusions

1. Algorithm 1 was developed for mandrels with constant elliptical cross-section and assuming strand interference. It is based on an analytical method and gave reasonable results. The characteristics of the resulting braid angle, strand spacing, and cover factor functions were explained using physical arguments. The major conclusions for Algorithm 1 are:

   - The results for mandrels with aspect ratios greater than one show that the braid

angle is higher at points near the minor axis of the elliptical mandrel than at points near the major axis.

- The results for mandrels with aspect ratios greater than one show that the strand spacing is higher in the minor-axis region than in the major-axis region.

- The results also show that the cover factor decreases from the major-axis region to the minor-axis region.

- For larger mandrels, the braid angle at any same point on the perimeter is higher.

- Another effect of the mandrel size is that for larger mandrels the strand spacings (at similar points on the perimeter) are higher.

- A third effect of the mandrel size is that for larger mandrels, the cover factors are lower.

- If other factors are kept the same, a higher aspect ratio causes a lower 'major-axis' braid angle and a higher 'minor-axis' braid angle.

- A higher aspect ratio produces a lower 'major-axis' strand spacing and a higher 'minor-axis' strand spacing.

- A higher aspect ratio causes a higher 'major-axis' cover factor and a lower 'minor-axis' cover factor.

2. Algorithm 2 was developed for varying section size mandrels, assuming strand non-interference. It is based on a numerical integration method. The results indicate that the contact ring for this situation is non-planar.

3. Algorithm 2 models only one of the two sets of strands (clockwise and counter-clockwise). Algorithm 2 was modified to create Algorithm 3. Algorithm 3 sums the longitudinal movements of the strand contact points of the two sets of strands, which results in a planar contact ring. The results agree with those of Algorithm 1.

7.2 Recommendations

- Consider the effect of the forming ring. It is believed that if the formation ring is sufficiently larger than the mandrel, then the formation ring radius could be substituted for the carrier circle radius in the present equations as was done in Du, Popper, Chou [1]. However this question has yet to be investigated.

- Create an algorithm (if possible) to find the desired traverse speed versus location, (z), of contact point on mandrel, to give a desired property distribution. Perhaps do this by inverting the formulas developed herein.

- Create an algorithm for mandrels with cross-sections which change not only in size but also in aspect ratio, and/or rotate, as z increases.

- Create algorithms for more mandrel section shapes, for example:
  - a triangle with convex curved sides and rounded corners
  - a similarly rounded rectangle
  - any general section. Section could be defined by two or more functions.

REFERENCES

[1] C. Pastore and F. Ko, CIM of Braided Preforms for Composites, National SAMPE Symposium and Exhibition (Proceedings), 1988, May, pp. 133-155.

[2] G-W. Du, P. Popper, T-W. Chou, Process Model Of Circular Braiding, ASME MD, v 19, 1990, pp. 119-133.

[3] W. Michaeli and U. Rosenbaum, Structural Braiding of Complex Shaped FRP Parts, International SAMPE Symposium, 1989, May 8, pp. 1834-1842.

[4] J.B. Sainsbury-Carter, Fabrication Techniques of Tubular Structures from Braided Preimpregnated Rovings, Society of Manufacturing Engineers, EM85-100, 1985.

[5] L.R. Sanders, Braiding - A Mechanical Means of Composite Fabrication, SAMPE Quarterly, 1977, January, pp. 38-43.

[6] R.J. Post, Braiding Composites - Adapting The Process For The Mass Production of Aerospace Components, 22nd National SAMPE Symposium, 1977, pp. 486-503.

[7] H.B. Soebroto, T. Hager, C.M. Pastore, F.K. Ko, Engineering Design of Braided Structural Fiberglas Composites, 35th International SAMPE Symposium, 1990, April, pp. 687-696.

[8] F.Ko, C.Pastore, A.Head, Handbook of Industrial Braiding, Atkins & Pearce Inc.,Covington, 1990

[9] M.R.Spiegel, Mathematical Handbook of Formulas and Tables, McGraw-Hill Book Company, 1968

[10] M.Abramowitz and I.A.Stegun, Handbook of Mathematical Functions, Dover Publications Inc., New York, 1972

[11] C R C Handbook of Chemistry and Physics, The Chemical Rubber Company, Cleveland, 1969

BIBLIOGRAPHY

[1] R.T. Brown, Through-the-Thickness Braiding Technology, 30th National SAMPE Symposium, 1985, March, pp. 1509-1518.

[2] W. Michaeli, M. Goedel, H. Greif, M. Jehrke, Rational Manufacture of Fibre-Reinforced Plastics Components, Kunststoff - German Plastics, v 81 n 10 Oct, 1991, pp. 56-58.

[3] J.H. Byun, T.W. Chou, Three-dimensional Textile Composites. A Review, Winter Annual Meeting of the American Society of Mechanical Engineers, 1991, AMD v 129, pp. 47-55.

[4] D. Brookstein, Evolution of Fabric Preforms for Fibre Composites, Fiber Society 50th Anniversary Technical Conference, 1991, n 47, pp. 487-500.

[5] D. Brookstein, Comparison of Multilayer Interlocked Braided Composites with Other 3D Braided Composites, International SAMPE Symposium and Exhibition, 1991, v 36 pt 1, pp. 141-150.

[6] A.K. Munjal and P.F. Maloney, Braiding For Improving Performance And Reducing Manufacturing Costs of Composite Structures For Aerospace Applications, 22nd International SAMPE Technical Conference, 1990, v 22, pp. 1231-1242.

[7] D. Brookstein, Interlocked Fibre Architecture. Braided And Woven, 35th International SAMPE Symposium, 1990, v 35, pp. 746-756.

[8] A. Munjal, D. Spencer, E. Rahnenfuehrer, B. Pickett, P. Maloney, Design And Fabrication of High Quality Graphite/Epoxy Braided Composite Tubes for Space Structures, 35th International SAMPE Symposium, 1990, v 35, pp. 1954-1967.

[9] F.K. Ko, Recent Advances In Textile Structure Composites, ASM Advanced Composites Conference, 1985, pp. 83-94.

[10] J.B. Sainsbury-Carter, Braided Composites: A Material Form Providing Low Cost Fabrication Techniques, National SAMPE Symposium, v 30, 1985, 1486-1497.

[11] M. Hammad, W. Li, A. El-Shiekh, Structural Mechanics of 3-D Braided Preforms for Composites. Part 3: The 2-step Tubular Braiding, ASME Materials Division, MD v 5, 1988, pp 65-72.

[12] S.A. DeYoung, Braiding Machine for Composite Structures, Society of The Plastics Industry, Reinforced Plastics/Composites Institute, Annual Conference, 43rd, 1988, pp 9C.1-9C.3.

[13] J.B. Sainsbury-Carter, Braided Composite Tubes, Automotive Challenge And Plastics Response: Automotive Plastics, RETEC'87, 1987, Nov, pp 193-197.

[14] J. Archer, Composite Braided Structures - Characterization and Applications, 7th International Conference of the Society for the Advancement of Material and Process Engineering, European Chapter, 1986, v 35, pp 61-66.

[15] J.A. Vaccari, Automating Composites Fabrication, American Machinist and Automated Manufacturing, v 131 n 11 Nov, 1987, pp 87-98.

[16] P.F. Maloney, Composite Directions at Kaman, Vertiflite, v 33 n 5 Sept-Oct, 1987, pp 26-31.

Appendix A

Table 1, Data Results For Algorithm 1

X (cm)	Y (cm)	BA(deg)	FS (cm)	CF
0.089	1.992	21.49	0.179	0.938
0.196	1.961	23.71	0.199	0.902
0.307	1.904	28.23	0.240	0.833
0.422	1.813	34.80	0.308	0.745
0.540	1.683	43.02	0.409	0.661
0.658	1.506	51.68	0.549	0.600
0.770	1.277	59.49	0.727	0.563
0.868	0.992	65.32	0.931	0.540
0.946	0.649	69.31	1.136	0.526
0.993	0.228	71.64	1.296	0.519
0.940	-0.682	70.22	1.187	0.526
0.775	-1.265	62.44	0.813	0.554
0.668	-1.489	55.77	0.628	0.583
0.571	-1.643	48.85	0.494	0.621
0.478	-1.757	41.98	0.393	0.673
0.387	-1.844	35.43	0.315	0.737
0.295	-1.911	29.87	0.257	0.808
0.203	-1.958	25.53	0.215	0.874
0.109	-1.988	22.59	0.188	0.921
0.011	-2.000	21.28	0.176	0.943

$a = 2.0$ cm, $b = 1.0$ cm, $\omega_c = 0.116$ rad/sec, $v_t = 0.15$ cm/sec

$R = 16.0$ cm, $N_s = 18$, $w_t = 0.125$ cm

Braid Angle, Filament Spacing, and Cover Factor Distributions.
First and Second Quadrants. Case 1 Conditions.

Appendix B

Table 2, Data Results For Algorithm 2

FILAMENT 1						FILAMENT 2					
X	Y	Z	BA deg	FS cm	CF	X	Y	Z	BA deg	FS cm	CF
0.00	2.00	0.00	69.3	0.18	*	0.18	1.97	0.00	69.9	0.23	*
0.06	2.00	0.02	69.1	0.18	*	0.24	1.94	0.02	69.7	0.23	*
0.12	1.99	0.04	68.9	0.18	*	0.30	1.91	0.05	69.5	0.23	*
0.18	1.97	0.07	68.7	0.19	*	0.37	1.86	0.08	69.2	0.24	*
0.24	1.94	0.09	68.5	0.19	*	0.45	1.79	0.12	69.0	0.25	*
0.30	1.91	0.12	68.3	0.19	*	0.53	1.70	0.17	68.8	0.26	*
0.37	1.86	0.16	68.1	0.20	*	0.62	1.57	0.23	68.5	0.29	1.00
0.45	1.79	0.20	67.9	0.21	*	0.71	1.40	0.31	68.2	0.32	0.98
0.53	1.70	0.25	67.7	0.23	*	0.81	1.17	0.41	68.0	0.36	0.94
0.62	1.57	0.31	67.4	0.25	*	0.90	0.87	0.54	67.7	0.40	0.89
0.71	1.40	0.39	67.2	0.29	0.99	0.97	0.48	0.70	67.4	0.42	0.85
0.81	1.17	0.50	66.9	0.33	0.95	1.00	0.03	0.88	67.1	0.42	0.84
0.90	0.87	0.63	66.6	0.37	0.90	0.98	-0.43	1.08	66.8	0.41	0.85
0.97	0.48	0.80	66.4	0.40	0.86	0.91	-0.84	1.26	66.4	0.39	0.87
1.00	0.04	1.00	66.1	0.40	0.85	0.81	-1.18	1.41	66.1	0.38	0.88
0.98	-0.42	1.20	65.8	0.38	0.87	0.70	-1.43	1.53	65.9	0.37	0.89
0.91	-0.84	1.39	65.5	0.36	0.89	0.59	-1.61	1.63	65.6	0.37	0.89
0.81	-1.18	1.55	65.2	0.35	0.90	0.50	-1.74	1.70	65.4	0.37	0.88

-0.84	1.10	10.17	55.3	0.48	0.59	-0.52	1.71	10.32	55.2	0.48	0.59
-0.73	1.37	10.38	55.1	0.48	0.60	-0.43	1.81	10.41	55.2	0.48	0.59
-0.62	1.57	10.53	55.0	0.47	0.60	-0.35	1.88	10.49	55.1	0.48	0.59
-0.52	1.71	10.65	54.9	0.47	0.60	-0.27	1.93	10.55	55.1	0.49	0.59
-0.43	1.81	10.75	54.9	0.47	0.60	-0.20	1.96	10.60	55.1	0.49	0.59
-0.35	1.88	10.82	54.8	0.47	0.60	-0.14	1.98	10.65	55.1	0.49	0.59
-0.27	1.92	10.89	54.8	0.48	0.60	-0.08	1.99	10.70	55.1	0.49	0.59
-0.20	1.96	10.94	54.8	0.48	0.59	-0.02	2.00	10.74	55.2	0.49	0.59
-0.14	1.98	10.99	54.8	0.48	0.59	0.04	2.00	10.78	55.2	0.49	0.59
-0.08	1.99	11.03	54.8	0.48	0.59	0.10	1.99	10.82	55.2	0.49	0.58
-0.02	2.00	11.07	54.9	0.48	0.59	0.16	1.98	10.86	55.2	0.49	0.58
0.04	2.00	11.11	54.9	0.48	0.59	0.22	1.95	10.91	55.2	0.49	0.58
0.10	1.99	11.16	54.9	0.48	0.59	0.28	1.92	10.96	55.2	0.49	0.58
0.16	1.98	11.20	55.0	0.48	0.59	0.35	1.87	11.01	55.2	0.49	0.58
0.22	1.95	11.24	55.0	0.48	0.59	0.42	1.81	11.08	55.2	0.49	0.58
0.28	1.92	11.29	55.0	0.48	0.59	0.50	1.73	11.16	55.1	0.50	0.58
0.35	1.87	11.35	54.9	0.48	0.59	0.59	1.62	11.26	55.0	0.50	0.57
0.42	1.81	11.42	54.9	0.49	0.59	0.68	1.46	11.38	54.9	0.51	0.57
0.50	1.73	11.50	54.9	0.49	0.59	0.78	1.25	11.54	54.8	0.53	0.55
0.59	1.62	11.60	54.8	0.49	0.58	0.87	0.98	11.75	54.7	0.54	0.53

-0.07	-1.99	29.77	51.1	0.53	0.51	-0.25	-1.93	29.50	51.4	0.53	0.51
-0.13	-1.98	29.82	51.2	0.53	0.51	-0.32	-1.89	29.56	51.4	0.53	0.51
-0.19	-1.96	29.87	51.2	0.53	0.51	-0.39	-1.84	29.63	51.4	0.53	0.51
-0.25	-1.93	29.93	51.3	0.53	0.51	-0.47	-1.77	29.72	51.4	0.53	0.51
-0.32	-1.89	29.99	51.3	0.53	0.51	-0.55	-1.67	29.82	51.4	0.54	0.51

* a CF of * indicates yarn jamming

Braid Angle, Filament Spacing, and Cover Factor Distributions, as a Function of 3D surface co-ordinates, Case 2 Conditions.

FILAMENT 3						FILAMENT 4					
X	Y	Z	BA deg	FS	CF	X	Y	Z	BA deg	FS	CF
0.37	1.86	0.00	70.3	0.38	0.95	0.62	1.57	0.00	70.5	0.77	0.63
0.45	1.79	0.04	70.1	0.38	0.95	0.72	1.40	0.07	70.2	0.77	0.62
0.53	1.70	0.08	69.8	0.39	0.93	0.81	1.17	0.16	69.9	0.78	0.61
0.62	1.57	0.14	69.6	0.41	0.91	0.90	0.86	0.28	69.6	0.79	0.59
0.71	1.40	0.21	69.3	0.43	0.88	0.97	0.47	0.42	69.3	0.79	0.58
0.81	1.17	0.30	69.0	0.46	0.85	1.00	0.03	0.59	68.9	0.79	0.58
0.90	0.86	0.43	68.7	0.49	0.81	0.98	-0.43	0.77	68.6	0.77	0.58
0.97	0.48	0.58	68.4	0.51	0.78	0.91	-0.85	0.93	68.3	0.75	0.59
1.00	0.03	0.76	68.1	0.51	0.77	0.81	-1.18	1.07	67.9	0.74	0.59
0.98	-0.43	0.94	67.7	0.50	0.78	0.70	-1.43	1.18	67.6	0.73	0.59
0.91	-0.85	1.12	67.4	0.48	0.79	0.59	-1.61	1.27	67.4	0.72	0.59
0.81	-1.18	1.26	67.1	0.47	0.79	0.49	-1.74	1.34	67.1	0.72	0.59
0.70	-1.43	1.38	66.8	0.46	0.79	0.41	-1.83	1.39	66.9	0.71	0.59
0.59	-1.61	1.47	66.5	0.46	0.79	0.33	-1.89	1.43	66.7	0.71	0.59
0.49	-1.74	1.54	66.3	0.46	0.79	0.25	-1.94	1.47	66.5	0.71	0.58
0.41	-1.83	1.59	66.1	0.46	0.78	0.19	-1.97	1.50	66.3	0.70	0.58
0.33	-1.89	1.64	65.9	0.46	0.78	0.12	-1.99	1.53	66.1	0.70	0.58
0.25	-1.93	1.67	65.7	0.46	0.78	0.06	-2.00	1.56	66.0	0.69	0.58
-0.27	1.93	10.21	55.4	0.51	0.57	-0.08	1.99	10.00	55.6	0.58	0.52
-0.20	1.96	10.27	55.4	0.51	0.57	-0.02	2.00	10.04	55.7	0.58	0.52
-0.14	1.98	10.31	55.4	0.51	0.57	0.04	2.00	10.08	55.7	0.58	0.52
-0.08	1.99	10.36	55.4	0.52	0.57	0.10	1.99	10.12	55.7	0.58	0.52
-0.02	2.00	10.40	55.4	0.52	0.57	0.16	1.98	10.16	55.7	0.58	0.52
0.04	2.00	10.44	55.4	0.52	0.57	0.22	1.95	10.21	55.7	0.58	0.52
0.10	1.99	10.48	55.5	0.52	0.57	0.28	1.92	10.26	55.7	0.58	0.52
0.16	1.98	10.52	55.5	0.52	0.57	0.35	1.87	10.31	55.7	0.58	0.52
0.22	1.95	10.56	55.5	0.52	0.57	0.42	1.81	10.38	55.6	0.58	0.52
0.28	1.92	10.61	55.5	0.52	0.57	0.50	1.73	10.46	55.6	0.58	0.52
0.35	1.87	10.67	55.5	0.52	0.57	0.59	1.61	10.56	55.5	0.58	0.52
0.42	1.81	10.74	55.4	0.52	0.56	0.68	1.46	10.68	55.4	0.59	0.51
0.50	1.73	10.81	55.4	0.52	0.56	0.78	1.25	10.84	55.3	0.60	0.50
0.59	1.62	10.91	55.3	0.52	0.56	0.87	0.97	11.04	55.1	0.61	0.49
0.68	1.46	11.04	55.2	0.53	0.55	0.95	0.61	11.30	55.0	0.62	0.48
0.78	1.25	11.20	55.1	0.55	0.54	1.00	0.18	11.60	54.8	0.62	0.48
0.87	0.97	11.40	54.9	0.56	0.52	0.99	-0.28	11.93	54.7	0.60	0.49
0.95	0.61	11.66	54.8	0.58	0.51	0.93	-0.72	12.24	54.5	0.59	0.50
1.00	0.18	11.97	54.6	0.57	0.51	0.84	-1.08	12.51	54.4	0.57	0.51
0.99	-0.28	12.30	54.5	0.56	0.52	0.73	-1.36	12.72	54.2	0.56	0.52
-0.32	-1.89	29.13	51.4	0.54	0.51	-0.55	-1.67	28.96	51.5	0.55	0.50
-0.39	-1.84	29.20	51.4	0.54	0.51	-0.64	-1.53	29.09	51.4	0.56	0.49
-0.47	-1.77	29.29	51.4	0.54	0.51	-0.74	-1.34	29.26	51.4	0.57	0.49
-0.55	-1.67	29.39	51.4	0.54	0.51	-0.84	-1.09	29.47	51.3	0.58	0.48
-0.64	-1.53	29.52	51.4	0.55	0.50	-0.92	-0.77	29.74	51.2	0.59	0.47
-0.74	-1.35	29.69	51.3	0.56	0.49	-0.98	-0.36	30.07	51.1	0.60	0.46
-0.84	-1.10	29.90	51.2	0.57	0.48	-1.00	0.09	30.44	50.9	0.59	0.47

(Cont'd)

FILAMENT 5

X	Y	Z	BA deg	FS	CF
0.90	0.86	0.00	70.1	1.30	0.40
0.97	0.47	0.14	69.8	1.28	0.40
1.00	0.02	0.31	69.4	1.25	0.40
0.98	-0.44	0.48	69.1	1.22	0.41
0.90	-0.85	0.64	68.8	1.19	0.41
0.80	-1.19	0.78	68.4	1.16	0.41
0.70	-1.44	0.88	68.1	1.14	0.41
0.59	-1.61	0.97	67.8	1.13	0.41
0.49	-1.74	1.03	67.6	1.12	0.41
0.40	-1.83	1.08	67.3	1.11	0.41
0.32	-1.89	1.13	67.1	1.10	0.41
0.25	-1.94	1.16	66.9	1.09	0.41
0.18	-1.97	1.19	66.7	1.08	0.41
0.12	-1.99	1.22	66.6	1.07	0.41
0.06	-2.00	1.25	66.4	1.07	0.41
0.00	-2.00	1.27	66.3	1.06	0.41
-0.06	-2.00	1.30	66.1	1.05	0.41
-0.11	-1.99	1.32	66.0	1.04	0.42

FILAMENT 6

X	Y	Z	BA deg	FS	CF
0.98	-0.44	0.00	69.0	1.04	0.47
0.90	-0.86	0.16	68.7	1.01	0.47
0.80	-1.19	0.30	68.3	0.99	0.47
0.70	-1.44	0.40	68.0	0.98	0.47
0.59	-1.62	0.49	67.7	0.96	0.47
0.49	-1.74	0.55	67.5	0.95	0.47
0.40	-1.83	0.60	67.2	0.95	0.47
0.32	-1.89	0.65	67.0	0.94	0.47
0.25	-1.94	0.68	66.8	0.93	0.47
0.18	-1.97	0.71	66.6	0.93	0.47
0.12	-1.99	0.74	66.5	0.92	0.47
0.06	-2.00	0.77	66.3	0.92	0.47
0.00	-2.00	0.80	66.2	0.91	0.47
-0.06	-2.00	0.82	66.0	0.90	0.47
-0.11	-1.99	0.85	65.9	0.90	0.47
-0.17	-1.97	0.87	65.8	0.89	0.47
-0.24	-1.94	0.91	65.6	0.88	0.47
-0.30	-1.91	0.94	65.5	0.88	0.47

0.10	1.99	9.73	55.8	0.68	0.46
0.16	1.97	9.77	55.8	0.68	0.46
0.22	1.95	9.81	55.8	0.67	0.46
0.28	1.92	9.86	55.8	0.67	0.46
0.35	1.87	9.92	55.8	0.67	0.46
0.42	1.81	9.98	55.8	0.67	0.46
0.50	1.73	10.06	55.7	0.67	0.46
0.59	1.61	10.16	55.6	0.67	0.46
0.68	1.46	10.28	55.5	0.67	0.46
0.78	1.25	10.44	55.4	0.68	0.45
0.88	0.97	10.65	55.3	0.69	0.44
0.95	0.60	10.90	55.1	0.70	0.44
1.00	0.17	11.21	54.9	0.69	0.44
0.99	-0.29	11.53	54.8	0.67	0.45
0.93	-0.72	11.84	54.6	0.65	0.46
0.84	-1.09	12.10	54.5	0.64	0.47
0.73	-1.36	12.32	54.3	0.63	0.47
0.62	-1.56	12.48	54.2	0.63	0.47
0.52	-1.70	12.60	54.1	0.63	0.47
0.43	-1.80	12.70	54.1	0.63	0.47

0.28	1.92	9.40	55.8	0.63	0.48
0.35	1.87	9.46	55.8	0.63	0.48
0.43	1.81	9.52	55.7	0.63	0.48
0.51	1.73	9.60	55.7	0.63	0.48
0.59	1.61	9.70	55.6	0.63	0.48
0.69	1.46	9.82	55.5	0.64	0.48
0.78	1.25	9.98	55.4	0.65	0.47
0.88	0.96	10.19	55.2	0.66	0.46
0.95	0.60	10.44	55.1	0.66	0.46
1.00	0.17	10.75	54.9	0.66	0.46
0.99	-0.29	11.07	54.8	0.64	0.47
0.93	-0.73	11.38	54.6	0.63	0.48
0.84	-1.09	11.65	54.4	0.61	0.48
0.73	-1.36	11.86	54.3	0.60	0.49
0.62	-1.56	12.02	54.2	0.60	0.49
0.52	-1.70	12.15	54.1	0.60	0.49
0.43	-1.80	12.24	54.1	0.60	0.49
0.35	-1.87	12.32	54.0	0.60	0.49
0.27	-1.92	12.39	54.0	0.60	0.49
0.21	-1.96	12.44	54.1	0.60	0.49

-0.84	-1.09	29.04	51.3	0.60	0.47
-0.92	-0.76	29.31	51.2	0.61	0.46
-0.98	-0.36	29.64	51.1	0.61	0.45
-1.00	0.10	30.01	51.0	0.60	0.46
-0.96	0.55	30.37	50.8	0.58	0.47
-0.88	0.95	30.70	50.7	0.56	0.48
-0.78	1.26	30.97	50.6	0.55	0.49

-1.00	0.10	29.56	50.9	0.59	0.46
-0.96	0.56	29.92	50.8	0.57	0.48
-0.88	0.95	30.25	50.7	0.56	0.49
-0.78	1.26	30.52	50.6	0.54	0.50
-0.67	1.49	30.73	50.5	0.54	0.50
-0.56	1.65	30.89	50.5	0.54	0.50
-0.47	1.77	31.01	50.5	0.54	0.50

(Cont'd)

FILAMENT 7

X	Y	Z	BA deg	FS	CF
0.69	-1.44	0.00	68.2	0.49	0.80
0.59	-1.62	0.08	67.9	0.49	0.80
0.49	-1.74	0.15	67.6	0.48	0.79
0.40	-1.83	0.20	67.4	0.48	0.79
0.32	-1.89	0.24	67.2	0.48	0.78
0.25	-1.94	0.28	67.0	0.48	0.78
0.18	-1.97	0.31	66.8	0.48	0.78
0.12	-1.99	0.34	66.6	0.48	0.78
0.06	-2.00	0.36	66.5	0.48	0.78
0.00	-2.00	0.39	66.3	0.47	0.77
-0.06	-2.00	0.41	66.2	0.47	0.77
-0.11	-1.99	0.44	66.0	0.47	0.77
-0.17	-1.97	0.47	65.9	0.47	0.77
-0.24	-1.94	0.50	65.7	0.47	0.77
-0.30	-1.91	0.53	65.6	0.47	0.77
-0.37	-1.86	0.57	65.4	0.47	0.76
-0.45	-1.79	0.62	65.2	0.47	0.76
-0.53	-1.70	0.67	65.0	0.47	0.75

FILAMENT 8

X	Y	Z	BA deg	FS	CF
0.40	-1.83	0.00	68.2	0.26	9.99
0.32	-1.89	0.04	68.0	0.26	9.99
0.25	-1.94	0.07	67.8	0.26	9.99
0.18	-1.97	0.10	67.6	0.26	9.99
0.12	-1.99	0.13	67.4	0.26	1.00
0.06	-2.00	0.16	67.2	0.26	1.00
0.00	-2.00	0.18	67.1	0.26	1.00
-0.06	-2.00	0.21	66.9	0.27	1.00
-0.12	-1.99	0.23	66.7	0.27	1.00
-0.17	-1.97	0.26	66.6	0.27	1.00
-0.24	-1.94	0.29	66.4	0.27	0.99
-0.30	-1.91	0.32	66.3	0.27	0.99
-0.37	-1.86	0.36	66.1	0.28	0.99
-0.45	-1.79	0.40	65.9	0.28	0.98
-0.53	-1.70	0.46	65.7	0.30	0.97
-0.62	-1.57	0.53	65.5	0.31	0.95
-0.71	-1.41	0.61	65.3	0.34	0.91
-0.81	-1.18	0.73	65.0	0.37	0.86

0.51	1.72	9.17	55.7	0.52	0.56
0.59	1.61	9.26	55.6	0.53	0.56
0.69	1.45	9.39	55.5	0.54	0.55
0.78	1.24	9.55	55.4	0.55	0.54
0.88	0.96	9.75	55.3	0.57	0.52
0.95	0.60	10.01	55.1	0.58	0.51
1.00	0.16	10.31	55.0	0.58	0.51
0.99	-0.30	10.64	54.8	0.56	0.52
0.93	-0.73	10.95	54.6	0.54	0.53
0.84	-1.09	11.21	54.5	0.53	0.54
0.73	-1.37	11.42	54.3	0.52	0.55
0.62	-1.57	11.58	54.2	0.52	0.55
0.52	-1.71	11.71	54.2	0.52	0.55
0.43	-1.80	11.81	54.1	0.52	0.55
0.35	-1.87	11.88	54.1	0.52	0.55
0.27	-1.92	11.95	54.1	0.52	0.55
0.20	-1.96	12.00	54.1	0.52	0.55
0.14	-1.98	12.05	54.1	0.52	0.55
0.08	-1.99	12.10	54.2	0.53	0.54
0.02	-2.00	12.14	54.2	0.53	0.54

0.78	1.24	9.19	55.6	0.51	0.57
0.88	0.96	9.39	55.5	0.53	0.56
0.95	0.59	9.65	55.3	0.54	0.54
1.00	0.16	9.95	55.2	0.54	0.54
0.99	-0.30	10.27	55.0	0.53	0.55
0.93	-0.74	10.58	54.8	0.51	0.57
0.84	-1.10	10.84	54.7	0.49	0.58
0.73	-1.37	11.05	54.5	0.49	0.58
0.62	-1.57	11.21	54.4	0.48	0.59
0.52	-1.71	11.33	54.3	0.48	0.59
0.43	-1.81	11.43	54.3	0.48	0.58
0.35	-1.88	11.51	54.3	0.48	0.58
0.27	-1.92	11.57	54.3	0.49	0.58
0.20	-1.96	11.63	54.3	0.49	0.58
0.14	-1.98	11.68	54.3	0.49	0.58
0.08	-1.99	11.72	54.3	0.49	0.58
0.02	-2.00	11.76	54.4	0.49	0.58
-0.04	-2.00	11.80	54.4	0.49	0.58
-0.10	-1.99	11.85	54.4	0.49	0.58
-0.15	-1.98	11.89	54.5	0.49	0.58

-0.78	1.26	30.08	50.6	0.53	0.51
-0.67	1.49	30.28	50.6	0.52	0.51
-0.56	1.65	30.44	50.5	0.52	0.51
-0.47	1.77	30.56	50.5	0.52	0.51
-0.38	1.85	30.66	50.5	0.53	0.51
-0.30	1.91	30.74	50.5	0.53	0.51
-0.23	1.95	30.81	50.6	0.53	0.51

-0.47	1.77	30.13	50.5	0.52	0.52
-0.38	1.85	30.23	50.5	0.52	0.51
-0.30	1.91	30.31	50.6	0.52	0.51
-0.23	1.95	30.37	50.6	0.52	0.51
-0.17	1.97	30.43	50.7	0.52	0.51
-0.10	1.99	30.48	50.8	0.53	0.51
-0.04	2.00	30.53	50.8	0.53	0.51

(Cont'd)

FILAMENT 9						FILAMENT 10			
X	Y	Z	BA deg	FS	CF	X	Y	Z	BA deg
0.18	-1.97	0.00	68.7	0.19	9.99	-0.00	-2.00	0.00	69.3
0.12	-1.99	0.03	68.5	0.19	9.99	-0.06	-2.00	0.02	69.1
0.06	-2.00	0.05	68.3	0.19	9.99	-0.12	-1.99	0.04	68.9
0.00	-2.00	0.07	68.1	0.19	9.99	-0.18	-1.97	0.07	68.7
-0.06	-2.00	0.10	67.9	0.19	9.99	-0.24	-1.94	0.09	68.5
-0.12	-1.99	0.12	67.8	0.19	9.99	-0.30	-1.91	0.12	68.3
-0.18	-1.97	0.15	67.6	0.20	9.99	-0.37	-1.86	0.16	68.1
-0.24	-1.94	0.17	67.4	0.20	9.99	-0.45	-1.79	0.20	67.9
-0.30	-1.91	0.20	67.2	0.21	9.99	-0.53	-1.70	0.25	67.7
-0.37	-1.86	0.24	67.0	0.21	9.99	-0.62	-1.57	0.31	67.4
-0.45	-1.79	0.28	66.8	0.22	9.99	-0.71	-1.40	0.39	67.2
-0.53	-1.70	0.34	66.6	0.24	9.99	-0.81	-1.17	0.50	66.9
-0.62	-1.57	0.40	66.4	0.26	1.00	-0.90	-0.87	0.63	66.6
-0.71	-1.40	0.49	66.2	0.29	0.98	-0.97	-0.48	0.80	66.4
-0.81	-1.18	0.60	65.9	0.33	0.93	-1.00	-0.04	1.00	66.1
-0.90	-0.87	0.74	65.7	0.37	0.88	-0.98	0.42	1.20	65.8
-0.97	-0.49	0.91	65.4	0.40	0.84	-0.91	0.84	1.39	65.5
-1.00	-0.04	1.12	65.1	0.40	0.83	-0.81	1.18	1.55	65.2

1.00	0.16	9.62	55.4	0.53	0.55	0.83	-1.10	10.17	55.3
0.99	-0.31	9.94	55.3	0.52	0.56	0.73	-1.37	10.38	55.1
0.93	-0.74	10.24	55.1	0.50	0.58	0.62	-1.57	10.53	55.0
0.84	-1.10	10.50	54.9	0.48	0.59	0.52	-1.71	10.65	54.9
0.73	-1.37	10.71	54.8	0.48	0.60	0.43	-1.81	10.75	54.9
0.62	-1.57	10.87	54.7	0.47	0.60	0.35	-1.88	10.82	54.8
0.52	-1.71	10.99	54.6	0.47	0.60	0.27	-1.92	10.89	54.8
0.43	-1.81	11.08	54.6	0.47	0.60	0.20	-1.96	10.94	54.8
0.35	-1.88	11.16	54.5	0.47	0.60	0.14	-1.98	10.99	54.8
0.27	-1.92	11.22	54.5	0.48	0.59	0.08	-1.99	11.03	54.8
0.20	-1.96	11.28	54.5	0.48	0.59	0.02	-2.00	11.07	54.9
0.14	-1.98	11.33	54.5	0.48	0.59	-0.04	-2.00	11.11	54.9
0.08	-1.99	11.37	54.6	0.48	0.59	-0.10	-1.99	11.16	54.9
0.02	-2.00	11.41	54.6	0.48	0.59	-0.16	-1.98	11.20	55.0
-0.04	-2.00	11.45	54.6	0.48	0.59	-0.22	-1.95	11.24	55.0
-0.10	-1.99	11.50	54.7	0.48	0.59	-0.28	-1.92	11.29	55.0
-0.16	-1.98	11.54	54.7	0.48	0.59	-0.35	-1.87	11.35	54.9
-0.22	-1.95	11.58	54.7	0.48	0.59	-0.42	-1.81	11.42	54.9
-0.28	-1.92	11.64	54.7	0.48	0.59	-0.50	-1.73	11.50	54.9
-0.35	-1.87	11.69	54.7	0.48	0.59	-0.59	-1.62	11.60	54.8

-0.23	1.95	29.94	50.7	0.52	0.51	-0.04	2.00	29.68	51.0
-0.17	1.97	30.00	50.7	0.52	0.51	0.01	2.00	29.72	51.0
-0.10	1.99	30.05	50.8	0.52	0.51	0.07	1.99	29.77	51.1
-0.04	2.00	30.10	50.9	0.53	0.51	0.13	1.98	29.82	51.2
0.01	2.00	30.15	51.0	0.53	0.51	0.19	1.96	29.87	51.2
0.07	1.99	30.20	51.1	0.53	0.51	0.25	1.93	29.93	51.3
0.13	1.98	30.25	51.1	0.53	0.51	0.32	1.89	29.99	51.3

(Cont'd)